DISSERTATION

Defence held on 07/12/2018 in Bordeaux

to obtain the degree of

DOCTEUR DE L'UNIVERSITÉ DU LUXEMBOURG

EN PHYSIQUE

AND

DOCTEUR DE L'UNIVERSITÉ DE BORDEAUX

EN PHYSICO-CHIMIE DE LA MATIÈRE CONDENSÉE

by

Catarina REALISTA COELHO DOS SANTOS PEDROSA

Born on 9 September 1990 in Lisbon (Portugal)

BIOACTIVE NANOTOPOGRAPHIES FOR THE CONTROL OF MESENCHYMAL STEM CELL DIFFERENTIATION FOR APPLICATIONS IN BONE TISSUE ENGINEERING

Dissertation defence committee

Dr Marie-Christine Durrieu, dissertation co-supervisor
Professor, Université de Bordeaux

Dr Sivashankar Krishnamoorthy, dissertation co-supervisor
Research director, Luxembourg Institute of Science and Technology

Dr Ana Paula Pêgo, Chairman
Professor, Universidade do Porto

Dr Lars Pleth Nielsen
R&D director, Teknologisk Institut

Nanotopographies bioactives pour le contrôle de la différenciation des cellules souches mésenchymateuses pour applications en ingénierie de tissu osseux

Résumé

Les nanotopographies de surface présentant des dimensions comparables à celles des éléments de la matrice extracellulaire offrent la possibilité de réguler le comportement cellulaire. L'étude de l'impact de la nanotopographie de surface sur la réponse cellulaire a été toujours limitée compte tenu des précisions limitées sur les géométries produites, en particulier sur les grandes surfaces. Des matériaux base silicium présentant des nanopiliers avec des géométries parfaitement contrôlées ont été fabriqués et leur impact sur la différentiation ostéogénique de cellules souches mésenchymateuses humaines (hMCSs) a été étudié. Des matériaux avec des nanopiliers de dimensions critiques comprises entre 40 et 200 nm et des écarts types inférieurs à 15% sur un wafer de silicium ont été réalisés en profitant de la capacité d'auto-assemblage des copolymères à blocs. Pour mettre en évidence si des modifications de la chimie de la surface des nanopiliers pourraient favoriser la différenciation des MSCs, des peptides mimétiques ont été greffés sur les matériaux fabriqués. Un peptide connu pour sa capacité d'améliorer l'adhésion cellulaire (peptide RGD), un peptide synthétique capable d'améliorer l'ostéogenèse (peptide mimétique BMP-2) et une combinaison de ces deux peptides ont été immobilisés de manière covalente sur les matériaux silicium présentant des nanopiliers de différentes géométries (diamètre, espacement et hauteur).

Les essais d'immunofluorescence et de réaction en chaîne de la polymérase quantitative (RT-qPCR) révèlent un impact des nanotopographies sur la différenciation ostéogénique des hMSCs. De plus, il a été constaté que la différenciation des cellules dépendait de l'âge du donneur. La fonctionnalisation de surface a permis une augmentation supplémentaire de l'expression des marqueurs ostéogéniques, en particulier lorsque le peptide RGD et le peptide mimétique BMP-2 sont co-immobilisés en surface. Cette étude met clairement en évidence l'impact de nanostructures avec différentes bioactivités sur la différentiation de MSCs. Ces matériaux pourront trouver leur place dans des cultures in vitro, dans l'élaboration de nouveaux biomatériaux osseux et dans de nouveaux produits d'ingénierie tissulaire.

Mots clés: Cellules souches mésenchymateuses, Biomatériaux, Nano-structuration de matériaux, Autoassemblage de polymères, Chimie de surface.

Bioactive nanotopographies for the control of mesenchymal stem cell differentiation for applications in bone tissue engineering

Abstract:

Nanotopography with length scales of the order of extracellular matrix elements offers the possibility of regulating cell behavior. Investigation of the impact of nanotopography on cell response has been limited by inability to precisely control geometries, especially at high spatial resolutions, and across practically large areas. This work allowed the fabrication of well-controlled and periodic nanopillar arrays of silicon to investigate their impact on osteogenic differentiation of human mesenchymal stem cells (hMSCs). Silicon nanopillar arrays with critical dimensions in the range of 40-200 nm, exhibiting standard deviations below 15% across full wafers were realized using self-assembly of block copolymer colloids. To investigate if modifications of surface chemistry could further improve the modulation of hMSC differentiation, mimetic peptides were grafted on the fabricated nanoarrays. A peptide known for its ability to ameliorate cell adhesion (RGD peptide), a synthetic peptide able to enhance osteogenesis (BMP-2 mimetic peptide), and a combination or both molecules were covalently grafted on the nanostructures. Immunofluorescence and quantitative polymerase chain reaction (RT-qPCR) measurements reveal clear dependence of osteogenic differentiation of hMSCs on the diameter and periodicity of the arrays. Moreover, the differentiation of hMSCs was found to be dependent on the age of the donor. Surface functionalization allowed additional enhancement of the expression of osteogenic markers, in particular when RGD peptide and BMP-2 mimetic peptide were co-immobilized. These findings can contribute for the development of personalized treatments of bone diseases, namely novel implant nanostructuring depending on patient age.

Keywords: Mesenchymal stem cells, Biomaterials, Material nanostructuration, Block copolymer self-assembly, Surface chemistry.

Unités de Recherche

3 BIOs group: BIOactive surfaces, BIOmaterials and BIOmimetic tissue-engineered products

Institut de Chimie et Biologie des Membranes et des Nano-objects

(CNRS UMR5248 CBMN)

Allée Geoffroy Saint Hilaire - Bât. 14, 33600 Pessac, France

Nano-enabled Medicine and Cosmetics group (NEMC)

Materials Research and Technology Department (MRT)

Luxembourg Institute of Science and Technology (LIST)

41, rue du Brill, L-4422 Belvaux, Luxembourg

Résumé

Nanotopographies bioactives pour le contrôle de la différenciation des cellules souches mésenchymateuses pour applications en ingénierie de tissu osseux

Dans le but de guider de manière contrôlée la réponse cellulaire (e.g. migration, prolifération, différentiation), des biomatériaux bioactifs capables de mimer le microenvironnement cellulaire *in vivo* (c'est-à-dire la matrice extracellulaire (MEC)) sont à l'étude [1, 2]. La compréhension des interactions biomatériau-cellule à l'échelle cellulaire (micromètre) ou même moléculaire (nanomètre) est donc essentielle pour la conception er l'élaboration d'implants de nouvelle génération utilisables en dentaire ou orthopédie, la synthèse de nouveaux produits d'ingénierie tissulaire ou pour la compréhension du microenvironnement cellulaire *in vivo* [3]. En particulier, pour l'ingénierie du tissu osseux, les cellules souches mésenchymateuses (MSC) représentent les cellules le plus utilisées en raison de leur capacité à proliférer et à se différencier vers divers lignages y compris le lignage ostéoblastique [4]. Ces cellules peuvent être isolées de différents tissus, notamment de la moelle osseuse, du tissu adipeux et des tissus dentaires [5, 6].

Les méthodes de nanofabrication classiquement utilisées dans l'électronique fournissent des outils intéressants pour fabriquer des substrats nanostructurés que peuvent être utilisés comme plateformes pour ces études d'interaction entre une cellule et le substrat. Ces techniques ont été majoritairement développées puis utilisées pour la structuration du silicium. Le silicium est considéré comme non cytotoxique, et toutes les particules susceptibles d'être libérées sont dégradées en acide silicique, également non toxique [7, 8].

Des études sur les interactions cellule-matériau ont été relevées à différents régimes d'échelle. Concernant la nano-échelle, des structures comprenant trous, piliers ou stries on été capables de produire des réponses cellulaires spécifiques sur plusieurs types cellulaires comme les MSC, les fibroblastes, les neurones, les ostéoblastes et les cellules

musculaires lisses, sans besoin de facteurs de croissance supplémentaires [9–11]. Cependant, il n'est pas encore compris comment chaque paramètre géométrique d'une nanostructure influence la différenciation des MSC en ostéoblastes. De plus, des résultats contradictoires sont souvent trouvés dans la littérature probablement car des protocoles de culture cellulaire différents sont utilisés [12, 13].

Par conséquent, dans cette étude, nous avons étudié l'influence des réseaux de nanopiliers contrôlés sur la différenciation des MSC humaines vers le lignage ostéoblastique. Les cellules ont été cultivées sur des échantillons nanostructurés dans un milieu minimum ne contenant que les molécules essentielles à la survie des cellules, afin d'éviter l'influence de tout autre paramètre que la topologie du matériau. La fabrication des réseaux de piliers à l'échelle nanométrique était basée sur l'auto-assemblage de copolymères diblocs (BCP) amphiphiles. Ces modèles à base de micelles inverses constituent une alternative à d'autres techniques lithographiques, comme par exemple la lithographie par faisceau d'électrons, en raison de leur facilité de formation des structures sur grandes surfaces, d'un contrôle orthogonal des variables géométriques, des coûts réduits et de leur compatibilité avec une large gamme de substrats [14]. Cette technique lithographique est largement utilisée dans les applications en nanoélectronique car elle permet la fabrication de matrices ordonnées à l'échelle nanométrique [15].

En ce qui concerne le contrôle de la réponse cellulaire par le biais de modifications de la chimie de surface d'un biomatériau, des molécules de différentes tailles, allant des protéines de la MEC aux peptides linéaires courts, ont été étudiées dans la littérature comme moyens possibles d'attribuer la bioactivité à la surface d'un matériau [16]. Des peptides sont normalement utilisés au détriment des protéines car ils peuvent être synthétisés avec une grande pureté, à un coût inférieur, et des sites actifs peuvent être crées de manière contrôlée [17]. Le motif le plus représentatif utilisé pour améliorer l'adhésion cellulaire est la séquence d'acides aminés arginine-glycine-acide aspartique (RGD), qui intervient in vivo dans la liaison des protéines de la MEC aux récepteurs transmembranaires de type intégrine [18, 19]. Les protéines morphogénétiques osseuses (BMP), en particulier la BMP-2, et ses peptides dérivés sont utilisées pour soutenir la différenciation ostéogénique des MSC [20–22]. Des effets synergiques de la combinaison d'un peptide favorisant l'adhérence cellulaire et d'un peptide favorisant la différenciation cellulaire ont été rapportés dans la littérature [21, 23].

Cette étude vise à étudier la différenciation ostéogénique de MSC humaines cultivées

sur des matrices de nanopiliers de silicium non-fonctionnalisées ou greffés avec un peptide RGD et / ou un peptide mimétique de la BMP-2. Les surfaces préparées ont été caractérisées par microscopie à force atomique (AFM), microscopie électronique à balayage (MEB) et spectroscopie photoélectronique à rayons-X (XPS). Pour évaluer dans quelle mesure la différenciaîon des MSC était favorisée, l'expression de marqueurs de différenciation ostéogéniques (facteur de transcription 2, Runx2, collagène de type I, Col1A1, ostéopontine, OPN, et ostéocalcine, OCN) a été étudiée par immunofluorescence et réaction en chaîne de la polymérase quantitative (RT-qPCR) [24].

Les micelles inverses des BCP ont permis la fabrication de matrices polymériques ordonnées avec une bonne uniformité sur grandes surfaces (wafers), qui pourraient ensuite être utilisées comme masques pour la structuration du substrat avec une reproductibilité élevée. Ces caractéristiques sont essentielles pour l'utilisation subséquente des nanopiliers de silicium dans les études de différenciation des MSC.

La caractérisation des surfaces réalisées par XPS avant et après le greffage de peptides (RGD ou BMP-2) a montré que la fonctionnalisation de surface se réalisait suivant le schéma théorique que ce soit sur les surfaces planes ou nanostructurées. La fonctionnalisation peptidique apparaît homogène sur les cinq régions analysées sur un même matériau. De plus, aucune différence significative dans la chimie de surface n'a pas été observée entre les échantillons, même avec différentes topographies.

Des MSC ont été cultivées pendant deux semaines dans un milieu basal indépendamment du test biologique à réaliser (immunofluorescence ou RT-qPCR). Des échantillons plats ou nanostructurés ont été testés soit juste après la fabrication, soit après leur fonctionnalisation avec un peptide mimétique de RGD et / ou de BMP-2 afin de déterminer quelle était la meilleure surface bioactive pour la promotion de la différenciation ostéogénique des MSC.

Les résultats obtenus par immunofluorescence et RT-qPCR ont démontré que les nanopiliers longs, de grand diamètre et espacement réduit, non-fonctionnalisés semblaient être la meilleure surface pour favoriser la différenciation des MSC vers le lignage ostéoblastique. En comparant l'expression des différents marqueurs (par immunofluorescence et par RT-qPCR) des cellules cultivées sur ces matrices non-fonctionnalisées et fonctionnalisées (RGD et/ou BMP-2), il apparait des niveaux d'expression des marqueurs ostéoblastiques plus élevés das le case des matériaux fonctionnalisés.

Le greffage d'un seul peptide (RGD ou BMP-2) sur les surfaces planes ou nano-

structurées n'a pas contribué à favoriser la différenciation cellulaire ; au contraire, l'expression des marqueurs a été réduite sur les surfaces fonctionnalisées avec les peptides RGD ou BMP-2 comparativement aus surfaces vierges. Quand les deux peptides ont été greffés simultanément, l'expression des marqueurs de différentiation sélectionnés a augmentée (en comparaison avec le greffage d'un peptide) et est restée constante sur toutes les topographies étudiées. Cette expression est similaire à l'expression observée pour les cellules cultivées sur les nanopiliers de grands diamètre et hauteur mais avec un espacement réduit (sans aucune fonctionnalisation.

Aucun effet synergique entre les modifications de chimie de surface et de la topographie n'a pas été observé concernant la différenciation cellulaire après deux semaines de culture. Au lieu de cela, nous avons observé que les nanopiliers ou la biofonctionnalisation de la surface (avec la combinaison d'un peptide adhésif et un peptide mimétique favorisant la différentiation en ostéoblastes) ont été capables d'induire la différenciation des MSC au même niveau. Un tel résultat indique que les deux approches peuvent être efficaces pour la modulation du comportement cellulaire. Ces conclusions peuvent être intéressantes pour le développement de nouveaux biomatériaux ou surfaces modèles où les deux types de stimuli ne peuvent pas être appliqués simultanément, car des signaux physiques ou chimiques peuvent être utilisés de manière indépendante pour promouvoir la différenciation des MSC vers un lignage spécifique.

Acknowledgments

There are so many people to whom I am grateful to for their encouragement during all the steps that brought me here. I am sure I will not be able to thank you all enough in this short section, but believe me, it would have been impossible to reach this moment without you.

First of all, I would like to thank my supervisors, Marie-Christine Durrieu and Sivashankar Krishnamoorthy, who had the idea of creating a highly multidisciplinary and appealing project, for their guidance, teaching (there were so many subjects that I had to learn), and support throughout these three overwhelming years. Thank you Marie for being always so positive, so patient, and so supportive even when everything seems like falling apart. Thank you Siva for all your support, and for sharing your knowledge and points of view with me.

Since this was a co-tutelle thesis, I had the opportunity of joining two institutes, but I had to go through various bureaucratic processes. For their help in managing this collaboration, I am specially grateful to Audrey Sidobre, Christopher Nielsen and Audrey Chancel from the University of Bordeaux, and Corinne Lavorel, Sabrina Morais and Alexis De Col from LIST.

At LIST, I must acknowledge all NEMC group for their kindness in welcoming me and for their guidance during the time we shared. Likewise, I am sincerely grateful to my colleagues in MRT with whom I had the honor to work with. Thank you Bianca-Rita and Stéphanie (I wish one day I could be an amazing person as you are!), Kevin (I am sorry for the infinite times I asked for your help, and for have written all the RIE's logbook), Didier (thank you for all the help, patience and friendship), Patrick (thanks for all the patience, and for all the talks about Bordeaux and Médoc), Petru (a.k.a. God of the Cleanroom), Noureddine (ALD and cleanroom boss), Guillaume (who helped me solving 1000 different issues in the lab), all MRT support team,... Thank you Olga (for allowing me to learn so much with you), Hameeda (my super friend), Kamal and Sergey (my coffee break mentors), and all my colleagues from

F1.14 (not forgetting king Hubert).

Abbreviations and Acronyms

AFM Atomic Force Microscopy

ALD Atomic Layer Deposition

ALP Alkaline Phosphatase

αMEM Alpha Modified Eagle Medium

APTES 3-aminopropyltriethoxysilane

BCP Block Copolymer

BMP Bone Morphogenetic Protein

BMP-2 Bone Morphogenetic Protein 2

BSA Bovine Serum Albumin

CAD Computer-aided Design

CAM Cell Adhesion Molecule

cDNA Complementary Deoxyribonucleic Acid

CMP Chemical Mechanical Polishing

Col1A1 Type I Collagen

Col1A2 Type II Collagen

CV Coefficient of Variation

DAPI 4',6-diamidino-2-phenylindole

DMF Dimethylformamide

DNA Deoxyribonucleic Acid

EBL Electron Beam Lithography

ECM Extracellular Matrix

FA Focal Adhesion

FBS Fetal Bovine Serum

GF Growth Factor

hMSC Human Mesenchymal Stem Cell

HSC Hematopoietic Stem Cell

ICAM Intercellular Adhesion Molecule

IPS Intermediate Polymer Stamp ®

iPS Induced Pluripotent Stem Cell

MSC Mesenchymal Stem Cell

$\boldsymbol{M_w}$ Molecular Weight

NP Nanoparticle

NIL Nanoimprint Lithography

OCN Osteocalcin

OPN Osteopontin

PBS Phosphate Buffered Saline

PCL Polycaprolactone

PDI Polydispersity Index

PET Polyethylene terephthalate

PFA Paraformaldehyde

PPIA Peptidylprolyl isomerase A

PS Polystyrene

PS-b-P2VP Polystyrene-block-poly(2-vinylpyridine)

PVD Physical Vapor Deposition

P2VP Poly(2-vinylpyridine)

RT-qPCR Quantitative Real Time Polymerase Chain Reaction

RIE Reactive Ion Etching

RNA Ribonucleic Acid

RT Room Temperature

Runx2 Runt-related Transcription Factor 2

SEM Scanning Electron Microscopy

SMP 3-(Maleimido)propionic acid N-hydroxysuccinimide ester

TCP Tissue Culture Plastic

$\boldsymbol{T_g}$ Glass Transition Temperature

TGFβ Transforming Growth Factor Beta

UV Ultraviolet

VCAM Vascular Cellular Adhesion Molecule

XPS X-ray Photoelectron Spectroscopy

Contents

List of Figures

List of Tables

1 | Introduction

The main considerations and objectives behind this project are introduced in this chapter. The basic theoretical concepts and previous works on the subject report in the literature are analyzed. Finally, the main nanofabrication approaches allowing the creation of nanostructure arrays for cell studies are summarized.

1.1   Problems and Objectives

The interaction of a material with biological tissues is known to impact the initial protein adsorption on its surface, and the subsequent cell response, namely its adhesion, proliferation or death [25, 26]. The cell-material interface can therefore be seen as a complex system comprising three main players: material properties, molecules on the material surface, and adherent cells. The understanding of this interplay at the length scales of cells (microscale) or even molecules (nanoscale) is of extreme interest for the improvement of implants used in dentistry or orthopedics, for the improvement of the properties of other biomaterials for tissue engineering applications, and for the understanding of the *in vivo* cell microenvironment [3]. Multiple cell types (including mouse Mesenchymal Stem Cells (MSCs), osteoblasts, cancer cells) have been extensively utilized for investigation of cell-substrate interactions. Nevertheless, it is important to keep in mind that the same material cue can induce a distinct response in two different cell types.

Human Mesenchymal Stem Cells (hMSCs) appear as promising candidates for cell-substrate interaction studies for bone tissue engineering applications, as they can be harvested from adult tissues, they can be easily cultured *in vitro*, and they have the ability to proliferate and to differentiate into various lineages, including the osteoblastic lineage [4]. These stem cells can be isolated from different tissues, including bone marrow, adipose tissue, and dental tissues, which potentiates their use in cell therapies

from the patient own cells (autologous cells), avoiding the risk of immune reactions, often associated with utilization of cells from a different donor [5, 6].

As referred, nanotopography with length scales of the order of Extracellular Matrix (ECM) elements offers the possibility of regulating cell behavior. Nonetheless, the investigation of the impact of nanotopography on cell response has been limited by inability to precisely control geometries, especially at high spatial resolutions, and across practically large areas. Moreover, biofunctionalization of biomaterial surfaces can be also engineered in order to further improve cell response.

Therefore, the present study aimed at creating well-controlled and periodic nanopillar arrays of silicon with critical dimensions close to the dimensions of elements of ECM on full wafers, to ensure that the number of samples required for biological studies was achieved. The nanostructures were afterwards functionalized with peptides or combination of peptides known to improve cell adhesion and osteoblastic differentiation of hMSCs. The impact of these physical and chemical cues on hMSC adhesion and differentiation was evaluated *via* the investigation of expression of proteins and genes related with such cell behaviors.

1.2 State of Art

1.2.1 Biomaterials and bone tissue engineering

The concept of biomaterials has been developed and expanded since its first definition in 1980s as non viable materials used in a medical device intended to interact with biological systems [27]. Nowadays, since it is well understood that the cells are able to interact and sense changes (of chemistry, topography or stiffness) on a material surface down to nanometer scale, a biomaterial can now have a broader definition as an engineered material that can be used alone or as a part of a complex system to regulate processes of living systems in order to control the course of any therapeutic or diagnostic procedure for medical purposes (in humans or veterinary) [1]. Biomaterials field is expected to have a continuous development, considering the aging population, the increasing standard of living in developing countries, and the growing ability to address previously untreatable medical conditions [28].

According to Rabkin and Schoen, the development of biomaterials and biomaterial

science can be divided in three main periods/generations, each one with distinct objectives [29]. Biomaterials used in the 1950s, which are described as first generation of biomaterials, were selected according to their physical properties – that should match the ones of the replaced tissue – and their bioinertness, since they should elicit the minimum possible host reaction, hence being biocompatible. Later, with improvements in technology areas, a second generation of biomaterials could be developed, aiming at creating a controlled response of the tissues into which the biomaterial had been implanted. Such bioactive biomaterials included resorbable materials, or materials able to release a drug in a controlled-localized way, for instance [28].

With respect to bone tissue, a biomaterial must meet a few basic requirements, namely biocompatibility, nontoxicity, corrosion resistance, durability, strength and ductility, and a low elasticity modulus (moduli of the biomaterials most commonly used in bone replacement are summarized in Table 1.1) [30]. Biocompatibility is an essential property of any biomaterial, since it must interact with the living systems and perform its function without causing immune responses or foreign body reactions [28]. According to the definition of Williams (2008), biocompatibility refers to the 'ability of a biomaterial to perform its desired function with respect to a medical therapy, without eliciting any undesirable local or systemic effects in the recipient or beneficiary of that therapy, but generating the most appropriate beneficial cellular or tissue response in that specific situation, and optimizing the clinically relevant performance of that therapy' [31]. In the same way, it is required that no ions or other harmful sub-products are released by a material, to impede any possibilities of allergy, inflammation, or necrosis, for instance. Alongside with nontoxicity, a biomaterial used in an implant in orthopedics must have a high corrosion resistance, to have a longer life in the host's body. Moreover, failures of an implant can be more likely avoided if the material has a high durability, that is, high fatigue strength, which is directly related with its resistance to corrosion and to releasing particles. Finally, the materials used in bone replacement should have a lower Young's modulus than the materials currently used in such applications, as they have elastic moduli 5 to 10 times higher than bone. This difference is often a cause of stress shielding, *i.e.* the implant bears more load than the surrounding bone which leads to the death of bone cells over time [28]. Table 1.1 summarizes the main properties of commonly used materials in bone implants.

Table 1.1 – Properties of examples of metal biomaterials. Comparison with cortical bone. [30]

Material	Density / g.cm⁻³	Young's modulus / GPa
Stainless steel	8.0	200
CoCr alloys	8.5	210-250
Ti-6Al-4V	4.4	90-115
Cortical bone	2.0	7-30

1.2.2 Stem cells

Regenerative medicine and tissue engineering rely on the utilization of stem cells since they have two unique and advantageous properties: self-renewal and potency (Figure 1.1). Stem cells are able to proliferate maintaining their undifferentiated char-
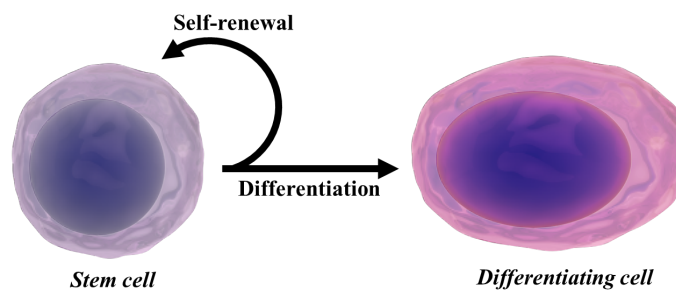
Figure 1.1 – Schematic representation of the capacities of stem cells to self-renewing and to differentiate into a more committed cell.

acteristics, and consequently maintaining a stem cell population. Moreover, they have the ability to differentiate into a more specialized cell type [32]. According to their differentiation capacity, stem cells can be divided into two main categories (Figure 1.2): pluripotent, if they are able to differentiate into cells of the three germ layers (endoderm, mesoderm, and exoderm), or multipotent, if they can differentiate only into cells of a specific germ layer.

Adult stem cells are normally defined as multipotent stem cells, even if in particular cases some of them may have the capacity to transdifferentiate into a cell type from other germ layer (*e.g.* differentiation of hMSCs into neurons). Examples of pluripotent stem cells are embryonic stem cells and Induced Pluripotent Stem Cells (iPSs). Embryonic stem cells are collected from the inner mass of the blastocyst from an embryo, which gives rise to a number of ethical factors concerning the use of human embryos

for research [33]. Alternatively, pluripotent cells can be created via the reprogramming of somatic cells into iPS with the help of key transcription factors (Figure 1.3).
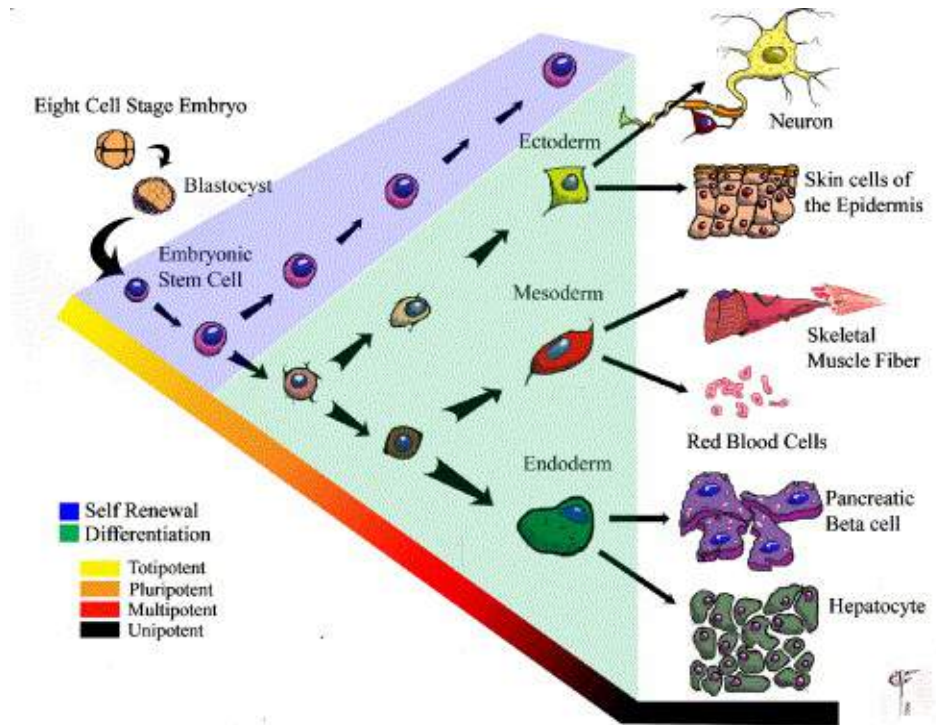
Figure 1.2 – Stem cell hierarchy. Progression of stem cells during development, highlighting their ability to self-renew or to differentiate into a more compromised state [34].
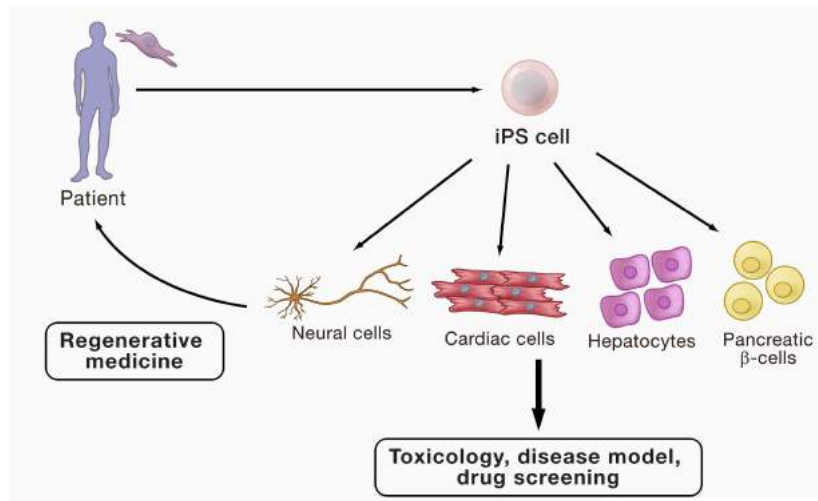
Figure 1.3 – iPS cell technology. Somatic cells from a patient can be reprogrammed, generating pluripotent cells. These cells can be differentiated into specialized cells and be applied in regenerative medicine, or in the development of disease models, for instance [35].

Such cells were first described for humans in 2007 (findings had been previously shown for mice) by the team of Yamanaka [36]. The generation of human iPS opened up the potential for the creation of autologous cells in sufficient number for applications in

regenerative medicine. Nevertheless, a few shortcomings still need to be overcome. For instance, there is no screening method to ensure that cells were fully reprogrammed. If cells are not correctly reprogrammed, they may not exhibit all the properties of stem cells, and there can be an increased risk of teratoma formation due to aberrant reprogramming [35].

1.2.2.A   Mesenchymal stem cells

In 1990s, MSCs were described as progenitor cells from bone marrow, which are able to proliferate almost indefinitely and to give rise to skeletal tissues, namely bone, and cartilage [37]. More recently, it was understood that these stem cells exist in other tissues besides the bone marrow, including adipose tissue, and that they actually have the ability to differentiate or trans-differentiate in numerous cell types from all germ lines, as represented in Figure 1.4 [38].
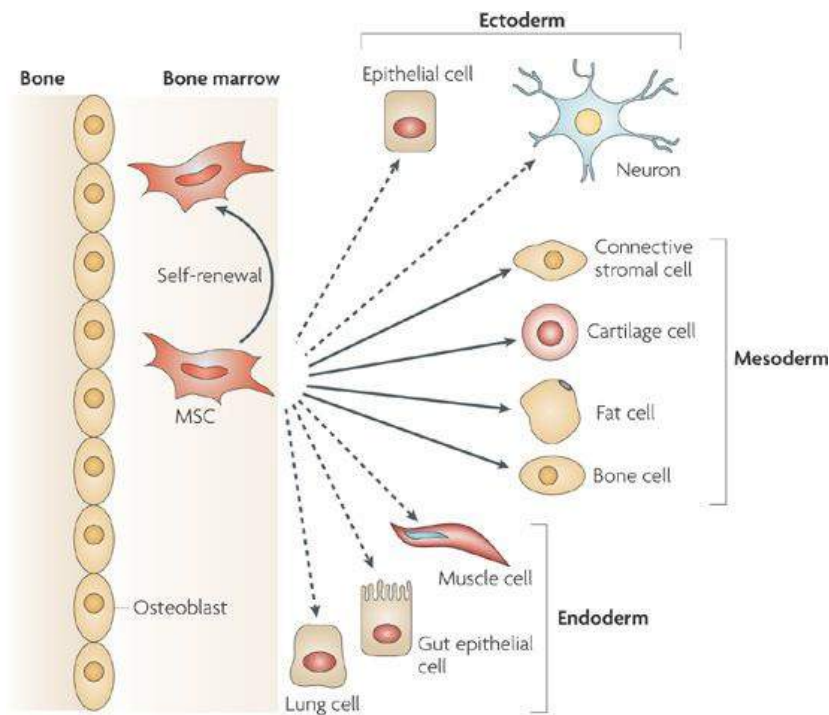
Figure 1.4 – MSC differentiation. Bone marrow MSCs have the capacity to self-renew and to differentiate into cells of mesoderm. It has also been reported that these stem cells may transdifferentiate across the other germ lines during *in vitro* culture. [38].

Although the fraction of MSCs in the body is rather low (between $1:10^4$ cells in a new-born and $1:10^6$ cells in an 80 year old person), their use in tissue engineering is preferred over other stem cell type, as iPS [39]. MSCs are advantageous for tissue engineering and cell therapy applications mainly due to their simple harvesting process

and *in vitro* culture, the potential to use patient-derived cells, which eliminates the risk of immune reactions, their immunomodulatory effect, and the reduced ethical constraints related with their utilization [38, 40].

1.2.3 Bone tissue

Bone is a mineralized connective tissue that constitutes the skeleton, together with the cartilage. It works closely together with the bone marrow almost as a single entity, ensuring the interactions between different types of cells which are critical for the equilibrium of hematopoiesis and the maintenance of skeletal health [41]. Bone is organized in a hierarchical way (Figure 1.5) and it comprises structures whose dimensions range from mili- to nanometer scale. Bone tissue can be either very dense, denominated cortical bone, or more cancellous, being called trabecular bone [42].
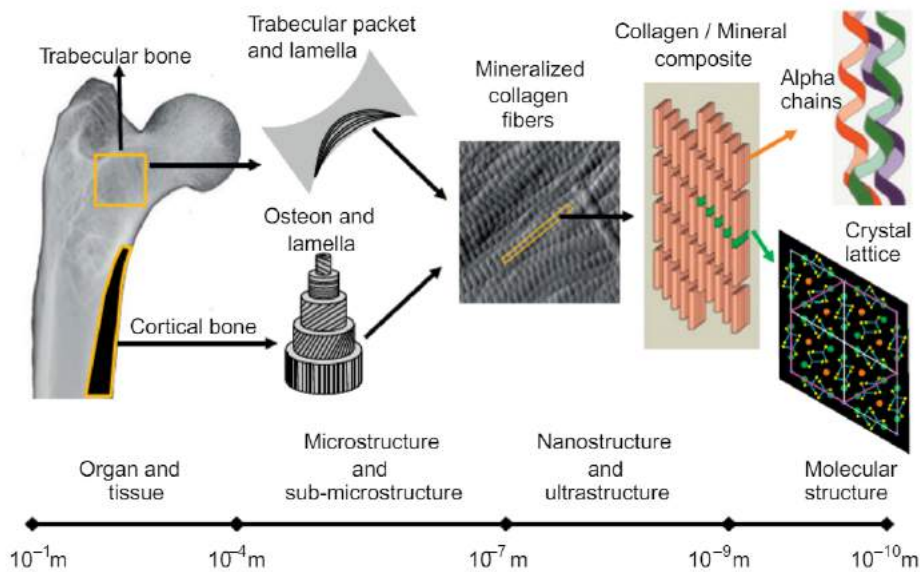
Figure 1.5 – Hierarchical organization of bone. Representation of bone organization from macro- to nanoscale levels [42].

Bone is composed mainly by a mineral phase (mostly carbonated apatite) corresponding to approximately 65 % of its weight, an organic matrix (mainly type I collagen), and around 10 % of water [42]. Collagen is the main responsible for bone viscoelasticity and structure organization. Other types of collagen together with a large number of non-collagenous proteins, as Osteocalcin (OCN), Osteopontin (OPN), bone sialoprotein, proteoglycans, glycoproteins, constitute a rather smaller fraction of the organic matrix. Non-collagenous proteins play a vital role on the regulation and

maintenance of bone's ECM [43].

Four main cell types constitute bone: osteoblasts, osteocytes, osteoclasts, and bone lining cells. These cells are responsible for the maintenance of the equilibrium between bone formation and resorption (Figure 1.6), complex processes relying on cell-cell communications for the preservation of skeletal integrity.
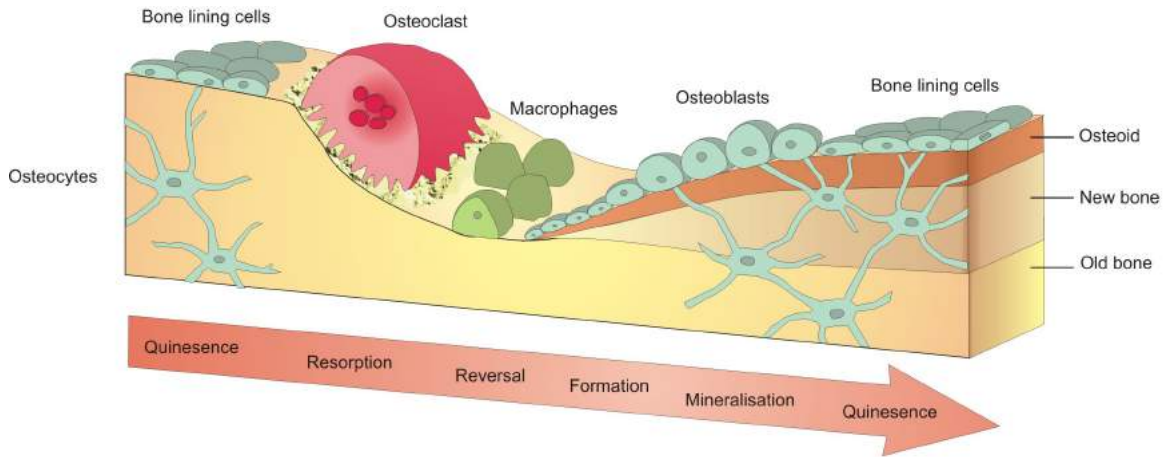
Figure 1.6 – Schematic representation of bone remodeling process. [44]

Perturbation of such communications is known to be related with abnormal bone density, leading to bone diseases as osteoporosis (characterized by loss of bone mass and structural deterioration of bone tissue) or osteopetrosis (when bone formation occurs faster than bone resorption, leading to very dense, but brittle bones)[45].

Bone cells originate from two types of stem cells: hematopoietic stem cells, in the case of osteoclasts, and mesenchymal stem cells, in the case of osteoblasts, osteocytes, and bone lining cells. Osteoclasts are large multinucleated cells (with four to twenty nuclei) derived from hematopoietic precursors of the monocyte-macrophage lineage that are found on bone surfaces. These cells are responsible for bone resorption, process that comprises two main steps: dissolution of hydroxyapatite crystals, and subsequent digestion of the organic compounds of bone matrix. In parallel, osteoclasts release factors limiting their own activity, and promoting osteoblast function. Osteoblasts derive from the differentiation of MSCs into osteoprogenitor cells which then differentiate into osteoblasts. These cells can later differentiate into osteocytes. The process of differentiation of bone marrow MSCs into the osteoblastic lineage is summarized in Figure 1.7.

Osteoblasts are responsible for the production of new bone, as they synthesize and secrete new collagen matrix and calcium salts in the growing portions of the bone.
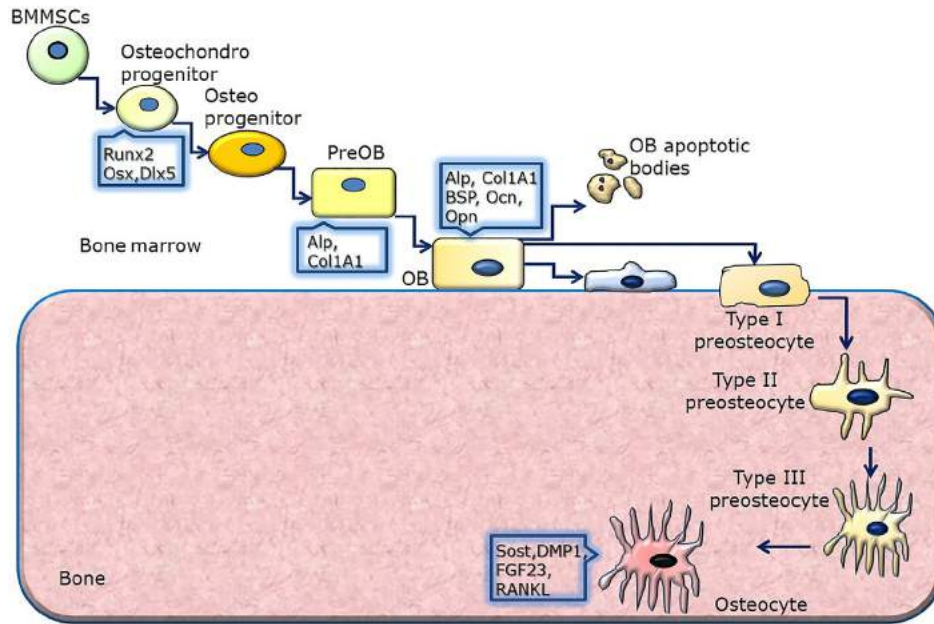
Figure 1.7 – Schematic representation of differentiation steps of bone marrow MSCs into osteoblasts and osteocytes. [46]

Osteoblasts express various osteogenic factors, namely Alkaline Phosphatase (ALP), OPN, OCN, and bone sialoprotein, known to be involved in the formation of the organic bone matrix (osteoid). As osteoblasts get surrounded by their secreted matrix which gets calcified and entraps them, these cells differentiate into mature osteocytes (most common type of bone cell) [41, 46]. Also, during bone formation, MSCs close to the growing bone tissue form a layer of undifferentiated cells forming the periosteum, which will be a reservoir for bone forming cells for later bone maintenance [47]. Bone lining cells derive from osteoblasts that are no longer synthesizing matrix, and become flattened, covering the inactive bone surface, and becoming bone lining cells [42].

1.2.4 Cell-substrate interactions

The control of the properties of biomaterials can be a powerful tool for the modeling of cell-ECM interactions. Furthermore, engineering of surface chemistry, topography or physical properties of a material at nanoscale has been reported to influence cell behavior, namely in the case of MSC (Figure 1.8)[16, 48, 49]. The investigation of cell-substrate interfaces at nanoscale can provide important insights on aspects of cell interactions with their *in vivo* microenvironment (*e.g.* different components of ECM), as well as ideas for the development of better scaffolds for bone tissue engineering or model systems for disease studies, for instance.
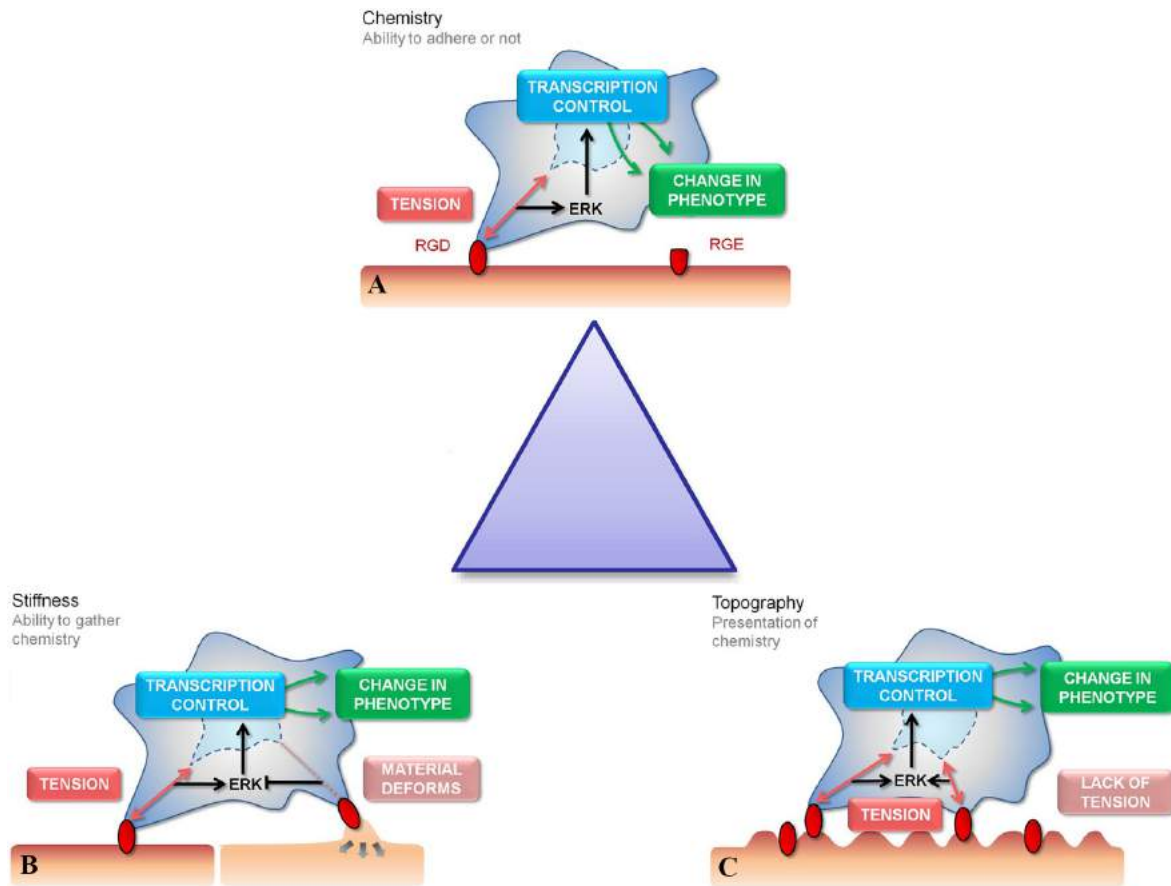
Figure 1.8 – Schematic representation of the control of cell response due to modifications of material chemistry(A), stiffness (B), and topography (C). Cells extend filopodia to 'find' adhesion ligands (in red). Binding of the cell through focal adhesions to ligands creates tension and activates signaling. Chemical functionality can be used to fabricate areas of high adhesion (red) or low adhesion for the cells to respond to. Stiffness will affect the cells ability to produce tension through focal adhesions formation. Topography will present the adhesion ligands to the cells in either a favorable or unfavorable manner, again affecting adhesion and subsequent tension and signaling. [50]

1.2.4.A   Biochemical surface modification

Surface modification processes that can add specific biological functions on the surface of a material, without impacting their bulk properties, can be called biofunctionalization methods, as they are able to turn a bioinert material into a bioactive cell-instructive one (Figure 1.9). These bioactive biomaterials can be engineered in such way that they are able to accurately reproduce the signaling microenvironment required for a cell response of interest, namely for bone development [49]. Alternatively, as the surface chemistry can be fine-tuned, it can be possible to investigate the impact of specific ECM components on cell behavior (Figure 1.10) [49].
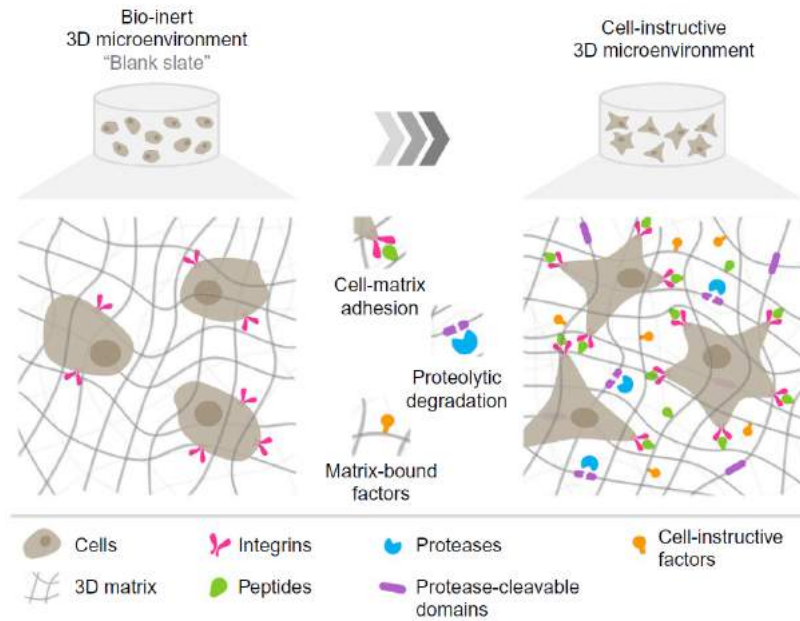
Figure 1.9 – Schematic representation of possible functionalization of hydrogels. Various bioactive molecules can be used in surface modification to create biomimetic cell instructive matrices [51].
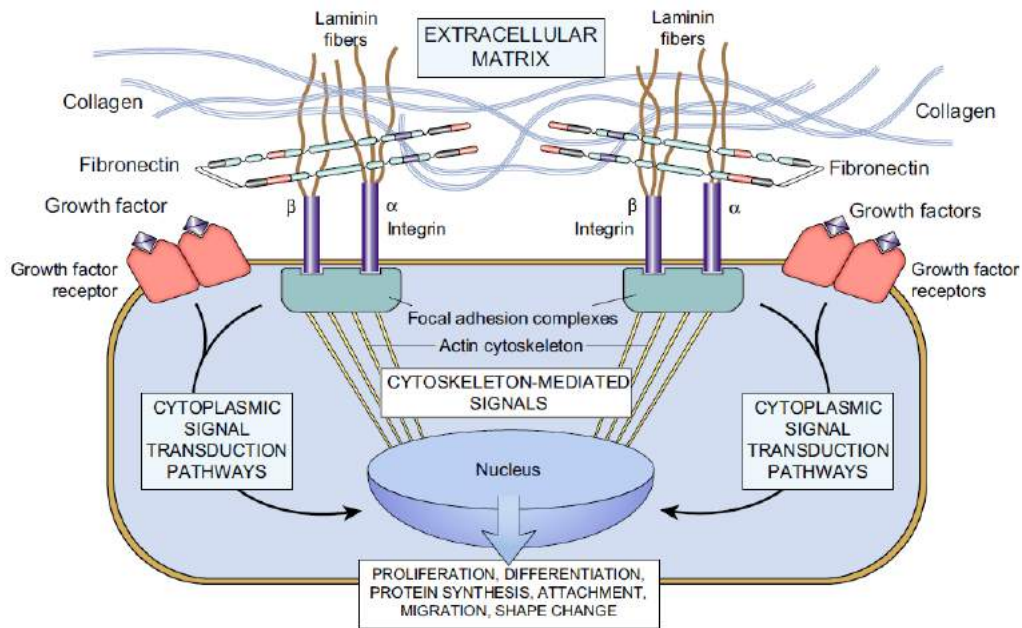
Figure 1.10 – Schematic representation of cell-ECM interactions. The interactions between cells and their surrounding ECM activate specific signaling pathways which can influence cell behaviour, namely their proliferation, differentiation, or protein synthesis.[28]

Nevertheless, it is essential to keep in mind that the ECM is a complex microenvironment comprising soluble (*e.g.* Growth Factors (GFs)) and non-soluble molecules. In addition, surface biofunctionalization is often advantageous over soluble presentation of biomolecules from the ECM (Figure 1.11), as it can enhance their biological

function due to a better mimicking of the *in vivo* microenvironment (given that most molecules are normally tethered to the ECM).
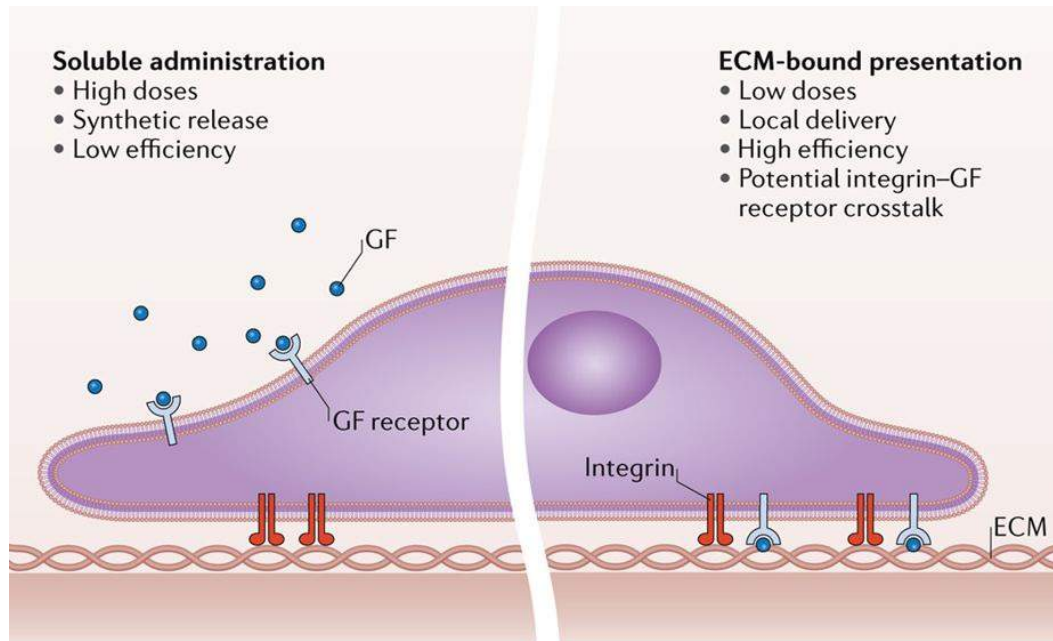
Figure 1.11 − Schematic representation of soluble and matrix-bound delivery of GF [16].

Moreover, this approach allows the possibility of a local delivery of biomolecules, in a controlled dose (much lower than the dose necessary for the delivery of such factors in solution), as well as it facilitates eventual crosstalking between integrins and GF receptors. [16].

Tailoring of surface chemistry is more often related with the covalent binding or adsorption of bioactive molecules onto the material, but the introduction of specific moieties has also been investigated as a possible tool for the control of cell response. It has been seen that hMSC differentiation can be controlled if chemical groups such as -OH, -CH$_3$, -COOH, or -NH$_2$ are created on the material surface [52]. These groups add specific surface properties to the materials, namely hydrophilicity (-OH), hydrophobicity (-CH$_3$), or positive (-NH$_2$) or negative (-COOH) charge at physiological pH, and are able to impact initial cell adhesion [53]. Phillips *et al.* reported that osteogenic differentiation was predominantly observed on surfaces modified with amine groups (positively-charged surfaces), when hMSCs were cultured for twelve days in osteogenic differentiation medium (Figure 1.12) [52]. Mineralized nodules were observed only on NH$_2$-functionalized surfaces (Figure 1.12a). Alizarin red staining was performed for investigation of matrix mineralization. The authors observed, in agreement with
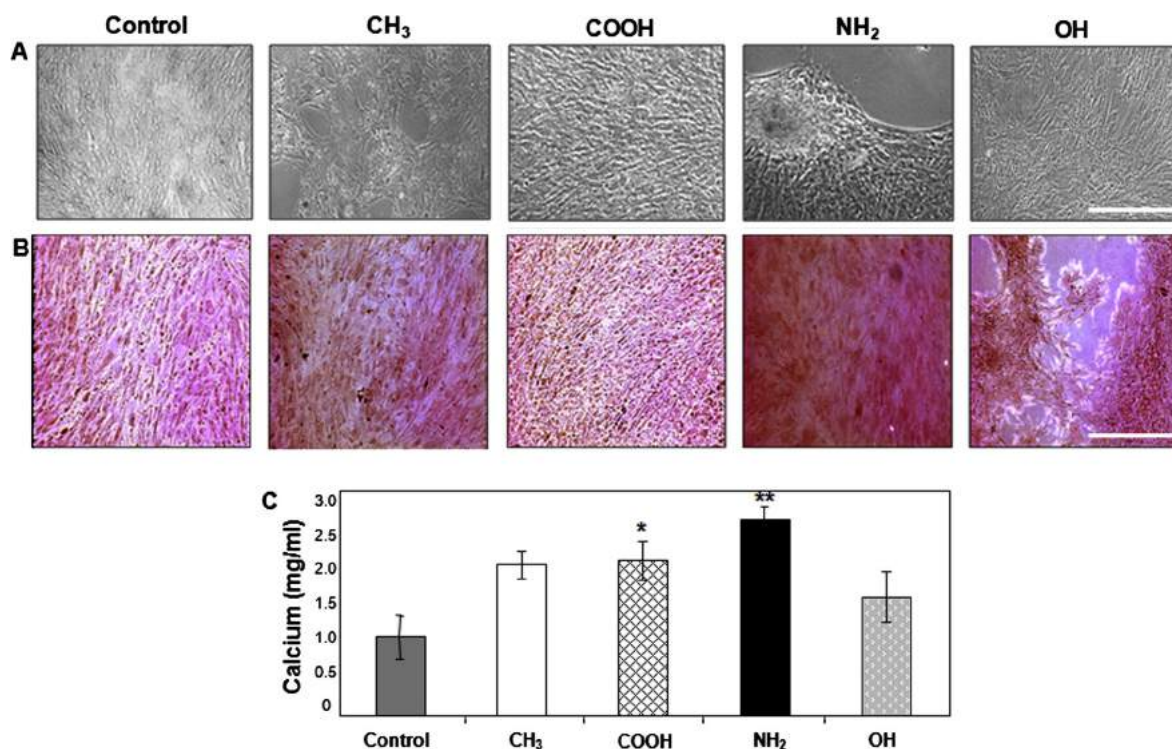
Figure 1.12 – Osteogenic differentiation of hMSCs on chemically modified surfaces. (A) Phase-contrast micrographs of cells after 12 days in culture. Scale bar 100 µm. (B) Alizarin red staining for investigation of matrix mineralization. Scale bar 50 µm. (C) Calcium content after 10 days in culture. ANOVA, $p < 0.05$, * vs. control, ** vs. control and OH). [52]

phase contrast images, enhanced intensity on amine-modified surfaces compared with all other conditions, indicating higher calcium content on this surface (Figure 1.12b and 1.12c).

Although the introduction of chemical moieties can be an interesting method of surface modification of a material, functionalization with proteins (usually from the ECM) or mimetic peptides representing specific sequences of such proteins appears to be a more congruous approach (idea which is supported by the much higher number of published studies of surface modification using peptides or proteins). The use of bioactive molecules for surface functionalization is a more robust method to mimic the *in vivo* ECM, therefore conveying stronger cues for the modulation of cell behavior [17]. Biofunctionalization of bone implant surfaces with peptide sequences from ECM proteins (*e.g.* fibronectin) has been investigated extensively (a list of some of such studies is presented in Table 1.2), and their action in improvement of cell adhesion and implant integration has been demonstrated.

13

Table 1.2 – Peptides derived from ECM proteins and growth factors known to have an impact on hMSC behavior.

Peptide sequence	Source	Function	Ref.
RGD	Fibronectin, Vitronectin, Collagen I	Cell adhesion	[54, 55]
PHSRN	Fibronectin	Cell adhesion	[56, 57]
GFOGER	Collagen I	Cell adhesion	[58, 59]
P15	Collagen I	Cell adhesion	[58]
DGEA	Collagen I	Cell adhesion	[58]
KRSR	Fibronectin, vitronectin (heparin binding domain)	Cell adhesion	[60]
FHRRIKA	Fibronectin, vitronectin (heparin binding domain)	Cell adhesion	[60]
KRIPKASSVPTELSAISTLYL	BMP-2	hMSCs osteogenic differentiation	[19, 21]

Being highly complex molecules, proteins can offer a plethora of signals to cells, alongside with multiple binding sites (for integrin, heparin, or GF binding) showing great affinity towards specific receptors [61]. Nonetheless, the use of full ECM proteins in such applications is not straightforward, due to their poor stability, safety concerns, difficult handling and complexity in production in large quantities [17]. Since most proteins are still produced by recombinant methods in living organisms, chemically defined products are not always obtained, which results in batch-to-batch variations, and different biological activity of these molecules. Furthermore, contaminants main remain after protein purification, which contributes to the possibility of infection or immunogenicity. Additionally, long-term stability of proteins cannot be always ensured since they can be enzymatically degraded, and are very sensitive to changes of pH and temperature, as well as to solvents [62]. Finally, biofunctionalization of large areas demand large quantities of molecules, which, in the case of full-length proteins, may be very costly, considering the necessary steps of extraction and purification. Other extremely demanding step is the control of conformation when binding to the surface, i.e. the control of available motifs for receptor binding is not possible which can hamper the biofunctionality of the bound proteins [63].

Such drawbacks may be circumvented using short synthetic peptides containing only the amino acid sequence necessary to support a given biological response, like cell adhesion (e.g. RGD peptide). ECM-derived peptides present several advantages over full-length proteins as ligands for surface functionalization. First and foremost, production methods of synthetic peptides allow their production in large scale with high purity, at low costs; therefore, batch-to-batch variability is eliminated, and there is no risk of immune reactions [17]. Moreover, synthetic peptides have better stability to pH and temperature changes, to solvents, and can be modified to be resistant to enzymatic degradation [62]. Also, the grafting of a synthetic molecule onto the material may be controlled specifically (and at high densities) without loss of biological activity, through the introduction of specific anchoring units in the peptide sequence [17].

Despite being a good alternative to full-length proteins for surface functionaliza-tion, synthetic peptides still show some limitations, mainly related with their inability to reproduce the biological activity and receptor specificity of ECM proteins. Usu-ally this issue arises from the high flexibility of linear peptides, which, contrary to proteins, can exhibit several different conformations, thus being able to bind to struc-

turally related receptors, decreasing the expected biological response. Furthermore, synthetic peptides normally encompass only one functional site, whereas proteins are multifunctional, which grants them much higher biological activity, with the possibility of exerting multiple interactions given their complementary domains, when compared with synthesized molecules. Such synergies are often required to trigger specific cell responses, which may not be achievable using only one synthetic ligand [17].

Functionalization of a material requires the immobilization of the biomolecules of interest on its surface. Two main approaches can be followed for that end: adsorption or covalent immobilization (Figure 1.13). If the functionalized material is porous, then biomolecules can get entrapped within its pores. A brief comparison of the advantages of these three methods is presented in Table 1.3.
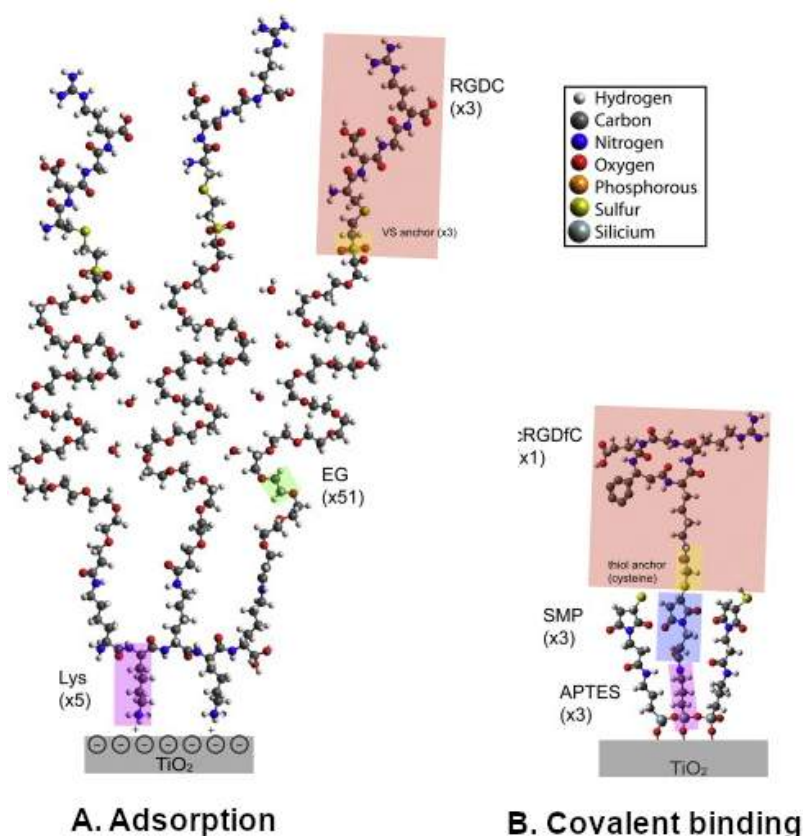
Figure 1.13 – Representation of immobilization of RGD on titania surfaces. (A) Poly-l-lysine-g-poly(ethylene glycol) layer adsorbed electrostatically onto a titania surface, followed by grafting of poly(ethylene glycol) side chains. RGDC peptide binds to the polymer brush by a double thiol binding (possible thanks to the cysteine). (B) Silanization of the TiO_2 by APTES and covalent attachment of a heterobifunctional maleimide crosslinker SMP followed by specific thiol tethering of the cysteine residue of a cyclic RGDfC peptide. (Adapted from [64])

Table 1.3 – Comparison of biomolecule immobilization methods (Adapted from [28]).

Method	Adsorption	Entrapment	Covalent Binding
Difficulty	Low	Moderate	High
Loading possible	Low	High	Depends on S/V
	(unless high S/V)		and site density
Leakage	High	Low to none	Low to none
Cost	Low	Moderate	High

S/V: surface/volume ratio.

Molecule adsorption can be achieved by dipping a material into the appropriate solution, being therefore a very fast and simple method. However, since it is based on weak interactions, as electrostatic interactions and van der Waals forces, changes in environmental conditions (*e.g.* pH) can cause a uncontrolled desorption of immobilized molecules [65]. On the other hand, covalent grafting of bioactive molecules ensures a stable immobilization of such molecules, which makes it a widely followed approach [18, 23, 66, 67]. Such strong and stable binding is advantageous when the biomolecules are able to interact with transmembrane cell receptors, like integrins. Nevertheless, if a controlled release of the molecules is necessary for their internalization by cells, an alternative method must be implemented due to the irreversible nature of covalent bonds [65].

With the aim of enhancing the biological performance of the simplest synthetic peptides, that is, linear peptides, several approaches have been investigated, including the grafting of a mixture of peptides, or the synthesis of cyclic peptides of peptidomimetics [18, 66, 68]. The co-immobilization of several synthetic peptides on a material is a simple strategy to increase a biological response or to add extra functions to a surface [17, 66]. For instance, it has been demonstrated that the concomitant grafting of RGD (Arg-Gly-Asp) and PHSRN (Pro-His-Ser-Arg-Asn) peptides has a synergistic effect on the improvement of osteoblast adhesion on titanium surfaces when compared with the biofunctionalization only with the RGD motif [56]. Similary, Bilem and colleagues showed that the co-immobilization of RGD and a Bone Morphogenetic Protein 2 (BMP-2) mimetic peptide enhances the osteogenic commitment of MSCs as compared

to BMP-2 modified surfaces [20, 23]. Alternatively, peptide structures comprising more than one peptide sequence have been shown to have greater efficiency on the modulation of cell response than the simple combination of peptides on the surface, as their disposition and spacing can be controlled. That could be achieved creating linear sequences with spacers between the different peptides, or branched structures, for example [69, 70]. Furthermore, increased stability against enzymatic degradation of peptides have been demonstrated by restraining their conformational freedom. Such restraint can be attained through the creation of cyclic peptides instead of linear [18, 68]. An alternative approach for the increase of stability and receptor selectivity is the use of peptidomimetics [2, 71]. These small protein-like molecules are synthetically designed to mimic natural peptides or proteins, and to bind to their receptors with similar affinity of the natural proteins from which they were derived. Hence, similar biological effects can be obtained using peptidomimetics [72]. The molecules can be designed not only to have a specific bioactivity, but also to have increased stability to enzymatic degradation, increased selectivity or potency [72].

Improvement of cell adhesion

In vivo, cell adhesion is mediated by Cell Adhesion Molecules (CAMs) located on cell surface. These proteins are involved in the binding of the cell with its surrounding ECM or with other cells (Figure 1.14).
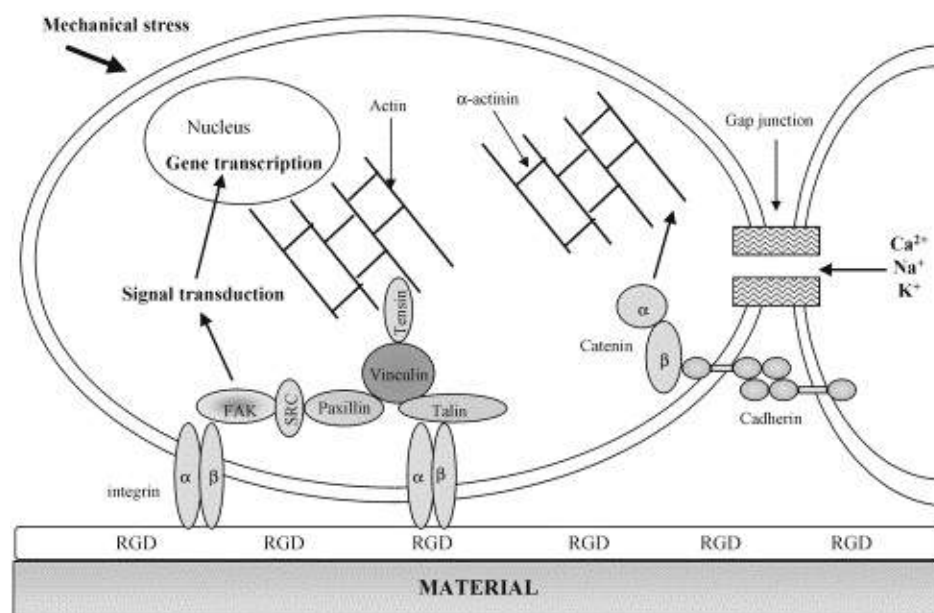
Figure 1.14 – Representation cell interactions with a material (via integrins) and other cells (via cadherins) [73].

Typically, CAMs are transmembrane receptors composed of three domains: an intracellular domain that interacts with the internal cell skeleton, a transmembranar spanning section, and an extracellular domain that interacts with the ECM or with other CAMs [74]. As previously referred, ECM proteins are large proteins with multiple binding sites for adhesion receptors, namely collagens, fibronectin, and elastin. The most important ECM adhesion receptors are integrins, though there are other receptor families, as syndecans [75]. Integrins are heterodimeric, transmembrane proteins comprising two subunits (α and β) [74]. Different combinations of α and β subunits grant the possibility of cell binding to one or more ECM ligands, as summarized in Table 1.4. Moreover, various ECM proteins can act as ligands for more than one integrin [63]. Integrins exist in two states: a resting state, in which the two subunits do not interact with the ECM, and an activated state in which the subunits are able to bind to ECM proteins (schematic representation in Figure 1.15).
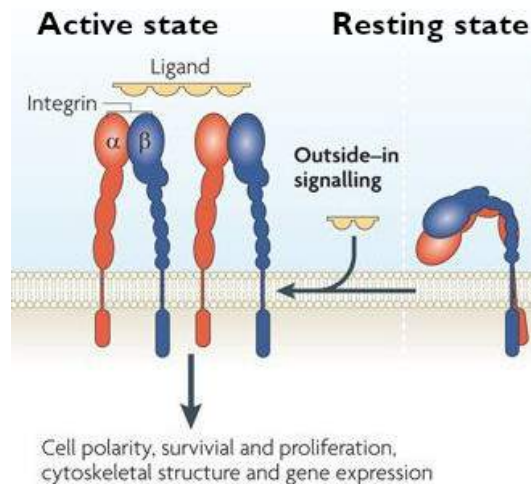
Figure 1.15 – Representation of integrin activation upon binding to a ligand (Adapted from [76]).

Once the binding occurs, intracellular protein aggregates, known as Focal Adhesions (FAs) (Figure 1.16), start to form. A series of proteins form a FA: talin and vinculin, actin-binding proteins are responsible for the linkage of the integrin receptor to the actin fiber, and α-actinin, an actin crosslinker [77].

Table 1.4 – Possible combinations of integrin subunits and their ligands (Adapted from [73, 78]).

Subunits		Ligands
β1	α1	Collagens, Laminins
	α2	Collagens, Laminins
	α3	Laminins, Fibronectin, Thrombospondin
	α4	Vitronectin, VCAM
	α5	Fibronectin
	α6	Laminins
	α7	Laminins
	α8	Fibronectin, Tenascin
	α9	Tenascin
	α10	Collagens
	α11	Collagens
	αv	Fibronectin, Vitronectin
β2	αL	ICAM
	αM	Fibrinogen, ICAM, iC3b
	αX	Fibrinogen, iC3b
	αD	VCAM, ICAM
β3	αIIb	Collagen, Fibronectin, Vitronectin, Fibrinogen, Thrombospondin
	αv	Fibronectin, Vitronectin, Fibrinogen, Thrombospondin
β4	α6	Laminins
β5	αv	Vitronectin
β6	αv	Fibronectin, Tenascin
β7	α4	Fibronectin, VCAM, MAdCAM
	αE	E-cadherin
β8	αv	Collagens, Laminins, Fibronectin

Vascular Cellular Adhesion Molecule (VCAM); Intercellular Adhesion Molecule (ICAM) .
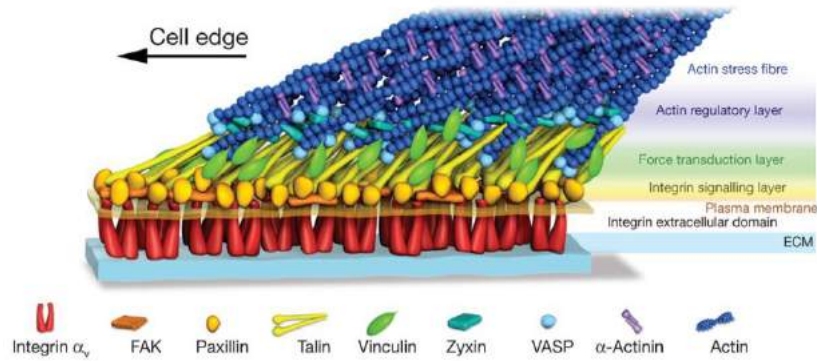
Figure 1.16 – Representation of nanoscale structure of a FA highlighting the integrin extracellular domain, integrin signaling layer, force transduction layer, actin regulatory layer and actin stress fiber (Adapted from [79]).

Since integrins are one of the most relevant messengers between cells and their surrounding ECM, functionalization of biomaterials with integrin-binding molecules (namely RGD) have been extensively reported in the literature for the investigation of modulation of cell behavior by biomaterials.

RGD (Arg-Gly-Asp), the major recognition sequence for integrins, is present in different ECM proteins, as fibronectin, collagen, laminin, pronectin and vitronectin [80]. Almost half of the known integrins are able to bind to ECM proteins due to the presence of RGD sequences, namely $\alpha 3\beta 1$, $\alpha 5\beta 1$, $\alpha 8\beta 1$, $\alpha IIb\beta 3$, $\alpha v\beta 1$, $\alpha v\beta 3$, $\alpha v\beta 5$, $\alpha v\beta 6$, $\alpha v\beta 8$, $\alpha 2\beta 1$, $\alpha 4\beta 1$ [63]. Therefore, this amino acid sequence is the most widely used in ligands for the promotion of cell adhesion, either alone, either as part of longer peptide sequences which may improve RGD effect [81]. As previously referred, several studies have shown that the combination of RGD and PHSRN peptides can have a synergistic effect, contributing to enhanced cell adhesion of MSCs and osteoblasts, when compared with the utlization of only RGD [57, 69, 70]. Conversely, the collagen-mimetic peptide GFOGER (Gly-Phe-Pyl-Gly-Arg) has also been reported as an effective motif for surface functionalization due to its capacity of improving not only cell adhesion but also osteoblastic differentiation of MSCs [58, 59]. Improvement of bone repair in critically-sized defects was observed in rat models after the implantation of Polycaprolactone (PCL) scaffolds coated with GFOGER, even after 4 weeks of treatment, without the need of implanted cells or GFs [59]. These results are summarized in Figure 1.17.

Other studies have also shown good prospects on the utilization of two heparin binding domains for amelioration of cell adhesion, especially with regard to osteoblasts:

KRSR (Lys-Arg-Ser-Arg) and FHRRIKA (Phe-His-Arg-Arg-Ile-Lys-Ala) (Figure 1.18) [60].
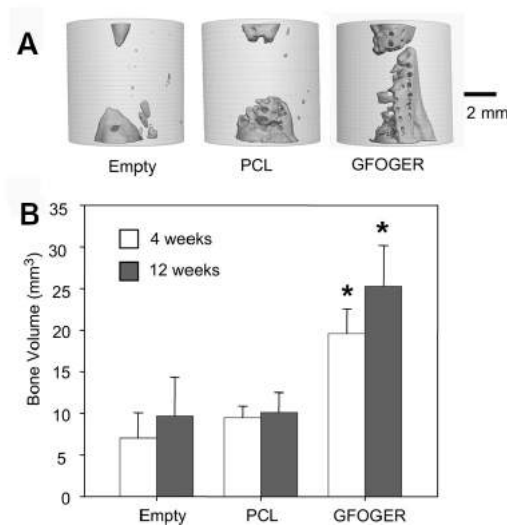
Figure 1.17 – GFOGER-coated scaffolds significantly enhance bone formation in critically-sized defects in rat models compared to uncoated PCL scaffolds and empty defect controls. (A) MicroCT shows enhanced bone formation in GFOGER-coated PCL at 12 weeks after implantation. (B) Likewise, bone volume is significantly greater in GFOGER-treated scaffolds at 4 and 12 weeks. * represents p-value < 0.05. (Adapted from [59])
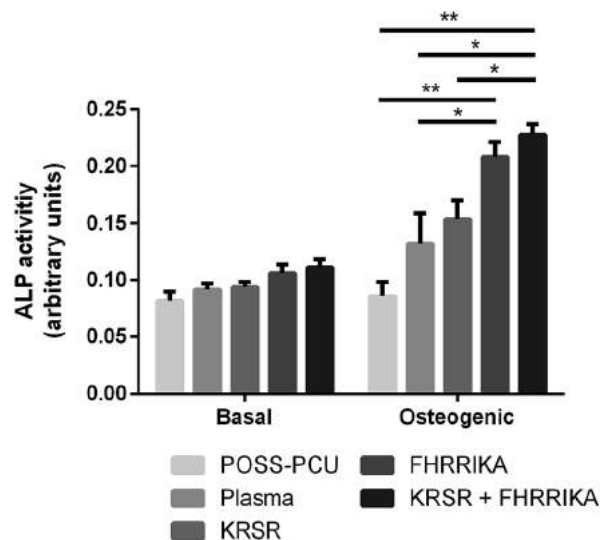
Figure 1.18 – ALP activity of rat MSCs on untreated, plasma treated, and functionalized substrates after 21 days of culture. * represents p-value < 0.05, and ** p < 0.01 [82]

.

The authors observed that materials functionalized with the two peptides significantly enhanced ALP activity of MSCs cultured in osteogenic medium. It was proposed that such increase in activity could be mainly related with the presence of the FHRRIKA peptide, known to improve bone mineralization, whereas KRSR has been

22

shown to improve cell adhesion[82]. Furthermore, targeting integrin and heparin signaling pathways simultaneously has been reported to further improve cell adhesion of osteoblasts when compared with the use of one of the peptides alone [60, 83, 84]. Yet, other studies reported that little or no cell response improvement is observed when functionalizing a surface with a combination of these peptides both *in vitro* as well as *in vivo* [85, 86]. Mas-Moruno (2018) advocated that different concentration and proportion of peptides used along with their spatial presentation may be factors responsible for such contradictory results reported in literature [17].

Promotion of osteoblastic differentiation of hMSCs

In addition to the peptides and peptide combinations already presented in the previous section (*e.g.* GFOGER, FHRRIKA), improvement of osteoblastic differentiation of MSCs through surface functionalization with Bone Morphogenetic Proteins (BMPs) (in particular BMP-2) or their mimetic peptides has been the main strategy reported in literature. BMPs constitute a group of proteins of the Transforming Growth Factor Beta (TGFβ) family, known for their ability to regulate cell proliferation and differentiation [87]. TGFβ acts in synergy with Runt-related Transcription Factor 2 (Runx2) to promote osteoblastic differentiation of MSCs [88]. BMPs regulate a large set of processes including skeletal formation, hematopoiesis, neurogenesis, or cell differentiation during embryonic development [89]. From this group, BMP-2 is the most powerful GF for the induction of bone formation, being even approved for use in clinic for bone therapy, along with BMP-7 [90].

Zouani *et al.* (2010, 2013) showed that Polyethylene terephthalate (PET) substrates functionalized with a BMP-2 mimetic peptide (KIPKACCVPTELSAISMLYL) were able to significantly enhance osteoblast precursor differentiation when compared with the control substrate, or with BMP-2 in solution (Figure 1.19) [21, 22].

Since no differentiation was observed on cells cultured in growth medium with BMP-2 mimetic peptide in solution, the authors suggested that binding of BMP-2 to the matrix is essential for induction of osteoblastic differentiation [22]. Following a similar *rationale*, Bilem *et al.* (2016) reported enhanced osteoblastic differentiation of hMSCs on glass functionalized with a BMP-2 peptidomimetics (Figure 1.20) [20]. Moreover, the authors observed a synergistic effect of the combination of RGD peptide with the BMP-2 mimetic peptide, as represented in Figure 1.20.
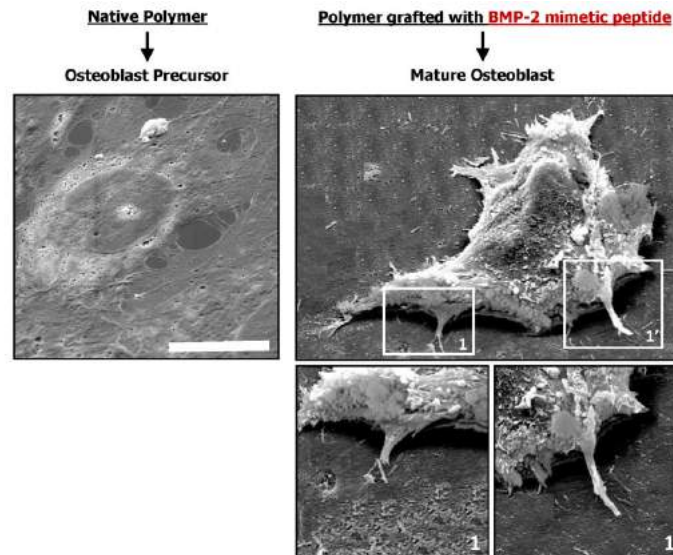
Figure 1.19 – Osteoblast precursor response to PET and PET grafted with BMP-2 peptidomimetics after 24 hours of culture. Scale bar 20 µm (Adapted from [22])

.
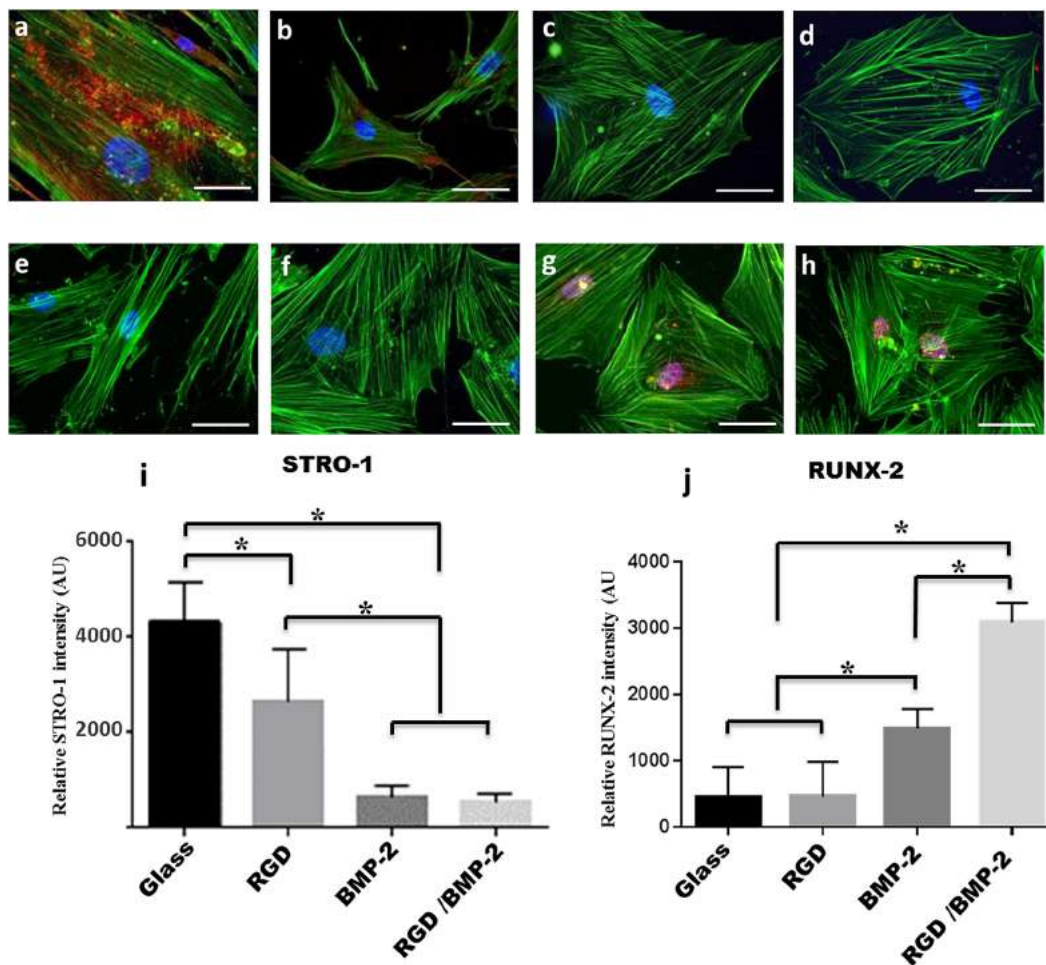
Figure 1.20 – Osteogenic comitment of hMSCs cultured for 4 weeks on glass (a, e), glass functionalized with RGD (b, f), BMP-2 (c, g), and RGD/BMP-2 (d,h). Staining in red for STRO-1 (stemness marker) (a-d), or Runx2 (e-h) analyzed in (i) and (j), respectively. Blue – nucleus, green – F-actin. Scale bar 50 µm [20]

.

A very detailed study of the influence of short peptide sequences on MSC differentiation was patented by Zouani (2018) [91].

1.2.4.B   Biological responses to surface topographies

The change of topography of a biomaterial is a way of creating physical cues to modulate cell behavior, and to study the mechanisms of mechanotransduction. Such process describes the transduction of a mechanical stimulus into a chemical signal inside a cell, giving rise to alterations of gene expression [49]. The investigation of the impact of surface topography on cell response was first described in 1960s, when contact guidance of fibroblastic cells was observed, *i.e.*, it was observed that fibroblasts were sensitive to surface topology, aligning to grooves created in materials [92]. Contact guidance is now currently understood as being a mechanism through which cells respond to the underlying surface topology, namely by altering their cytoskeleton organization, proliferating, or migrating. With the development of semiconductor industry for electronics, the creation of a large variety of patterns on different materials, and the decrease in feature dimensions – down to nanoscale – became possible. This allowed further investigations of contact guidance, but also of the impact of topographic features whose dimensions are in the range of those of proteins and other components of ECM [49]. A simplified representation of interactions of cells with a bone implant topography at different scales is illustrated in Figure 1.21.

Macroscale surface modifications are valuable mainly for the improvement of mechanical support of bone tissue and to facilitate osseointegration of the prosthesis. Microscale structures, being at the same scale range of cells, can potentially boost interactions between cells and implant, contributing as well for a better osseointegration. The investigation of how nanoscale topography of a biomaterial can elicit a specific cell behavior, including alterations in cell adhesion, cell migration, cytoskeletal changes, and gene expression started to be reported in the late 1990s, beginning of 2000 [94–96]. Nanoscale features appear to be more advantageous than microscale for modulating cell response since they offer an exceptionally large surface area for protein adsorption as well as more adhesion sites for integrins, which facilitates the interaction of integrins with the proteins adsorbed on the surface [97]. Nonetheless, there is still the need for further investigation on this subject, as it was not yet possible to encompass and interpret all the complex cell-substrate interactions happening at nanoscale level.
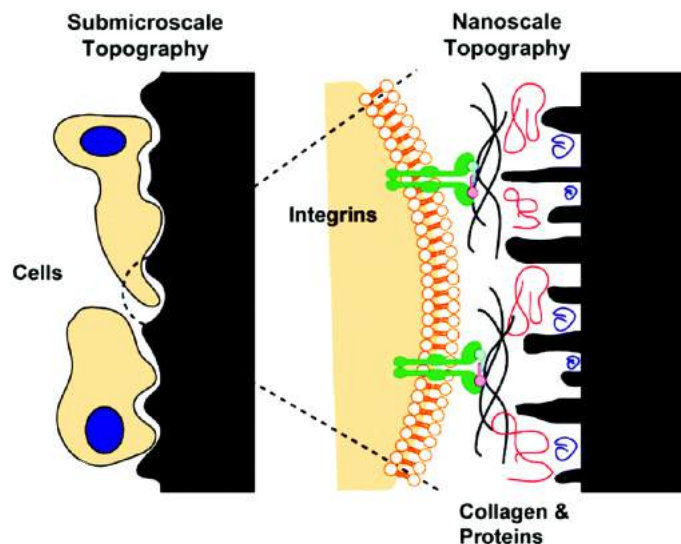
Figure 1.21 – Schematic representation of the interactions of cells with bone implants at different scale. Nanoscale topographies are at the same size regime of subcellular structures. Integrins (in green) and other transmembrane receptors are able to interact with the structures at nanoscale as well as with collagen and other proteins (represented by the lines in blue, red and black) (Adapted from [93]).

Not only the shape and dimensions of surface topography have the capability of regulating cell response, but also their degree of order is know to influence cell fate [97]. Such degree of organization of topography features on a surface can be categorized as random, partially ordered, or ordered. If limited or no control is exerted over orientation and pattern geometry during material structuring, then randomly organized features are obtained. Random patterns include for example, the increase of surface roughness or porosity, or the creation of fibrous surfaces, which can be fabricated by wet etching, anodization, or electrospinning, for instance [98–101]. If the patterns show features of controlled dimension and short-range order, they can be classified as partially ordered, whereas if the array features show a precise organization at long-range, they may designated periodically ordered arrays, as illustrated in Figure 1.22 [11, 97, 102, 103].

Tubes are the most common example of partially ordered surface patterns in biomaterials [11, 104, 105]. Ordered patterns comprise arrays of pillars/protrusions, pits, grooves, or more intricate matrices, for instance [106–109].

With regard to partially to well ordered nanoarrays, features such as pillars, tubes, pits, or a combination of micro- and nanostructures have been fabricated for cell fate studies, as summarized in Table 1.5.

Table 1.5 – Examples of studies of the impact of nanoscale topographies on hMSC behavior.

Pattern	Material	Diameter / Width	Height	Spacing	Culture medium	Outcome	Ref.
Pillars	SiO$_2$	10-30 nm	20-50 nm	50-120 nm	Basal	Adhesion and proliferation independent of feature dimensions. Higher pillars promote osteogenesis.	[106]
	TiO$_2$	50-200 nm	50-200 nm	90-185 nm	Osteogenic	Larger features favor cell adhesion, spreading, and osteoblastic differentiation.	[110]
	TiO$_2$	25 nm	8-15 nm	20-50 nm	Basal	Larger features promote osteogenesis. hMSCs interact with topographies down to 8 nm height.	[111]
	TiO$_2$	20-55 nm	8-100 nm	30-115 nm	Basal	Smaller features promote osteogenesis.	[10, 102, 112]
Grooves	Polyimide	2-15 μm	200 nm, 2 μm	2-15 μm, 650 nm	Osteogenic	Topography supports differentiation initiated by induction medium.	[113]
	PMMA	140-415 nm	100-200 nm	140-415 nm	Osteogenic	Poor osteogenesis.	[114]
	PDMS	250 nm	250 nm	500 nm	Basal	Neurogenic differentiation is promoted.	[115]
	PDMS	350 nm	280 nm	700 nm	Basal	Fibronectin coating. Cells align according to pattern, but their adhesion is low.	[116]

Table 1.5 – Examples of studies of the impact of nanoscale topographies on hMSC behavior.

Pattern	Material	Diameter / Width	Height	Spacing	Culture medium	Outcome	Ref.
	Polyurethane	400-1400 nm	300 nm	400-1400 nm	Osteogenic	Smaller width/pitch improves osteogenesis.	[108]
Tubes	TiO_2	30-100 nm	n/a	n/a	Basal	Improved cell adhesion on smaller tubes. Improved osteogenesis on larger features.	
	TiO_2	15-100 nm	n/a	n/a	Osteogenic	BMP-2 coating. Smaller diameter tubes promote osteogenesis, whereas larger diameter promotes chondrogenesis.	[117]
	TiO_2	45 nm	n/a	n/a	Basal	Decrease of cell adhesion compared with flat TiO_2.	[100]
Pits	PCL	120 nm	100 nm	300 nm	Basal	Topography can maintain stemness up to 8 weeks.	[118]

[0]PCL: Polycaprolactone; PDMS: Polydimethylsiloxane; PMMA: Polymethyl methacrylate. n/a: not applicable.
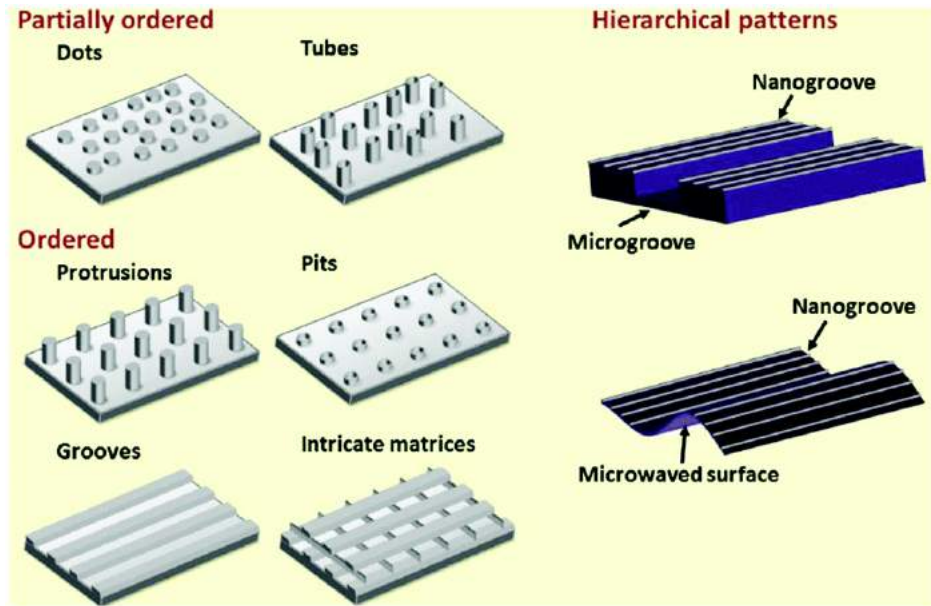
Figure 1.22 – Schematic representation of topographic features used for the studies of cell response for applications in bone tissue [97].

Pillars

Nanoscale pillars are typically fabricated in titanium oxide or silicon oxide by Electron Beam Lithography (EBL) or reverse micelle lithography followed by electrochemical anodization or Reactive Ion Etching (RIE) of the material.

Fiedler *et al.* (2013) investigated the behavior of hMSCs cultivated in basal medium, on silica nanopillars. They observed that even though adhesion and proliferation of hMSCs were similar on all the patterns, their osteoblastic differentiation was enhanced on higher features (50 nm) when compared with shorter ones (20 or 35 nm) [106]. Moreover, the authors compared proliferation rates of hMSCs and human osteoblasts, and observed that proliferation of hMSCs was augmented on all topographies (compared with a flat control), whereas osteoblast proliferation appear to be sensitive to pillar height, with greater rates towards short pillars (20 nm). The authors suggested that different topographies may be able to induce distinct mechanical stimuli, leading to a specific stress on actin fibers (as previously reported by Dalby *et al.* as well as Biggs *et al.*) [106, 119, 120].

De Peppo *et al.* (2014) observed the same tendency of osteoblastic differentiation of hMSCs with increasing nanopillar size [110]. The authors reported that larger features (diameter 105 or 185 nm, height 130 or 240 nm, respectively) were able to sustain increased cell proliferation and differentiation than smaller features (diameter 50 nm, height 90 nm). After 2 weeks, cells cultured on flat surfaces or on pillars of diameter

of 185 nm expressed a significant higher level of Runx2 and ALP (markers of early osteogenic differentiation), and produced more mineralized matrix than on pillars of 50 nm diameter. De Peppo *et al.* suggested that, since cells adhere only to the top part of the features (as depicted in Figure 1.23), increased cell adhesion and proliferation on flat and larger features can be directly related with a larger surface area available for cell adhesion.
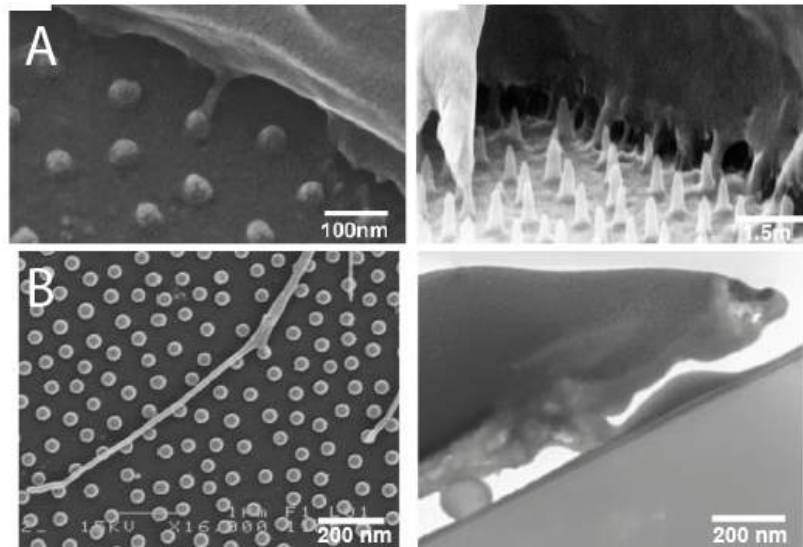
Figure 1.23 – Detail of SEM pictures showing the interaction of hMSCs with nanopillars. (A) Fiedler et al. [106]; (B) de Peppo et al. [110]

.

Furthermore, as described by Tang *et al.* (2010), osteogenic differentiation potential is directly correlated with the number of cell-cell contacts, thus, it can be expected that a nanostructured surface which enhances cell proliferation (therefore increasing the possibility of cell-cell interaction) may also promote MSC differentiation [110, 121].

Despite reporting similar trends on the impact of nanostructures on hMSC osteoblastic differentiation, it is important to note that the two studies differ in several aspects. First of all, Fiedler finds feature height as the most relevant parameter for the control of cell fate whereas de Peppo highlights the importance of surface area at the top, given by the diameter [106, 110]. Moreover, material (SiO_2, and TiO_2, respectively), feature shape (conical vs. *quasi*-round), and culture medium (basal and osteogenic, respectively) differ. Finally, the osteogenic markers evaluated are not expressed at the same stage of differentiation, and different approaches were followed. Fiedler investigated the expression of OCN (a late stage marker) by immunofluorescence but on the other hand, de Peppo quantified gene expression for the early differ-

entiation marker Runx2 and the activity of ALP. de Peppo reported high expression for large features as well as for flat surfaces (related with a larger area available for cell adhesion). Yet, Fiedler observed a significantly lower expression of OCN on flat TiO_2, when compared with the nanostructured surfaces, even if the larger pillar diameter was 30 nm.

Contrary to the findings of Fiedler and de Peppo, Sjöstrom *et al.* (2009, 2013) as well as McNamara *et al.* (2011) reported that shorter nanopillars are actually more effective on the stimulation of osteogenic differentiation of hMSCs [10, 102, 112]. In their studies, the authors observed that hMSC spreading, cytoskeleton organization, and expression of osteogenic markers (ALP, OPN, OCN) were inversely proportional to the height of TiO_2 nanopillars (15 to 100 nm range). In particular, 15 nm high features were reported to be the best condition for the promotion of osteogenic differentiation, along with the formation of large focal adhesions when compared not only with higher pillars as previously referred, but also with flat control and 8 nm high features. Mc-Namara *et al.* highlighted also the importance of selecting an adequate control for cell studies, whose surface chemistry resembles the chemistry of the nanostructured materials [112]. The authors evaluated the utilization of Tissue Culture Plastic (TCP) and flat TiO_2, as controls in metabolomic assays for the comparison with TiO_2, nanostructures. It was observed that the metabolic profile of hMSCs cultured on flat or patterned titania were congruent, but differed significantly from the profile of cells cultured on TCP, which indicated that the latter was unsuitable to be used as control surface.

Grooves

Grooves are commonly fabricated in polymeric substrates by photolithography or Nanoimprint Lithography (NIL) methods, with dimensions in the micron and sub-micron scales [97]. Several studies have shown that this type of topography is not able to induce osteogenic differentiation of MSC *per se*, requiring the use of adjuvants as osteogenic medium, or surface coating with ECM proteins or mimetic peptides [108, 113–116]. Due to the difference in scale regime (as this review focuses on nanoscale topographies), this type of pattern will not be discussed in detail. Examples of the use of grooves for the investigation of differentiation of hMSC can be found in Table 1.5.

Tubes

Nanotubes are routinely fabricated *via* electrochemical anodization of titanium, which gives rise to vertically arranged TiO$_2$ tubular structures [97] (Figure 1.24).
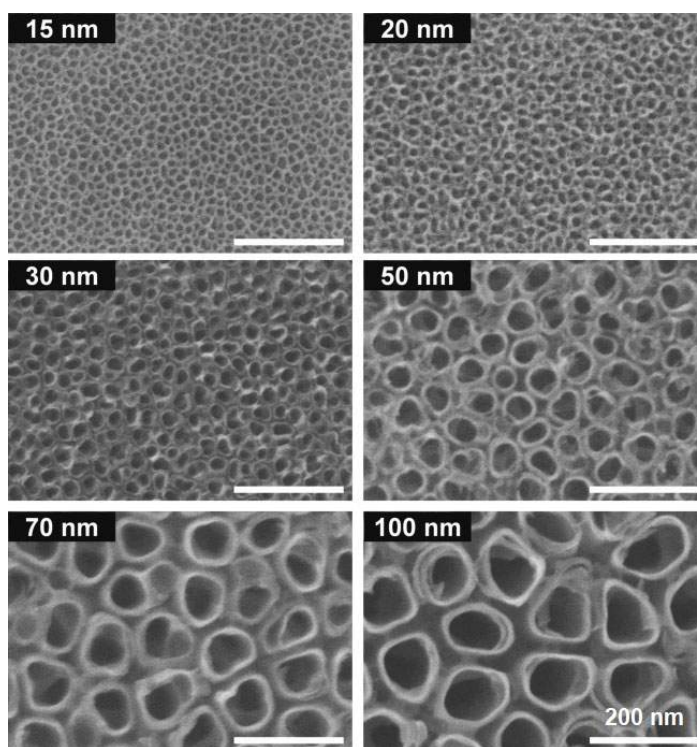
Figure 1.24 – Top-view SEM images of titania nanotubes with diameters ranging from 15 to 100 nm [104].

Brammer *et al.* (2009, 2012) emphasized two interesting features of such nanotopography: superhydrophilicity and the possibility of fluid flow between nanotube walls [105, 122]. The authors demonstrated thatthe contact angle of titanium (approximately 80° for a flat titanium sample) decreases to almost 0° after anodization, which can contribute for an improvement of cell adhesion. The existence of interconnecting spaces between nanotube walls may ensure flow of culture media and exchanges of gas, nutrients and other molecules even when cells reach confluence, contributing to an enhanced cell environment [105, 122]. Several works have been published on the investigation of the modulation of cell fate by nanotube diameter reporting conflicting results [11, 104, 122, 123]. It has been hypothesized that such discrepancies may be related with not only the use of different cell types and distinct culture conditions, but also with different material phase of the TiO$_2$, nanotubes (amorphous or anatase phase) [122].

Oh and colleagues (2009) reported that it was possible to modulate hMSC behavior changing only the TiO$_2$ diameter (from 30 to 100 nm), without the use of osteogenic

induction medium or other chemical cues [11]. The authors observed enhanced cell adhesion on narrow tubes (30 nm of diameter) compared with the other conditions. Moreover, increasing cell elongation and osteoblastic differentiation was observed with the increase of feature diameter. Highest expression of osteogenic markers ALP, OPN, and OCN was noticed on features of diameter of 100 nm. Oh *et al.* advocated that the density of protein adsorption on the structures impacts the extent of cell adhesion as smaller nanotubes shown a complete coverage by proteins contrary to large tubes [11]. hMSCs were more stretched (10 times longer on 100 nm tubes than on 30 nm ones), which can lead to cytoskeleton rearrangement, with subsequent differentiation of the cells [11]. Similar results were reported for human osteoblasts cultured in basal medium on titania nanotubes by Brammer (2009) [122]. Contrarily, Park *et al.* (2007, 2009, 2012) investigated the impact of titania nanotubes of diameters between 15 and 100 nm on the fate of different types of cells, namely rat MSCs and human Hematopoietic Stem Cells (HSCs) [104, 117, 124]. The authors observed identical results for all cell types, with small diameter features (15 nm) ensured high cell adhesion and proliferation, as well as differentiation into osteoblasts (in the case of MSCs) or osteoclasts (from HSCs). It was suggested that 15 nm tubes, being of a similar size of the extracellular ligand binding domain of integrins, contributes for a stronger integrin clustering, triggering specific intracellular signaling pathways and actin stress fiber formation, which leads to cell differentiation [117]. Larger nanotubes (100 nm) did not support proper cell adhesion, and eventually contributed to cell apoptosis. As highlighted before, it is worth noting that cells were cultured in a differentiation induction medium, and that titania was in its amorphous phase (whereas Oh and Brammer utilized titania in anatase phase, which has a different atomic organization), which can contribute for observations differing from the works of other research groups [105].

Pits

The use of nanopits created on polymeric substrates for the control of cell fate has been investigated predominantly at the University of Glasgow since early 2000s [125]. Diameter of pits as well as their arrangement on the surface (ordered vs. increasing degree of disorder) is known to influence the fate of cells (including hMSCs, osteoblasts, fibroblasts) cultured on such surfaces (as exemplified in Figure 1.25) [118–120, 125].

McMurray *et al.* (2011) showed that hMSCs cultured on ordered nanopit arrays
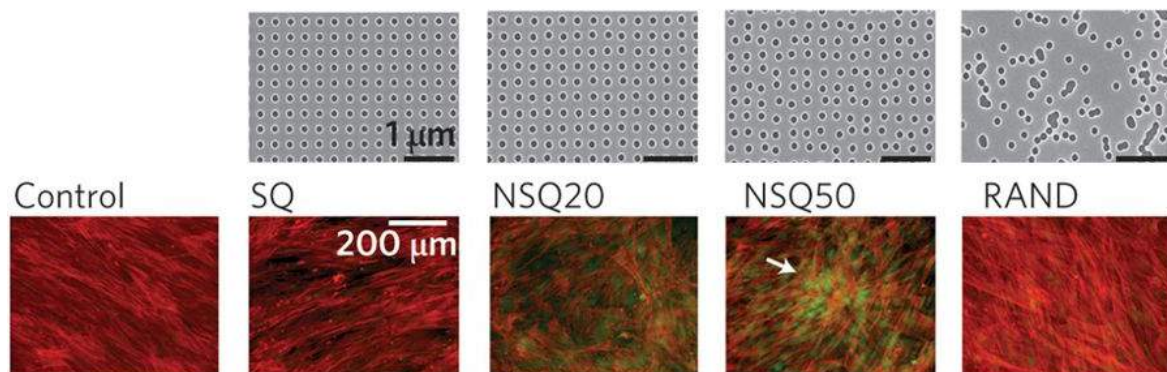
Figure 1.25 – Expression of OPN by hMSCs cultured on nanopit arrays of varied order. Red: actin. Green: OPN (Adapted from [119]).

(diameter 120 nm, depth 100 nm, spacing 300 nm) were able to maintain their stemness characteristics for 8 weeks (duration of the study) [118]. Instead, if hMSCs were cultured on nanopits of the same dimensions, but with a random displacement of ± 50 nm from their position in a true square, the expression of osteogenic differentiation markers in enhanced (compared with flat control, ordered array, or randomly displaced pits). Moreover, larger focal adhesions were observed on such slightly disordered arrays, along with a rearrangement of the cytoskeleton related with a high intracellular tension [13, 107, 119]. Figure 1.26 schematically summarizes such results.
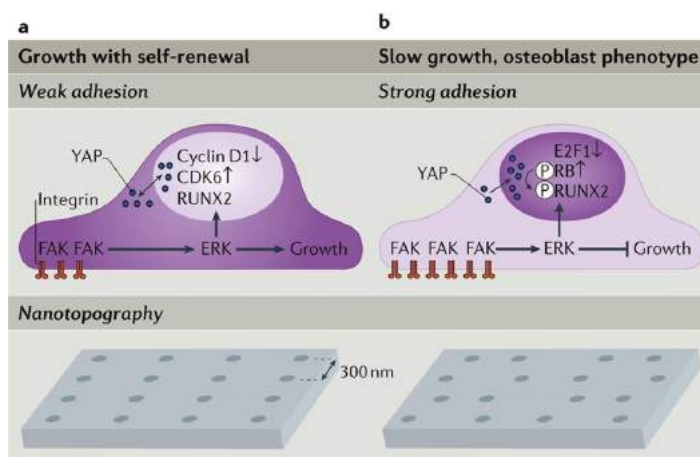
Figure 1.26 – Schematic representation of MSC fate by nanotopographies. (a) Self-renewing MSCs adhere to the matrix more weakly than differentiating cells, resulting in lower levels of integrin-mediated focal adhesion kinase (FAK)-triggered signalling. Runx2 remains inactive. No cytoskeleton tension is observed. Nanotopographies exhibiting regular patterns can be used to mimic weak adhesion. (b) Strong adhesion decreases cell growth and increases osteogenesis. Integrin-mediated formation of focal adhesions and the recruitment and activation of FAKs lead to the inhibition of cell growth, and the phosphorylation of Runx2 (initiating osteogenic differentiation). Increased cytoskeletal tension drives the translocation of YAP into the nucleus to further stimulate osteogenesis, again through Runx2 activation. (Adapted from [16]).

34

1.3 Nanostructuring of Biomaterials

The modification of surface topography on biomaterials relies on the commonly and vastly developed techniques used in micro- and nanofabrication methods used in electronics industry. The main approaches offering the possibility of feature fabrication with nanoscale resolution are summarized in this section. The nanofabrication methods utilized during this work are described in more detail later in this section.

1.3.1 Electron-beam lithography

EBL is a very interesting technique for the fabrication of very uniform and reproducible features with resolutions down to 10 nm. It is based on the exposure of an electron-sensitive polymer layer coated on the biomaterial by a highly focused electron-beam to write out a pattern designed with Computer-aided Design (CAD) tools. The beam induces a change in molecular structure and solubility of the polymer film. Following exposure to the electron-beam, the polymer is developed in a suitable solvent to selectively dissolve either the exposed or unexposed areas of the polymer (depending on polymer characteristics). Nonetheless, EBL is a very expensive and time-consuming method, not offering the possibility of high throughput, or patterning of large areas. EBL has been used in several studies of cell-substrate interactions at nanoscale [119, 126–128]. Figure 1.27 represents a SEM image of a nanoscale array created for studies of interaction of MSCs with nanoscale topographies. EBL is not only used for the patterning of a material, but also to create masks or molds for electrochemical anodization or NIL, respectively.
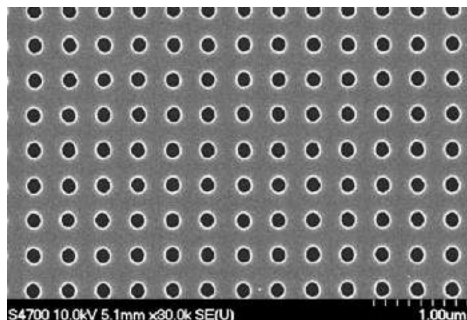
Figure 1.27 – Nanopit Si arrays fabricated by EBL with 120 nm of diameter, 100 nm of depth, and 300 nm of pitch [120].

1.3.2 Electrochemical anodization

Electrochemical anodization is a rather simple, cost-effective method which allows the patterning of a material (usually alumina or titania) in a controllable and reproducible way. This process offers the possibility of fabricating two distinct types of features: tubes, and short pillars [10, 11, 102, 122, 129]. The basis of this method consists on the utilization of a sheet of the biomaterial as anode and a platinum (most commonly) cathode. These material sheets are immersed in a electrolyte solution (*e.g.* hydrofluoric acid) and an electric field is applied to the system (as represented in Figure 1.28). The duration and magnitude of power supplied to the system determines the height and diameter of the nanotubes [105].
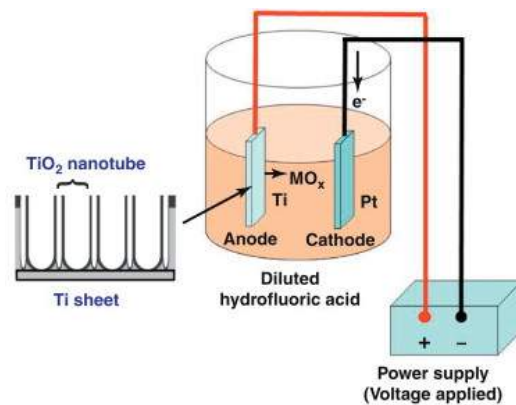
Figure 1.28 – Schematic representation of the anodization process for the fabrication of TiO$_2$ nanotubes [105].

If a mask is used to protect specific regions of the biomaterial during anodization, then nanopillars are obtained, instead of nanotubes [10, 102, 130]. Examples of the possible nanoscale structures fabricated by electrochemical anodization are represented in Figure 1.29.
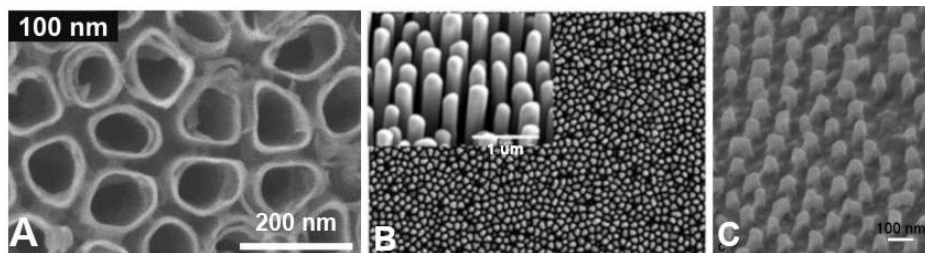
Figure 1.29 – Nanoscale tubes (A) and pillar arrays (B and C) obtained by anodization (Adapted from [102, 104, 130]).

1.3.3 Self-assembly of block copolymer films

Block copolymers

Block Copolymers (BCPs), macromolecules formed by sequences of two or more unimer species, can be arranged various ways, namely linearly, or in a radial arrangement. In particular, a diblock copolymer AB, the simplest form of BCP, consists in a sequence of two chains of different homopolymers, covalently bound at their ends. In addition to an AB configuration, the homopolymers A and B can also form ABA or BAB triblocks, and $(AB)_n$ linear multiblocks [131]. The molecular structure of BCPs, and in particular their segmental incompatibility, grants unique solution and associative properties to these molecules, namely their surfactant characteristics, and ability to self-assemble [131]. This difference in chemical nature of the blocks relates with the coexistence of two types of forces [132]. The first one consists in 'long-range repulsive interactions' between the two blocks. Particularly, in amphiphilic diblock copolymers, such repulsion occurs for very short block lengths, as their segmental incompatibility is related with differences in solubility (in a selective solvent) of each block. The latter kind of forces consists on 'short-range attractive interactions' due to the covalent bond between the two blocks, which is responsible for a microphase separation and for the constraint of further separation at macroscale [133].

Micellization of block copolymers

In solution, for a selective solvent for one of the blocks, amphiphilic BCPs can undergo two main processes depending on their concentration: micellization, for reduced concentrations, and gelation for higher concentrations [133]. The first process leads to a organization of the micelles in solution. The micellization of BCPs in a selective solvent for one of the blocks is possible due to their colloidal properties, analogous to the characteristics of classical surfactants, granting new structural and flow characteristics to the system [131, 134]. If dissolved in a solvent that is thermodynamically good solvent for one of the blocks and precipitant for the other, BCP chains tend to aggregate reversibly, in order to minimize the free energy of the system, forming micelles of specific morphologies (and of nanometer length scales) [131]. These micelles usually consist on a 'core' formed by the insoluble blocks, which swelling extent depends on the quality of the solvent for this block, surrounded by a flexible 'corona' constituted

by the soluble blocks [131]. The size of the formed micelles depends mainly on the size of their cores, principally when the insoluble block is very short [135]. Moreover, depending on the polarity of the solvent and the solvent quality for each block, BCPs form regular (aggregates with a more non-polar core and a more polar corona) or reverse (aggregates with a more polar core and a more non-polar corona) micelles [136]. The process of micellization occurs in dilute solutions of BCPs in a selective solvent, if the concentration of the BCP is above a critical micelle concentration, and the solution is maintained at a fixed temperature [131]. This critical micelle concentration corresponds to the concentration limit above which the system is no longer characterised by unimers in solution, but instead by an equilibrium between micelles and unimers [131]. In addition to the critical micelle concentration, and the equilibrium between unimers and micelles in solution, a micellar system is also characterized by variables including micelle morphology, micelle molecular weight, aggregation number, and radius of gyration and hydrodynamic radius. Two different processes are usually followed to attain a BCP micellar system [131]. The BCP can be firstly dissolved in a common solvent for the two blocks, and afterwards conditions like temperature, or solvent quality are changed in a way that leads to the formation of micelles. Usually, the solvent composition is changed by gradually adding a solvent which is a precipitant for one of the blocks. Alternatively, the BCP can be directly dissolved in a selective solvent, and subsequently let to anneal by standing, mechanical agitation, or thermal treatment [133]. Micelles are kinetically frozen when the core-forming block is below its Glass Transition Temperature (T_g) and the polymer is not extensively swollen by the solvent [137].

Block copolymer templates

Block copolymer micelles can adopt different morphologies, being spherical the most common shape. These type of micelles can create ordered arrays of hexagonal distribution that form a thin film (thickness lower than 100 nm) when coated on a flat substrate (Figure 1.30). The characteristic dimensions of the polymer templates obtained depend not only on the dimensions of the initial micelles in solution, but also on the conditions of deposition, which will mainly influence the speed of vapor evaporation [137].

Such polymeric templates may be potentially used as masks for subsequent pat-
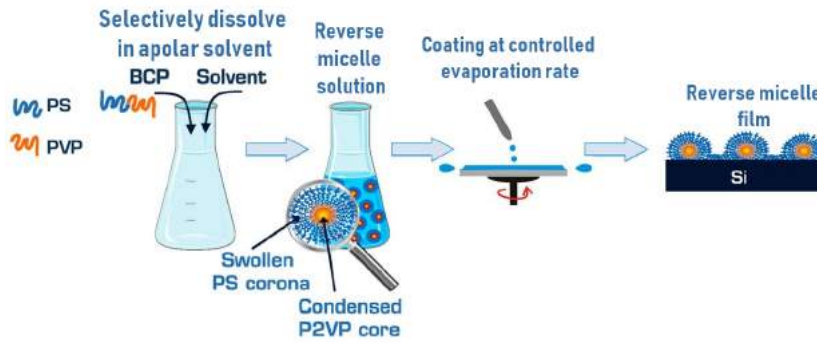
Figure 1.30 – Schematic representation of the formation of PS-b-P2VP thin films on a Si substrate. (Adapted from [15])

terning of the underlying substrate, allowing the creation of structures with spatial resolution of tens of nanometers across full wafers[14]. Top-down direct writing techniques (*e.g.* EBL) also allow the creation of high resolution patterns. However, contrary to self-assembly-based lithography, they require the use of very expensive equipment, and they cannot ensure pattering of large areas [138].

Improvement of pattern transfer

BCP films can be used as masks for substrate patterning. For that, the polymeric templates are usually subjected to a brief oxygen plasma to remove the intermediate layer in order to increase selectivity of pattern-transfer into underlying substrate [14]. Nonetheless, due to low thickness (typically 10 to 30 nm), these polymer masks cannot withstand long etching times, thus requiring alternative ways to increase selectivity. Hard masks with high selectivity for the etching process grant the possibility for the creation of uniform, reproducible features, with low standard deviations. Two main approaches are normally followed: an oxide thin film deposited on the substrate is used as an intermediate mask, or Nanoparticles (NPs) are created inside micelle cores and used as masks for controlled etching [14, 15]. Two main approaches are normally followed: an oxide thin film deposited on the substrate is used as an intermediate mask, or NPs are synthesized *in situ* inside micelle cores and used as masks for controlled etching [14, 15]. This enables nanopillars with desired heights beyond what is possible with only the polymer templates, and also contributes to higher uniformity on a wafer, and better batch-to-batch reproducibility.

In the first case (Figure 1.31), a thin oxide film (usually 25 to 50 nm thick) is thermally grown (more common approach) or deposited onto the substrate before the

coating with BCP micelle solution. The polymeric layer is briefly exposed to an oxygen plasma to remove the thin (normally less than 5 nm thick) corona-based layer, exposing the oxide. An etching approach allowing anisotropic pattern transfer (*e.g.* RIE) is then used for the patterning of the oxide, and for the subsequent substrate etching. The uniformity and reproducibility of the nanopillar array obtained depend on the characteristics of the initial BCP template and on the selected etching method [14].
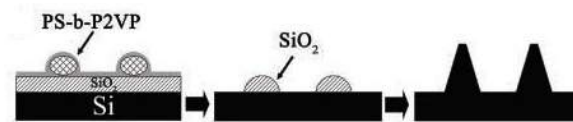
Figure 1.31 – Schematic representation of nanopillar fabrication using an intermediate silica mask. (Adapted from [14])

If the separation between reverse micelle cores forming the polymer template is very reduced or if the thickness of the polymeric film is very low, it may not be possible to use the polymer as mask for the patterning of the oxide layer. The substitution of the polymer template by an inorganic template (*(e.g.* titania NPs) can be an alternative to overcome such problem (Figure 1.32).
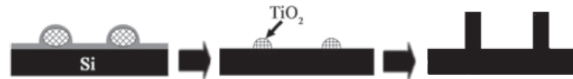
Figure 1.32 – Schematic representation of nanopillar fabrication using a titania NP mask for features with sub-10 nm dimensions and separation. (Adapted from [14])

If the core-forming block of the BCP is able to react with a precursor, namely a metal ion, then micelle cores can be used as 'confined reactors' for the formation of nanoparticles. Two main approaches are normally followed for the incorporation of NPs into BCP micelles: exposure of BCP to precursors in solution prior coating on a surface (Figure 1.33), or exposure of BCP films coated on a surface to the liquid- or gas-phase precursors (Figure 1.34) [14, 15, 139].

With regard to particles of metal oxides, exposure to vapor-phase precursors after micelle deposition on a surface appears to be the most suitable approach, particularly if the exposure takes place inside an Atomic Layer Deposition (ALD) reactor [15]. This method is designated sequential vapor infiltration synthesis. If such procedure is followed different parameters, namely spacing and particle diameter, can be independently controlled. BCP characteristics and coating conditions can be fine-tuned in
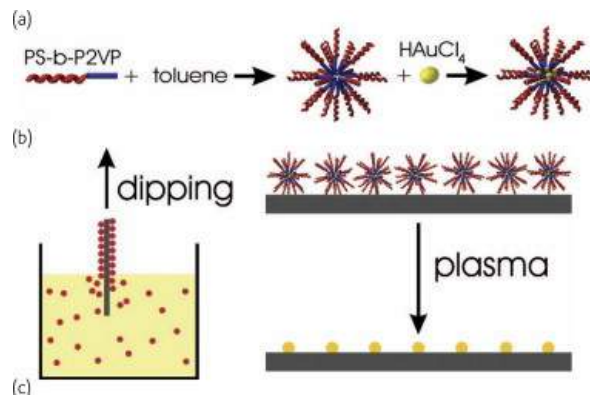
Figure 1.33 – Schematic representation of (a) micelle loading with a metal salt, and (b) subsequent coating of a material with the new complex by dip-coating. (Adapted from [137])
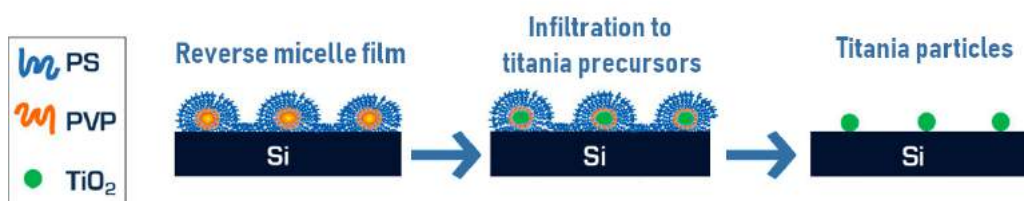
Figure 1.34 – Schematic representation of the formation of titania NPs on surface, guided by a BCP template. Titania NPs are formed inside P2VP cores after sequential exposure to titania precursors. Exposure of the film to an oxygen plasma allows a complete removal of the polymer, exposing the titania NP array. (Adapted from [15])

order to create arrays with the desired spatial resolution. Afterwards, exposure conditions can be accurately controlled by the ALD machinery, granting the growth of NP of specific dimensions. Parameters influencing particle growth and size include temperature, pressure, chemical environment, and dosing of precursors during the reaction [14].

1.3.4 Nanoimprint lithography

NIL is a high-throughput lithography technique which relies on the deformation of a polymer layer (sensitive to temperature or radiation), as represented in Figure 1.35.

It is therefore limited by the minimum feature size possible to be fabricated for the mold (by other technique, as EBL), which grants it very high resolution [141]. It has been reported by Hua (2004) that it is possible to achieve resolutions at sub-5 nm length scale using carbon nanotubes as imprinting templates (Figure 1.36) [142].

Other parameters must also be fine-tuned to achieve imprinted films with high uniformity and resolution. These include the choice of substrate and mold material (rigid
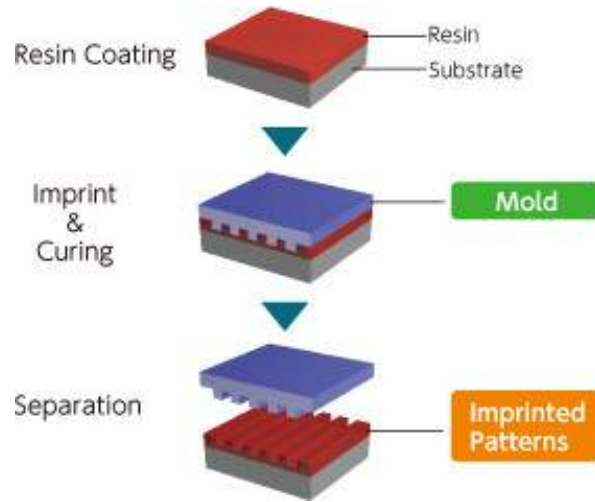
Figure 1.35 − Schematic representation of main NIL steps [140].
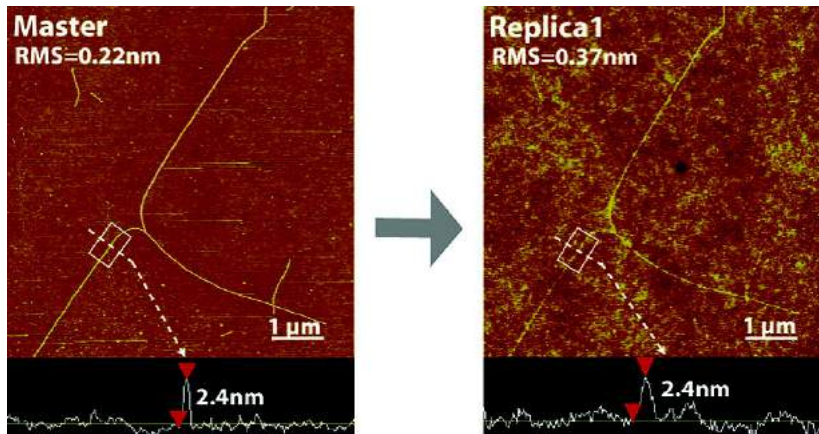
Figure 1.36 − AFM images of a carbon nanotubes master (a) and imprinted structures obtained by NIL [142].

or flexible), imprinting conditions (temperature, pressure, Ultraviolet (UV) power, duration of imprinting), and polymer characteristics, for instance [143].

As previously referred, very high resolutions can be achieved as this technique relies only on mechanical replication (Figure 1.37) [143]. Nonetheless, there are challenges when performing nanoimprinting, related mainly with the alignment of the sample and template, and the fabrication of a template with accurate feature definition [143].

Two main techniques of NIL can be followed: thermal NIL, and UV–NIL. The principle behind the former consists in pressing template with a surface relief defining the negative of the expected final features against a polymeric material (thermosetting or thermoplastic) cast on a substrate, at controlled pressure, and temperature above the T_g of the polymer (approximately 70 to 90 °C above T_g) [141]. The mold can be released after cooling down the resist below its T_g. Alternatively, if the polymer utilized is UV-curable, then, after being put in contact with the mold, it can be crosslinked
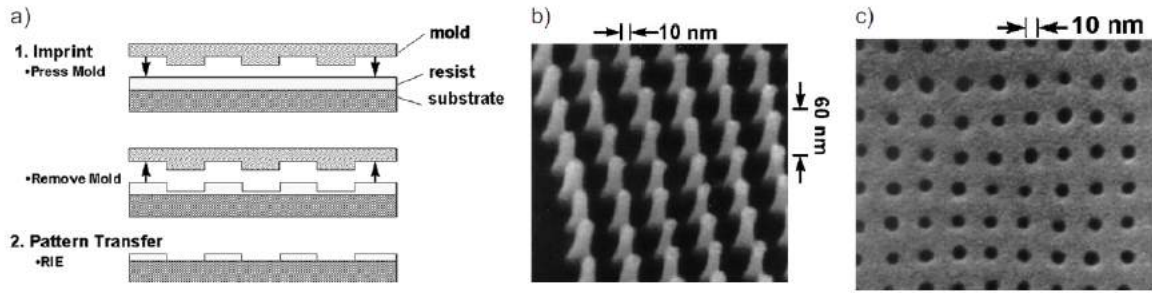
Figure 1.37 – (a) Schematic representation of NIL process. Example of (b) mold with 10 nm diameter pillar array and (c) imprinted hole array [144].

if subjected to UV light [141]. In both approaches, the obtained pattern is typically transferred into the substrate by RIE.

Thermal NIL, also denominated hot embossing, requires a good flow ability and incompressibility of the resist layer in order to achieve a complete filling of the mold cavities. The resists used for thermal imprinting are either thermoplastic or thermosetting polymers.

This can be attained through the increase of temperature above the T_g of the polymer, and the application of pressure in the range of 20 to 100 bar [145]. As the process has to be performed at relatively high pressure, the mold material must have high mechanical strength to withstand it. Furthermore, thermal NIL requires that the stamp has high thermal stability, low thermal expansion coefficient, and low roughness [145].

UV–NIL is an alternative approach offering several advantages over thermal NIL. UV–NIL allows quick (in a few seconds) replication, at low temperatures and pressures, and enabling high-throughput, large-area patterning with less demands on the substrate or the molds [143]. As referred, the patterning of UV–crosslinkable polymers can also be conducted using soft molds, which allow a more conformal contact between the stamp and the resist layer for larger patterning areas, reduce the high demolding force characteristic of UV–NIL processes using hard stamps, and since a particle contamination causes only a local deformation, which can improve the process yield. Nevertheless, the use of flexible molds not only limits the resolution of the imprinted features, but also reduces their uniformity, due to the possibility of mold deformation during imprinting. Moreover, since the resist layer needs to be exposed to UV radiation, it is necessary that either the stamp or the substrate onto which the polymer is spin-coated is UV–transparent, which can increase the experiment costs

when compared with thermal NIL processing [145].

Nanoimprint processing can be categorized into single-step or multi-step imprinting if the patterning of the resist film using is performed at once, using a stamp of a size comparable to the substrate size, or if it consists on the step and repetition of the imprinting on a large surface, using a stamp of reduced size [143]. Additionally, nanoimprinting can also be referred as single level imprinting or multilevel imprinting if monolayer or multilayer processing is considered, respectively [143].

Numerous variants of the main nanoimprinting processes previously described have been developed not only with the aim of achieving higher throughput, better resolution, and the reduction of number of imprint defects, but also with the aim of patterning larger surface areas, and obtaining 3D or functional features [143].

As previously referred, NIL requires the fabrication of a mold with accurate definition of surface relief structures, and able to withstand numerous repetitions of the imprinting process. Very high resolutions can only be attained using hard mold materials, as nanoscale structures must not deform, or collapse during imprinting, which can occur if an elastomeric stamp is utilized [141]. Nonetheless, it is possible to grant moderate flexibility to the mold if the rigid nanostructures are supported by a flexible substrate, since it can ensure the necessary local rigidity necessary for imprinting, but also a global flexibility, providing a more conformal contact between the stamp and the resist, hence contributing to a higher process throughput [141]. Additionally, thermal NIL processes require a precise control of the thermal expansion coefficients of stamp and substrate, since, as high temperatures (normally above 100 ºC) are used for resist processing, high imprinting accuracy can only be reached if materials with similar thermal expansion coefficients are used, in order to avoid pattern distortions or stress build-up during the cooling step [141]. A surface treatment of the stamps used for nanoimprinting is usually necessary in order to facilitate the release of the polymer layer after imprinting due to the strong adhesion of the resist to the mold, resultant from the large contact area between both [141]. Typically, the release process is improved applying a low surface energy coating to the mold prior to nanoimprinting — through the self-assembly of a fluorosilane monolayer —, but other options as the incorporation of an internal release agent into the resist formulation, or the selection of a stamp material with inherently low surface energy, such as fluoropolymers (e.g. PTFE AF) [141].

2 | Materials and Methods

2.1 Materials

Silicon wafers and silicon wafers with 25 nm of thermally grown SiO_2 were purchased from Silicon Valley Microelectronics (USA) and from Siegert Wafer (Germany).

All solvents, reagents, and acids were purchased from Sigma-Aldrich (France or Germany), unless stated otherwise.

PS-b-P2VP of Molecular Weight (M_w) of 55000-b-50000 g mol^{-1} or 248000-b-195000 g mol^{-1} with Polydispersity Index (PDI) of 1.05 and 1.08, respectively, were purchased from Polymer Source Inc (Canada) and used without further purification.

All consumables used for Chemical Mechanical Polishing (CMP) were acquired from Struers (Denmark).

NIL resists were purchased from Micro Resist Technology GmbH (Germany). Other consumables used for NIL were acquired from Obducat (Sweden).

APTES and SMP were purchased from Sigma Aldrich.

Peptides used for surface functionalization (GRGDSPC, afterwards designated as RGD peptide, and KRKIPKASSVPTELSAISMLYLC, afterwards designated as BMP-2 mimetic peptide) were synthesized by Genecust (Luxembourg).

Bone marrow hMSCs and hMSC growth medium and hMSC osteogenic induction medium were acquired from PromoCell (Germany). Other products, namely Alpha Modified Eagle Medium (αMEM), trypsin, sterile Phosphate Buffered Saline (PBS), and consumables, namely well-plates, were purchased from ThermoFisher Scientific. Ribonucleic Acid (RNA) extraction was performed using QIAGEN's RNeasy Mini Kit (QIAGEN SAS, France). RNA integrity assessment was performed using RNA 6000 Nano kit from Agilent (USA). The reagents used for RNA retrotranscription were purchased from ThermoFisher Scientific. The primers used in Quantitative Real Time

Polymerase Chain Reaction (RT-qPCR) were purchased from Sigma-Aldrich. SsoAdvanced Universal SYBR Green Supermix was purchased from Bio-Rad (USA).

2.2 Nanotopographies

The fabrication of nanopillar arrays required the creation of polymer templates of PS-b-P2VP, and the use of a hard mask for pattern transfer into the silicon substrate. It was possible to achieve uniform features over full wafers following the described protocols, both in silicon as well as in soft polymeric substrates.

2.2.1 Polymeric templates

Anhydrous toluene and anhydrous m-Xylene (Sigma Aldrich) were utilized for the preparation of reverse micelles of PS-b-P2VP (Figure 2.1), according to work of Krishnamoorthy *et al.* [137], given their selectivity as solvents for the Polystyrene (PS) block. These experiments were performed in a class 100 cleanroom, with ambient humidity between 45% and 55%, monitored by a hygrometer during sample processing. AFM (Innova, Bruker) and SEM (Helios 650 NanoLab, FIB-SEM, FEI Company, Hillsboro, OR, USA) were the techniques selected for the characterization of the polymer films, and the collected data was analyzed using NanoScope or ImageJ, respectively. In addition, MatLab was used to create a script allowing a better visualization of the distribution of micelles on a surface and an evaluation of deviations from the expected *quasi*-hexagonal feature distribution.
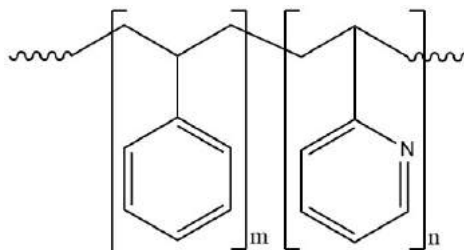
Figure 2.1 – PS-b-P2VP

More uniform and reproducible reverse micelles were created in m-xylene. Therefore this solvent was selected for the subsequent investigations. BCPs were dissolved in m-xylene in concentrations ranging from 0.4 to 1.0 wt %, and stirred for 24 hours to ensure that equilibrium is achieved. Si or SiO_2 on Si (SiO_2/Si) 4 inch substrates were

cleaned by oxygen plasma RIE (Plasma-Therm 790 Reactive Ion Etcher), followed by a cleaning with carbon dioxide snow jet, and used right after for the spin-coating of reverse micelle solutions at spin-speeds between 2000 and 8000 rpm for 30 seconds. The O_2 plasma allows the removal of organic residues and the hydrophilization of the surface, whereas CO_2 snow jet cleaning ensures further removal of hydrocarbon contaminants and the removal of particles present on the substrate surface down to nanometer size. Subsequent experiments were defined considering the conditions allowing the achievement of uniform polymer monolayers, since low concentrations and/or high spin-coating speeds can lead to a patchy coverage of the substrates, and high concentrations of polymer and/or low spin-speeds may lead to the formation of multi-layered films, hindering the objective of using such templates as masks for subsequent etching steps. Unless stated otherwise, further optimization steps were performed using PS-b-P2VP films spin-coated on clean substrates at 5000 rpm for 30 seconds, under controlled humidity, monitored by a hygrometer.

2.2.2 Hard mask fabrication

Since the selectivity of the polymer films for silicon etching is not sufficient to ensure the creation of features with the aspect ratios and profiles of interest, it was necessary to include an intermediate hard mask for the fabrication of the final arrays. Two different approaches were tested: patterning of a thin thermally grown SiO_2 layer by RIE, or incorporation of TiO_2 NPs in the micelle cores. On the other hand, the fabrication of nanopores (extra experiment to investigate the possible utilization of nanopore arrays for cells studies) required the pattering of a chromium thin film deposited by evaporation methods.

Silica mask

Regarding the use of a silica thin film, it was necessary to remove the thin PS layer between micelle cores, to expose the oxide. That was achieved subjecting the polymers to a brief Ar/O_2 plasma (18 sccm Ar / 2 sccm O_2, 4 mTorr, 4 W). The SiO_2 thin film was afterwards etched using a CHF_3/Ar plasma (12 sccm CHF_3 / 38 sccm Ar, 30 mTorr, 200 W, -90 °C). Finally the pattern could be transferred to the underlying silicon substrate by SF_6/O_2 plasma (50 sccm SF_6, 10 sccm O_2, 10 mTorr, 25 W). Any remaining silica mask was removed by etching with hydrofluoric acid (2 % v/v).

Titania nanoparticles

Conversely, the incorporation of the metal oxide particles was performed through a sequential infiltration of vapor phase precursors into the micellar cores, based on the work developed by Krishnamoorthy *et al.* (2011) and Ischenko *et al.* (2016) [14, 15]. The selective incorporation of a metal oxide in the micelle cores is possible due to the chemical differences between polymer blocks forming the core and corona of the reverse micelles. Polar precursors of TiO_2 (titanium tetrachloride and water, in the present study) are able to diffuse through the PS layer, and react with the pyridyl groups of P2VP (Figure 2.2), which allows the maintenance of structural uniformity of the initial micelles.
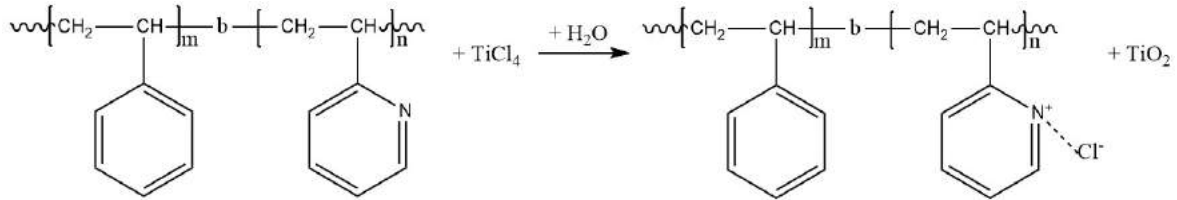
Figure 2.2 – Chemical reaction mechanism of samples exposed to $TiCl_4$. (Adapted from [15])

The samples were processed in an ALD reactor, as it allows a precise control of incorporation conditions, namely chemical environment, dosing of precursors, pressure, and temperature. The exposure to the precursors was performed at a temperature below the T_g of the BCP (approximately 97 °C). Before exposure to precursors, the ALD reactor was purged with nitrogen for 30 min for sample degassing. Sample processing was performed at a pressure of 4 mbar, for 50 precursor exposure cycles, corresponding to 100 ms pulses of $TiCl_4$ and water, intercalated with 1 min of purging with nitrogen to ensure the removal of unbound precursors from the chamber. The growth rate of TiO_2 was controlled by ellipsometry on flat silicon test samples included during deposition. The polymeric templates were subsequently removed by O_2 plasma RIE, exposing the titania particles. The number of exposure cycles for ALD was optimized, after the exposure of the BCP templates to increasing number of cycles. The maximum number of cycles (50) ensuring the incorporation of the precursors only inside the micelles, and not forming a TiO_2 shell around the micelles, was selected for the production of TiO_2 hard masks for Si patterning. Such shell can be created if the the processing conditions are not optimized for the amount of pyridyl groups available

for reaction. After exhausting all reactive groups in the micelle cores, precursors are still able to react with the recently formed TiO_2 or between themselves, which leads in a first step to NPs with a diameter larger than the initial P2VP diameter, and later to the deposition of a titania film onto the polymeric film, following a classic ALD process. Since reproducible and uniform nanopillar arrays were obtained using the silica mask, and since that process was less onerous than sequential vapor infiltration, the use of titania nanoparticles for silicon patterning was not further investigated.

Nanopores

With respect to nanopore arrays, chromium hard masks were created by mechanically assisted lift-off, following the studies of Popa *et al.* (2009) [146]. Chromium thin films with thickness of 15 nm were evaporated on the polymeric templates, and subsequently polished by gentle chemical mechanical polishing (Tegramin, Struers), as represented in Figure 2.3. The optimization of this process included investigations of the effects of different polishing cloths, slurries, and polishing conditions, namely force, spin speed and duration of treatment on the Cr thin film. Finally, polishing of 4 inch samples was performed using a solution of colloidal silica particles of 40 nm size at 40 rpm, applying a force of 5 N. Afterwards, samples were washed with concentrated soap solution to ensure the removal of the silica particles, which was confirmed by SEM. Samples could afterwards be potentially used for the fabrication of silicon nanopore arrays, if subjected to RIE for silicon etching followed by the removal of the chromium hard mask by etching. However, due to time constraints, it was not possible to give continuity to the fabrication of nanopore arrays.

2.2.3 Nanoimprint lithography

NIL is a powerful technique offering the possibilities of not only easily and rapidly replicating nanopatterns, but also of fabricating nanopatterns in different polymers using an existent master. Silicon nanopillar arrays of dimensions defined for cell studies were fabricated according the processes previously described and used as molds for NIL. Two main goals were envisaged for the application of this technique: the replication of the previously fabricated Si pillar arrays, and the fabrication of replicas of these arrays in materials of lower Young's moduli. The former aims at allowing a faster and easier production of Si nanopillar arrays, not having to follow the laborious approach
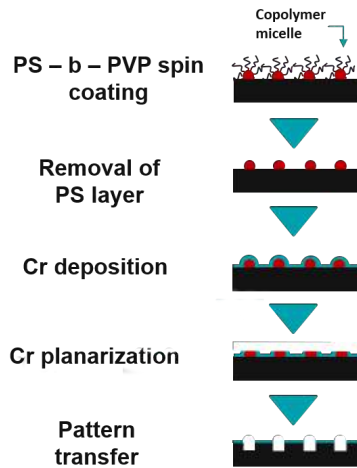
Figure 2.3 – Schematics of the process of creation of a etch mask for the fabrication of nanopore arrays.

previously described for the fabrication of the initial Si arrays, which includes at least self-assembly of BCP, substrate coating with reverse micelles and RIE of the hard mask and Si substrate. The relevance of the latter is related with the possibility of investigating not only the modulation of hMSC response by nanotopographies, but also the comparison of such modulation by nanostructured materials with different mechanical properties.

In order to achieve those objectives, nanoimprinting of several resists was evaluated following both thermal and UV processes, aiming to produce uniform patterns over large surface areas (4 inch wafers). Given its simple processing, Intermediate Polymer Stamp ® (IPS) was used for all intermediate steps required for the imprinting of the final polymer thin film. IPS patterning can be achieved following a fast process of thermal NIL, and its low surface energy confers it anti-sticking properties which can reduce processing time and effort, making it extremely interesting for all intermediate NIL steps.

Briefly, the fabrication of polymeric nanopillar arrays required the fabrication of an intermediate stamp, negative of the initial Si nanopillar array master, that could be subsequently used for the embossing of the polymer of interest, producing a uniform polymeric nanopillar array. The use of IPS for the fabrication of the auxiliary stamp avoided the need for anti-sticking treatments of both initial master and auxiliary stamp. The substrates chosen (silicon, quartz, and flexible NIL membranes) for the back support of the NIL resist required a pre-treatment with an adhesion-promoter for the improvement of adhesion of the polymer to the substrate. The resist was spin-

50

coated for a final thickness of 10 µm (due to its high viscosity further optimization would be necessary for lower thicknesses, and a high control over this parameter is not necessary as it is only vital that it ensures the fabrication of arrays with the original dimensions). Exposure to UV radiation for 5 min (at a power of 30 mW cm^{-2}) allowed the crosslinking of the polymer. After careful demolding (pressure applied during detachment from the stamp can damage features with high aspect ratio), the fabricated arrays were subjected to a hard-bake step for the improvement of feature stability.

Uniform soft polymeric nanopillar arrays with dimensions similar to the dimensions of the initial silicon arrays were therefore obtained on full wafers using soft or hard back substrates. SEM characterization of nanoimprinted polymer films was possible after sputtering of 20 nm thick platinum films.

2.2.4 Statistical analysis

All data is represented as mean $\pm$ standard deviation, except if stated otherwise. Statistical analysis of SEM images was performed using ImageJ (NIH, USA) and MatLab (MathWorks, USA). AFM data was analyzed using NanoScope Analysis (Bruker, USA).

2.3 Surface functionalization

For the investigation of possible synergistic effects between surface chemistry and nanotopography, 2 peptides were convalently grafted on the nanostructured Si surface. These peptides, RGD (Figure 2.4) and BMP-2 mimetic peptide(Figure 2.5), are well-described peptides known for their abilities to improve adhesion and enhance osteogenic differentiation of hMSC, respectively.
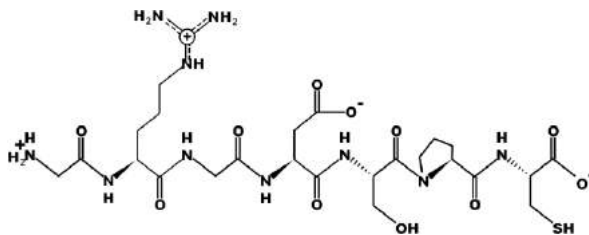
Figure 2.4 – Molecular structure of the synthesized RGD peptide.

The functionalization process, which is schematically illustrated in Figure 2.6, was based on the work of Porté-Durrieu *et al.* (2004) [18].
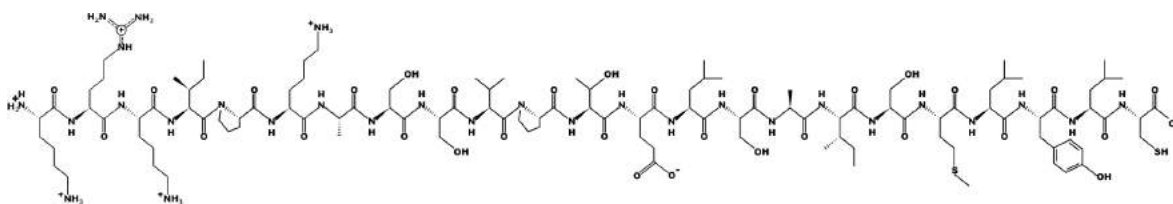
Figure 2.5 – Molecular structure of the BMP-2 mimetic peptide used.
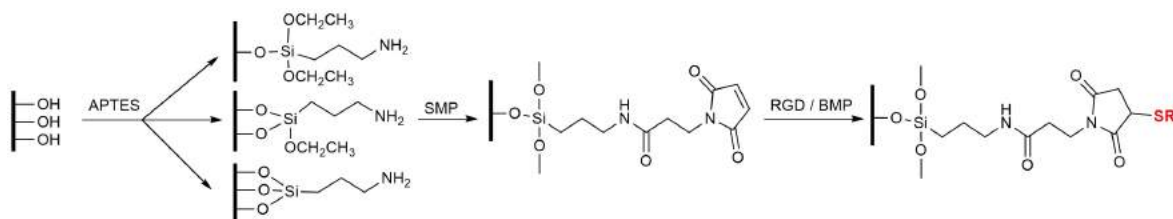
Figure 2.6 – Schematics of the process of surface functionalization of silicon with a peptide. Bonding of peptide highlighted in red.

A solution of hydrogen peroxide (30% wt) and concentrated sulfuric acid at a volume ratio 1:3 was used for cleaning and surface activation of the silicon samples for 30 min at Room Temperature (RT). Samples were thoroughly washed by sonication in deionized water. Cleaned samples were immediately transferred to a chamber under inert argon atmosphere where they were degassed under high vacuum (10^{-5} mbar) for 15 hours at 150 °C to further remove possible organic contamination.

Samples were subsequently silanized with APTES 10 % (v/v) in anhydrous hexane for 3 hours at RT, under inert atmosphere. After the reaction, samples were sonicated in anhydrous hexane to remove any excess of APTES molecules, and cured under high vacuum, during 2 hours at 100 °C.

Then, the samples were conjugated with a hetero-bifunctional crosslinker, SMP, at a concentration of 2 mM in Dimethylformamide (DMF) during 3 hours at RT. Once again samples were sonicated in the same solvent to remove molecules in excess and degassed under high vacuum for 2 hours at 70 °C.

Finally, RGD peptide, BMP-2 mimetic peptide or a combination of both peptides at a ratio 1:1 were immobilized on the surfaces. Samples were incubated for 24 hours at RT with solutions of peptides at 0.1 mM in deionized water. Samples were afterwards sonicated in deionized water to remove unbound peptides.

Samples were characterized by X-ray Photoelectron Spectroscopy (XPS) after each functionalization step to confirm that the process was successful. A K-Alpha (XPS system (ThermoFisher Scientific) with a monochromated AlKα source was utilized at 100 W, spot size of 400 μm.

2.4   hMSC studies

Bone marrow hMSC were cultured in basal medium and incubated in a humidified atmosphere at 37 °C and 5% CO_2. Basal medium consisted in αMEM supplemented with 10% Fetal Bovine Serum (FBS) and 1% penicillin-streptomycin.

Prior to cell seeding, the nanopatterned samples (both with or without grafted peptides) were sterilized overnight in 70% ethanol in a sterile environment, and subsequently washed thrice with PBS.

hMSCs were seeded at a density of 10^4 cells cm^{-2} in serum-free αMEM and incubated in such medium for 4 hours to avoid the sedimentation of a protein layer on the surface of the samples, impairing the adhesion of cells directly to nanotopographies. After that time, medium was changed to complete media, and cells were let grown during 2 weeks. Cell culture medium was replaced twice a week.

The cellular response to the modifications of surface chemistry and topography was characterized by immunofluorescence assays and RT-qPCR, techniques that allow, respectively, the study of expression of proteins and genes by cells. As previously referred, the expression of markers of osteogenic differentiation of hMSC, namely Runx2, Type I Collagen (Col1A1), OPN and OCN was investigated.

2.4.1   Immunofluorescence assays

At the defined time point, cell culture was stopped and cells fixed using a solution of 4% Paraformaldehyde (PFA) (incubation for 15 min). This step is fundamental at this stage since it ensures the preservation of cell morphology, strengthens their structure for further sample processing, and it inactivates the action of enzymes that could cause sample degradation.

Permeabilization of the fixed cells included two steps, *viz.* incubation in ice cold methanol for 15 min at -20 °C, followed by incubation in a solution of 0.5% TritonX 100 in PBS for 10 min at 4 °C. Afterwards, samples were incubated in a solution of 1% Bovine Serum Albumin (BSA) in PBS for 30 min at 37 °C to avoid nonspecific interactions of the antibodies with the cells undergoing analysis. Cells were then incubated with the primary antibodies (Table 2.1) in a humidified atmosphere, for 1 hour at 37 °C.

Table 2.1 – Primary antibodies used in immunofluorescence assays.

Antibody	Supplier	Marking
Runx2	Cell Signaling Technology	Osteoblastic differentiation (early phase)
OPN	Santa Cruz Biotechnology	Osteoblastic differentiation (late phase)

After washing with 0.05% Tween-20 in PBS, samples were incubated with the secondary antibodies – either AlexaFluor 488 or AlexaFluor 647 – for 1 hour at 37 °C in the dark, in a humidified atmosphere. Finally samples were mounted using Fluoroshield with 4',6-diamidino-2-phenylindole (DAPI) – for counterstaining of cell nuclei – mounting media.

Sample characterization was performed using a Leica DM5500B epifluorescence microscope controlled my Metamorph software. Briefly, a 40x oil immersion objective was used to observe and acquire images of the stained samples (excitation and emission spectra of the fluorochromes used is represented in Figure 2.7), which were later treated using ImageJ software, utilizing macros specifically written for the current project, having into consideration the intracellular localization of the proteins of interest.
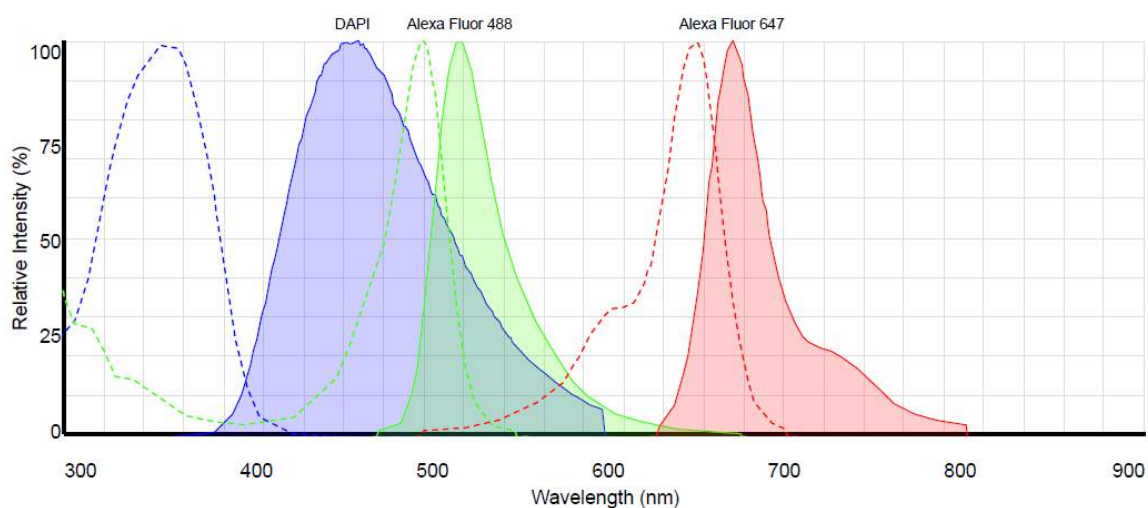
Figure 2.7 – Absorption and emission spectra of the fluorophores used in immunofluorescence.

2.4.2 RT-qPCR

In addition to immunofluorescence which allows the study of protein production by cells, RT-qPCR was also performed in order to investigate possible changes in ex-

pression of the genes involved in osteoblastic differentiation of hMSCs, namely Runx2, Col1A1, and OCN.

When performing RT-qPCR, it is fundamental to use reliable reference genes for normalization of gene expression between experiments. Since the expression of housekeeping genes has to be constant for all experimental conditions, expression of several candidates was evaluated prior to these studies. Finally, two reference genes were selected – Peptidylprolyl isomerase A (PPIA) and RPC53.

RT-qPCR requires the isolation of the total RNA from the cells of interest and its subsequent retrotranscription into Complementary Deoxyribonucleic Acid (cDNA), which can then be processed by RT-qPCR. However, since the quantity of RNA isolated from cells growing on each sample (of 1 cm^2), is not sufficient to run a RT-qPCR experiment, for each condition, cells from four chips were pooled together, ensuring that different genes can indeed be tested for the different conditions studied.

RT-qPCR requires, first of all, the extraction of total RNA from the cells in study. With that goal, two techniques were tested: a phenol-based approach, and a column method. The former, besides being more laborious than the column method, was also difficult to perform due to the low number of cells used (volume of cell pellet was so reduced, that in some steps it was not possible to even see it). Nevertheless, it was tested according to the protocol suggested by ThermoFisher Scientific (supplier of the TRIzol used for RNA extraction), and RNA was quantified using a spectrophotometer NanoDrop 1000 (ThermoFisher Scientific).

RNA extraction using RNeasy Mini Kit was performed according the manufacturer's protocol. Briefly, hMSCs were harvested using trypsin and lysed using the lysis buffer from the kit. Cell lysate was mixed with one volume of 70% ethanol, and centrifuged in a spin column. It was then incubated with a protein denaturating buffer. The spin column was centrifuged again, and samples were washed with RPE buffer. Finally RNA was eluted in RNase-free water. Genomic Deoxyribonucleic Acid (DNA) was removed using a TURBO DNA-free kit. NanoDrop 1000 spectrophotometer was used for RNA quantification. RNA integrity was investigated using an Agilent Bioanayzer 2100 with a RNA 6000 Nano kit.

Total RNA retrotranscription started with the incubation of the RNA solution with random primers for 5 min at 65 °C. Afterwards this solution was mixed with the retrotranscription master mix (retrotranscription buffer, dNTP mix, Reverse Transcriptase,

Ribonuclease in RNase-free water) and loaded in the thermal cycler. Retrotranscription included two main steps: incubation at 50 °C for 1 hour, followed by incubation at 72 °C for 15 min.

Aliquots of cDNA underwent dye-based RT-qPCR for the study of four genes (primers listed in Table 2.2). RT-qPCR was performed using 4 ng of cDNA, and primers at a concentration of 500 nM, for a final volume of 10 µL. The reaction was performed using a CFX Connect Real-Time PCR System (Bio-Rad). Forty amplification cycles were performed for each experiment, and consisted on incubating the solution at 95 °C for 5 seconds, followed by an incubation at 60 °C for 10 seconds. C_q values for the genes of interest were normalized against 2 reference genes which were selected using BestKeeper: PPIA and RPC53. Relative expression levels were calculated using the comparative method ($\Delta\Delta C_q$) and gene expression was normalized using flat silicon sample as control [147]. For each condition, three biological samples were tested, for which four technical replicates were done.

Table 2.2 – Primers used in RT-qPCR assays.

Gene	Primer sequence	Amplicon / bp
RPC53	5'-ACCCTGGCTGACCTGACAGA-3' (Forward) 5'-AGGAGTTGCACCCTTCCAGA-3' (Reverse)	71
PPIA	5'-CGGGTCCTGGCATCTTGT-3' (Forward) 5'-CAGTCTTGGCAGTGCAGATGA-3' (Reverse)	81
Runx2	5'-AAGTGCGGTGCAAACTTTCT-3' (Forward) 5'-TCTCGGTGGCTGGTAGTGA-3' (Reverse)	90
COL1A1	5'-ACATGTTCAGCTTTGTGGACC-3' (Forward) 5'-TGATTGGTGGGATGTCTTCGT-3' (Reverse)	117
OCN	5'-GACTGTGACGAGTTGGCTGA-3' (Forward) 5'-CTGGAGAGGAGCAGAACTGG-3' (Reverse)	119

2.4.3 Statistical analysis

Immunofluorescence data were analyses using ImageJ (NIH, USA) and GraphPad Prism (USA). RT-qPCR data were analyzed using CFX Maestro Software (Bio-Rad, USA). Significant differences were considered for p-values < 0.05 (* represents $p < 0.05$, ** $p < 0.01$, and *** $p < 0.001$).

3 | Results and Discussion

The main results obtained in this project regarding the preparation of nanoscale topographies, their functionalization with bioactive molecules, and the investigation of the impact of the bioactive topographies on hMSC behavior, are summarized in this chapter. From a materials perspective, the principal considerations behind these studies were the fabrication of highly uniform nanopillars arrays across large areas, as well as good homogeneity of peptides immobilized on the surface, due to the constraints imposed by biological studies. As previously referred, MSCs are highly sensitive to the surface characteristics of a biomaterial to which they are in contact with. Hence even reduced variations in surface chemistry or topography can lead to different responses from cells in culture. Moreover, biological assays, and in particular RT-qPCR, require the culture of a large cell number, and the replication of each experiment to ensure reproducibility.

Firstly, silicon nanopillar arrays were fabricated following an approach taking advantage of the ability to self-assemble of amphiphilic BCPs. The impact of such nanoarrays on the osteoblastic differentiation of bone marrow hMSCs from young and older donors was studied by immunofluorescence and RT-qPCR. This study is described in Section 3.1.

Considering that not only topography, but also the surface chemistry of biomaterials can be a tool for the modulation of cell response, the nanopillar arrays were functionalized with RGD peptide (to improve cell adhesion), BMP-2 peptidomimetics (to contribute to osteogenic differentiation), and the combination of both biomolecules. The differentiation of hMSCs when cultured on these biofunctionalized nanostructures was investigated and compared with the results obtained for bare nanotopographies. Section 3.2 summarizes this study.

Finally, Section 3.3 sums up different intermediate studies and optimizations which were fundamental for the achievement to the approach and results obtained that

granted the opportunity of preparing the two previous scientific articles. These includes the steps of optimization of the fabrication and surface functionalization of the nanoarrays, and of a basic understanding of hMSC behavior on the nanostructured materials.

3.1 hMSC response to Si nanopillar arrays

Controlled Nanoscale Topographies for Osteogenic Differentiation of Mesenchymal Stem Cells

Catarina R. Pedrosa [1-4], Didier Arl [4], Patrick Grysan [4], Irfan Khan[1-3,5], Stéphanie Durrieu [6,7], Sivashankar Krishnamoorthy [4,†,*], Marie-Christine Durrieu [1-3,†,*]

[1]Université de Bordeaux, Chimie et Biologie des Membranes et Nano-Objets (CBMN UMR5248), Pessac, France

[2]CNRS, CBMN UMR5248, Pessac, France

[3]Bordeaux INP, CBMN UMR5248, Pessac, France

[4]Materials Research and Technology (MRT) Department, Luxembourg Institute of Science and Technology (LIST), Belvaux, Luxembourg

[5]Dr. Panjwani Center for Molecular Medicine and Drug Research, International Center for Chemical and Biological Sciences, University of Karachi, Karachi, Pakistan

[6]Université de Bordeaux, ARNA laboratory, Bordeaux, France

[7]INSERM, U1212 – CNRS UMR 5320, ARNA laboratory, Bordeaux, France

*Equally contribution

[†] corresponding authors:

sivashankar.krishnamoorthy@list.lu, marie-christine.durrieu@inserm.fr

Abstract

Nanotopography with length scales of the order of extracellular matrix elements offers the possibility of regulating cell behavior. Investigation of the impact of nanotopography on cell response has been limited by inability to precisely control geometries, especially at high spatial resolutions, and across practically large areas. In this paper, we demonstrate well-controlled and periodic nanopillar arrays of silicon and investigate their impact on osteogenic differentiation of Human Mesenchymal Stem Cells (hMSCs). Silicon nanopillar arrays with critical dimensions in the range of 40-200 nm, exhibiting standard deviations below 15 % across full wafers were realized using self-assembly of Block Copolymer (BCP) colloids. Immunofluorescence and Quantitative Real Time Polymerase Chain Reaction (RT-qPCR) measurements reveal clear dependence of osteogenic differentiation of hMSCs on the diameter and periodicity of the arrays. Further, the differentiation of hMSCs was found to be dependent on the age of the donor. While osteoblastic differentiation was found to be promoted by the pillars with larger diameters and heights independent of donor age, they were found to be different for different spacings. Pillar arrays with smaller pitch promoted differentiation from young donor, while a larger spacing promoted those of an old donor. These findings can contribute for the development of personalized treatments of bone diseases, namely novel implant nanostructuring depending on patient age.

Keywords: nanoscale, topographies, block copolymer self-assembly, mesenchymal stem cells, osteogenic differentiation

1. Introduction

The interaction of a material with biological tissues is known to impact the initial protein adsorption on its surface, and the subsequent cell response, namely its adhesion, proliferation or death [25, 26]. Cell-material interface can be therefore seen as a complex system comprising three main players: material properties, molecules on the material surface, and adherent cells. The understanding of this interplay at the length scales of cells (microscale) or even molecules (nanoscale) is of extreme interest for the improvement of implants used in dentistry or orthopedics, for the improvement of the properties of other biomaterials for tissue engineering applications, and for the understanding of the *in vivo* cell microenvironment [3]. In particular, for bone tissue engineering, hMSCs appear as promising candidates for such studies, due to their ability to proliferate and to differentiate into various lineages, including osteoblastic lineage [4]. These stem cells can be isolated from different tissues, including bone marrow, adipose tissue, and dental tissues, but constitute a very heterogeneous cell population [5, 6]. Despite their limitations, hMSCs have been extensively used in the investigation of the mechanisms behind cell-material interactions [148, 149].

The interaction of a cell with a material topography was first observed in 1911 by Harrison, and it has been investigated at different scale regimes since then [150, 151]. Nanostructures ranging from holes, posts, grooves, etc. have been shown to elicit specific cell responses on several cell types, namely fibroblasts, neurons, osteoblasts and smooth muscle cells, without the need of additional growth factors or other chemical cues [9]. A very interesting study of the impact of nanoscale features on hMSC adhesion and differentiation was performed by Oh and colleagues who have demonstrated that titanium oxide nanotubes are able to promote osteogenic differentiation of these stem cells if their diameter is in the range of 70 - 100 nm, whereas nanotubes of lower diameter improve cell adhesion, but do not contribute for their differentiation [11]. However, in the same year, Park et al. showed completely opposite results for human osteoblast progenitor cells (cells of mesenchymal origin) cultured on similar nanostructures obtained after titanium anodization. In this study, cells showed enhanced adhesion and differentiation when grown on nanotubes of 15 nm diameter compared with larger feature diameter. Since the extracellular domain of an integrin is approximately 15 nm, the authors hypothesized that this dimension could support a maximum of cell responses to material surfaces and could be considered an 'universal spacing constant'

[104]. Nonetheless, it is important to note that osteogenic differentiation medium was utilized in this study (cells were initially cultured in basal medium, which was replaced by osteogenic medium at day 5), whereas Oh et al. cultured their hMSCs in basal medium (medium containing only the elements necessary for cell growth), and it is known that the chemical environment to which cells are subjected to (in this case, the composition of culture media) has a strong repercussion on cell response [152, 153]. Regarding the impact of nanotopographies on hMSC behavior, other studies have also shown that the organization of nanoscale features have an impact on cell fate. Nanopits created in polycaprolactone with 120 nm of diameter, spacing of 300 nm, and 100 nm depth organized in square lattice are able to maintain hMSC stemness for eight weeks, whereas the same pits with an offset of 50 nm from their true center (350 nm spacing) led to their differentiation into osteoblasts [118].

hMSC potential to undergo differentiation into different lineages has been shown to evolve with donor age [154, 155]. Aging is also known to be responsible for a lower proliferation rate of these cells, longer doubling time, greater extent of senescence and apoptosis [156–158]. Hence, the possible clinical use of MSCs from elderly people to treat bone diseases, such as osteoporosis, is highly impaired by these drawbacks. Yet, to the best of our knowledge, the investigation of osteogenic differentiation of MSCs from donors of different age on nanoscale topographies has not been performed. Since it is currently understood that material nanostructuring can convey specific cues to lead to a specific cell behavior, in the present study osteoblastic differentiation of hMSCs on nanopillar arrays was investigated for young and old donors, in order to have an insight on how such surfaces can be utilized for cell differentiation according to the patient age.

Although a myriad studies have been published on cell-material interactions, it is still unclear how each geometric parameter of a nanotopography influences hMSC differentiation into osteoblasts. As previously referred, conflicting findings are found in the literature, which can most probably be related with the fact that different protocols are used for cell culture, regulating hMSC fate in different ways. Therefore, in this study, we investigated the influence of controlled nanopillar arrays *per se* on the differentiation of hMSCs into the osteoblastic lineage. Cells were cultured on the nanostructured samples in a basal medium containing only the essential molecules for cell survival, to avoid the influence of any other parameter besides topology of the ma-

terial. The fabrication of the nanoscale pillar arrays was based on the self-assembly of amphiphilic diblock copolymers allowing the creation of polymeric masks for lithography. These micelle-based templates are an attractive alternative to other lithographic techniques, namely electron-beam lithography, due to their ease of formation on large surface areas, orthogonal control over geometric variables in steps down to 5 % of their mean value, short processing times, lower costs, and compatibility with a wide range of substrates [14]. Such lithographic technique is widely used in applications in nanoelectronics, quantum dot fabrication or nanowire formation as it allows the fabrication of ordered arrays of features at nanometer scale [159–162]. Still, few prior studies have showed the application of BCP self-assembly for the investigation of cell behavior, either for an accurate control of the presentation of molecules influencing cell adhesion or differentiation to the cells in culture, or for understanding the impact of nanoscale topographies on cells [10, 102, 110, 112, 163–165]. For example, Sjöstrom and McNamara have used BCP reverse micelles to create masks for the selective anodization of titanium surfaces, translating the polymeric template to the titanium sample, to study the impact of nanopillar height on the differentiation of hMSCs [10]. The nanopillars fabricated were distributed in a hexagonal array across the sample, and their top diameter was directly related with the diameter of the block copolymer micelles. The authors reported that titania pillars with diameters of 20 to 30 nm and 15 nm height are able to promote osteogenic differentiation of hMSCs cultured in basal medium, independently of feature separation (tested from 30 to 105 nm) and organization [10, 102, 112]. Contrarily, pillars of titanium dioxide with larger dimensions (diameter of 200 nm, spacing of 450 nm and height of 180 nm) showed a positive impact on the osteodifferentiation of hMSCs in a work performed by de Peppo [110]. It is worth noting that similar to the previously referred works of Oh and Park, the composition of cell culture media was not the same for all the studies, which may be one of the causes for divergences in the attained results. Whereas Sjöstrom and McNamara used a basal medium for hMSC culture, de Peppo used an osteogenic differentiation medium [10, 102, 110, 112]. Yet, there is still the need to investigate which geometric dimension (width, height, spacing) has more impact over hMSC behavior, particularly osteogenic differentiation. With this aim, nanoscale pillar arrays with fine-tunable dimensions and *quasi*-hexagonal distribution were fabricated on silicon substrates and used for the culture of hMSCs for investigation of their impact on cell fate. Even though

titanium and its alloys are the most common options as materials for bone implants due to their high biocompatibility and good mechanical properties, silicon was selected as model substrate for this study [28]. The extensive development of techniques for silicon structuration in electronics, its ease of patterning compared with titanium (or its alloys), together with its good biocompatibility, make it a more appropriate choice of material for the fabrication of features with dimensions of a few nanometers. The influence of the silicon nanostructures on cell behavior was studied by immunofluorescence and RT-qPCR. Such techniques allowed the evaluation of expression of markers related with osteogenic differentiation of hMSCs, namely Runt-related Transcription Factor 2 (Runx2), and Type I Collagen (Col1A1), expressed during early differentiation stages; Osteopontin (OPN), and Osteocalcin (OCN), expressed in late differentiation stages [24].

2. Experimental Section

Materials: Polystyrene-block-poly(2-vinylpyridine) (PS-b-P2VP) (M_w 55000-b-50000 g mol^{-1} and 248000-b-195000 g mol^{-1}, Polydispersity Indexs (PDIs) 1.05 and 1.08 respectively) were purchased from Polymer Source Inc (Montreal, Canada) and used without further purification. All solvents and surfactants were purchased from Sigma Aldrich, unless stated otherwise. Prime grade silicon wafers with a thermally grown silicon dioxide layer of 25 nm thickness were acquired from Siegert Wafer (Aachen, Germany). hMSCs from bone marrow were acquired from PromoCell (Heidelberg, Germany). Basal culture medium αMEM and Fetal Bovine Serum (FBS) were purchased from Gibco, ThermoFisher Scientific (France). All the reagents used in DNA digestion and RNA retrotranscription were acquired from ThermoFisher Scientific. The primers used for RT-qPCR were acquired at Sigma-Aldrich, whereas SsoAdvanced™ Universal SYBR® Green Supermix was purchased from Bio-Rad. Bovine Serum Albumin (BSA) and sample mounting media with DAPI (Fluoroshield™ with DAPI) were purchased from Sigma-Aldrich. The primary antibody against Runx2 (rabbit monoclonal) was purchased from Cell Signaling Technology Europe (Netherlands). Primary antibodies against Osteopontin (mouse monoclonal), Sox9, Type II Collagen (Col1A2) were purchased from Santa Cruz Biotechnology (USA). Primary antibodies against PPAR-γ and adiponectin were purchased from Abcam (France). Secondary antibodies were

acquired from Invitrogen, ThermoFisher Scientific.

Nanopillar fabrication: Si substrates with 25 nm of thermally grown oxide layers (25 nm SiO_2/Si) were cleaned by exposing them to oxygen plasma reactive ion etching (PlasmaTherm 790 RIE, FL, USA) at low bias, followed by use of carbon dioxide snow jet to any small sized particles prior to nanopillar preparation. Silicon nanopillar arrays were prepared using protocol described by Krishnamoorthy and coworkers [14]. Briefly, *quasi*-hexagonally ordered copolymer template with desired periodicity were obtained on 25 nm SiO_2/Si by spin-coating copolymer reverse micelle films from m-Xylene solutions. The substrates were then subjected to brief Ar/O_2 plasma descumming (18 sccm Ar / 2 sccm O_2, 4 mTorr, 4 W) for descumming the thin layer of polystyrene between the features, and subsequently transferred into thermal oxide layer by CHF_3/Ar (12 sccm CHF_3 / 38 sccm Ar, at -90 °C, 30 mTorr, 200 W) and then into Si by SF_6/O_2 plasma (50 sccm SF_6 / 10 sccm O_2, 10 mTorr, 25 W). Any remaining silica mask was removed by chemical etching with hydrofluoric acid (2 % v/v). The attained polymeric arrays as well as the nanopillar arrays were characterized in detail by AFM (Innova, Bruker, MA, USA) and SEM (FIB-SEM, Helios 650, FEI Company, OR, USA).

XPS characterization: The samples were characterized by X-ray Photoelectron Spectroscopy (XPS) to confirm that surface chemistry was identical on all surfaces. A K-Alpha (XPS system (ThermoFisher Scientific) with a monochromated AlKα source was utilized at 100 W, spot size of 400 µm. For each condition, 5 regions were analyzed to confirm the uniformity of the surface treatment.

Cell culture: Nanopillar chips were sterilized in 70 % ethanol overnight prior to their use as substrates for cell culture. hMSCs from bone marrow from donors of 36 or of 65 years old were seeded at passage 5 on the prepared samples at an initial density of 10^4 cells cm^{-2}. During the first 4 hours, cells were kept in serum-free medium to ensure cell interaction directly to the material surface, and incubated at 37 °C, 5 % CO_2. Afterwards, medium was changed to αMEM completed with 10 % FBS afterwards referred to as basal medium. Culture medium was replaced twice a week, and hMSCs were cultured for 2 weeks. Protein and gene expression were investigated by immunofluorescence assays and RT-qPCR.

Immunofluorescence assays: Immunostaining was performed after two weeks of cell culture to investigate the expression of osteogenic markers. Cells were fixed with paraformaldehyde (4 %), permeabilized with Triton-X 100 (0.5 %) and ice-cold methanol. To avoid non-specific interactions, samples were incubated with BSA (1 %). Samples were subsequently incubated with primary antibodies for 1 hour at 37 ℃. After washing with Tween-20 (0.05 %), samples were incubated for 1 hour at 37 ℃ with the secondary antibodies IgG coupled with AlexaFluor™ 488 and IgG coupled with AlexaFluor™ 647. Samples were again washed with a solution of Tween-20 (0.05 %) and mounted and counterstained with DAPI. Samples were observed using an epifluorescence microscope Leica DM5500B. Immunofluorescence assays for investigation of osteoblastic differentiation (Runx2 and OPN) were performed for n=3, considering the expression of at least 100 cells per sample. Adipogenic (PPAR-γand adiponectin) and chondrogenic (Sox9 and Col1A2) differentiation, the assays were only performed once (n=1), and the fluorescence signal was measured in 20 cells per sample.

RT-qPCR: Total RNA was isolated using RNeasy Mini Kit (QIAGEN), and genomic DNA was removed using TURBO DNA-free kit. Isolated RNA was quantified using a NanoDrop 1000 (ThermoFisher Scientific) and RNA integrity was assessed using an Agilent bioanalyzer 2100 with a RNA 6000 Nano kit (Agilent, USA). cDNA was synthesized from 500 ng of total RNA with the help of random primers and Maxima Reverse Transcriptase. RNA retrotranscription reaction included two main steps: incubation at 50 ℃ for one hour, followed by an incubation at 72 ℃ for 15 min. Aliquots of cDNA underwent dye-based RT-qPCR for the study of 4 genes (primers listed in Table 3.1). RT-qPCR was performed using 4 ng of cDNA, and primers at a concentration of 500 nM, for a final volume of 10 µL. RT-qPCR was performed using a CFX Connect™ Real-Time PCR System (Bio-Rad), using 2 genes of reference: RPC53 and PPIA. Forty PCR amplification cycles were performed for each experiment, and consisted on incubating the solution at 95 ℃ for 5 s, followed by an incubation at 60 ℃ for 10 s. *Cq* values for the genes of interest were normalized against 2 reference genes which were selected using BestKeeper: PPIA and RPC53 [147]. The relative expression levels were calculated using the comparative method ($\Delta\Delta Cq$) and the gene expression was normalized using flat Si sample as control. For each condition, 3 biological samples

were tested, for which 4 technical replicates were done.

Statistical analysis: All data are expressed as mean ± standard error of the mean, except if stated otherwise. Statistical analyses were performed using MatLab (Math-Works, USA) in the case of SEM data, NanoScope Analysis (Bruker, USA) for AFM data, CFX Maestro Software (Bio-Rad, USA) for RT-qPCR data, and GraphPad Prism (USA) for immunofluorescence data. Significant differences were considered for p-values < 0.05.

Table 3.1 – Primers used in RT-qPCR assays.

Gene	Primer sequence	Amplicon / bp
RPC53	5'-ACCCTGGCTGACCTGACAGA-3' (Forward)	71
	5'-AGGAGTTGCACCCTTCCAGA-3' (Reverse)	
PPIA	5'-CGGGTCCTGGCATCTTGT-3' (Forward)	81
	5'-CAGTCTTGGCAGTGCAGATGA-3' (Reverse)	
Runx2	5'-AAGTGCGGTGCAAACTTTCT-3' (Forward)	90
	5'-TCTCGGTGGCTGGTAGTGA-3' (Reverse)	
COL1A1	5'-ACATGTTCAGCTTTGTGGACC-3' (Forward)	117
	5'-TGATTGGTGGGATGTCTTCGT-3' (Reverse)	
OCN	5'-GACTGTGACGAGTTGGCTGA-3' (Forward)	119
	5'-CTGGAGAGGAGCAGAACTGG-3' (Reverse)	

3. Results

3.1. Nanopillar fabrication

The experimental strategy to obtain nanopillar arrays was based on the process developed by Krishnamoorthy [14]. Spin-coating of the PS-b-P2VP reverse micelle solutions on thoroughly cleaned substrates allowed the creation of organized, hexagonally distributed templates on 4-inch wafers, without the need for any further solvent annealing processing. The possibility of creating highly controlled nanoarrays on full wafers was one of the main considerations behind the choice of this process. hMSC culture and characterization required the utilization of hundreds of chips to ensure that experiments are reproducible and that statistically relevant results are obtained.

The use of BCPs of different M_w and block ratios allowed the fabrication of arrays of varying characteristic dimensions, as shown in Figure 3.1. Furthermore, the dependence of the array periodicity on evaporation speeds and solution concentrations was also used to arrive at desired pitch. Average feature diameter was determined for each condition over full wafer area by SEM, and the corresponding center-to-center distances, and feature densities by AFM, as summarized in Table 3.2.
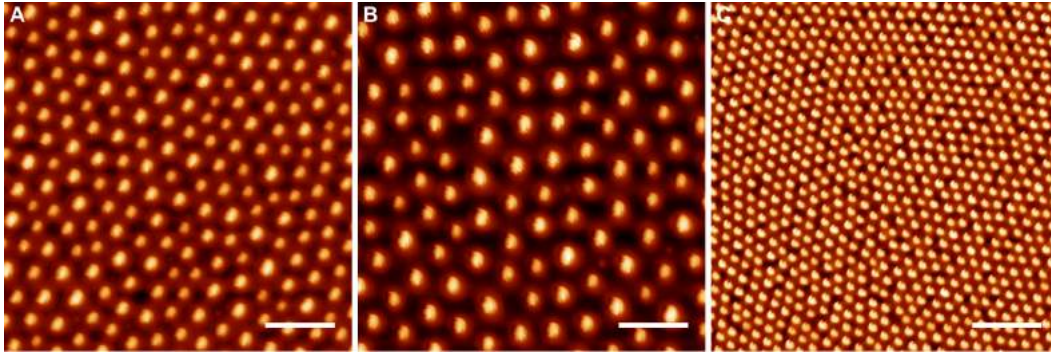
Figure 3.1 – Representative AFM images of BCP templates A, B, and C. Scale bar 400 nm.

Table 3.2 – Average characteristic dimensions of the produced BCP reverse micelle arrays. For simplicity, the arrays were labelled as A, B, and C. (Values represented as mean ± standard deviation)

Label	Mw/kg mol^{-1}	Spin speed/rpm	Diameter/nm	Periodicity / nm
A	148-b-195	2000	64 ± 6	135 ± 14
B	148-b-195	5000	60 ± 8	197 ± 23
C	55-b-50	5000	52 ± 4	68 ± 4

A small variation in periodicity, as well as a deviation from the expected hexagonal packing was observed during SEM characterization across the wafer surface, as depicted in Table 3, primarily due to different speeds of solvent evaporation during substrate coating. Nonetheless, the impact of such deviations on the full samples was within the range observed in previous studies, so it could be disregarded during the subsequent steps [14, 166]. Another interesting parameter to evaluate was the density of micelles on the surface, also presented in Table 3.3.

Table 3.3 – CVs for feature diameter and periodicity across wafers, percentage of features in a correct hexagonal packing, and density of features for the two BCP coated at 5000 rpm on 4 inch wafers.

Mw kg mol⁻¹	Region	CV diameter %	CV periodicity %	Coordination number 6	Density µm⁻²
55-b-50	Center	11	12	51	115
	Mid	9	10	65	136
	Edge	8	11	58	106
148-b-195	Center	12	12	62	26
	Mid	12	10	54	22
	Edge	10	12	57	21

Post etching characterization of the patterned wafers showed slight differences in feature dimensions from the initial ones. Once more, SEM was performed at full wafer scale to investigate the final characteristics of the nanopillar samples. These results are summarized in Table 3.4, and Figure 3.2 shows a detailed cross-section view of the 3 conditions with feature height of 80 nm. Wafers were subsequently treated with hydrofluoric acid and diced into 1 cm² chips to be compatible with ordinary cell culture systems.

Table 3.4 – Average characteristic dimensions of the produced nanopillar arrays. Labels A,B,C were defined in Table 3.2. 40/80 corresponds to the feature height.

Label	Diameter/nm	Periodicity/nm	Height/nm
A40	105 ± 14	137 ± 14	42 ± 6
A80	105 ± 14	141 ± 12	75 ± 6
B40	102 ± 10	196 ± 23	39 ± 3
B80	104 ± 13	201 ± 23	82 ± 6
C40	58 ± 4	70 ± 2	47 ± 4
C80	54 ± 5	73 ± 3	85 ± 5
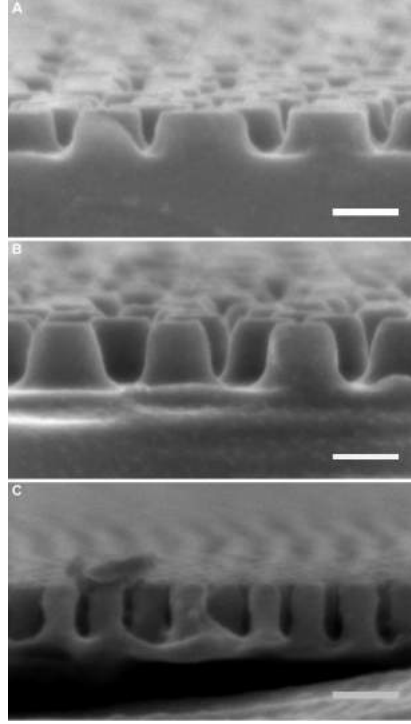
Figure 3.2 – Details of cross-sections of nanopillar samples obtained by SEM for the 3 conditions with feature height of 80 nm. (A) corresponds to A80, (B) to B80, and (C) to C80. (Scale bar 100 nm).

Since it is known that cells are able to sense and respond to not only surface topography, but also its chemistry, samples were characterized by XPS in order to verify that the surface chemistry to which hMSCs would be subjected to was the same for all arrays [167]. The results obtained after peak fitting are summarized in Table 3.5.

Table 3.5 – XPS characterization results of samples from all the topography conditions.

Element	Bond	eV	Atomic %						
			F	A40	A80	B40	B80	C40	C80
	Si^0	98.9-99.3	50.3	42.9	41.6	46.6	45.5	38.2	42.9
Si	$SiOC_3$	101.7-101.9	2.1	2.5	3.4	1.8	1.8	1.9	1.6
	SiO_2C_2, SiO_3C	102.7-103.1	5.6	9.1	7.7	8.0	8.3	11.2	9.5
	C-C	284.7-285.0	10.3	12.2	14.4	12.3	12.0	12.6	12.9
C	C-O	286.2-286.5	3.2	2.8	3.3	3.4	3.0	3.4	3.7
	COOH	288.7-289.2	0.6	0.7	0.7	0.8	0.5	0.6	0.4
N	$N-C-O_x$	401.7-401.8	0.3	0.2	0.2	0.3	0.3	0.3	0.5
O	O-C	532.2-532.6	27.6	29.6	28.7	26.8	28.6	31.8	28.5

70

3.2 Immunofluorescence

Immunofluorescence was performed to evaluate the expression of proteins known to be related with differentiation into the osteoblastic lineage (Runx2, OPN). The role and temporal expression of the selected markers during hMSC differentiation have been extensively studied previously, which makes them good tools for the understanding of cell response to the fabricated nanostructured materials [24, 99]. Since Runx2 is expressed in an early stage of differentiation into osteoblastic lineage, and OPN in a later phase, it could be possible to investigate to which extent the nanostructured samples were able to favor hMSC differentiation towards osteogenic lineage. Additionally, osteoblastic differentiation of hMSCs from a young and an old donor was characterized, to investigate possible variations according to nanotopography.

hMSC commitment to the osteoblastic lineage was characterized after 2 weeks of culture on the nanopatterned surfaces in basal media (example of marker expression on a flat silicon substrate in Figure 3.3). Fluorescence signal for each nanoarray was compared between topographies, and the results were normalized to flat control for simplicity (Figure 3.4).
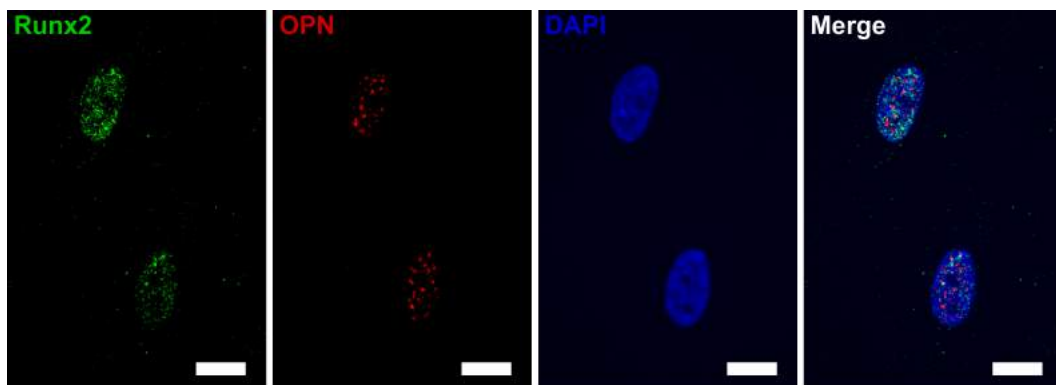
Figure 3.3 – Example of immunofluorescence images obtained for the characterization of Runx2 and OPN expression (nucleus marked with DAPI) for understanding of intracellular distribution of these proteins. (Scale bar 50 μm)

Expression of markers was found to be markedly different for cells from the two donors. Regarding the expression of the early osteogenic marker Runx2, hMSCs from a young donor (Figure 3.4 i) show a very high signal for the pattern A80 when compared with the remaining conditions (2.2 fold higher signal compared with F), whereas in the case of the old donor (Figure 3.4 ii) the highest Runx2 signal is observed on B80 samples (1.2 fold compared with control). This tendency is in agreement with the expression

71
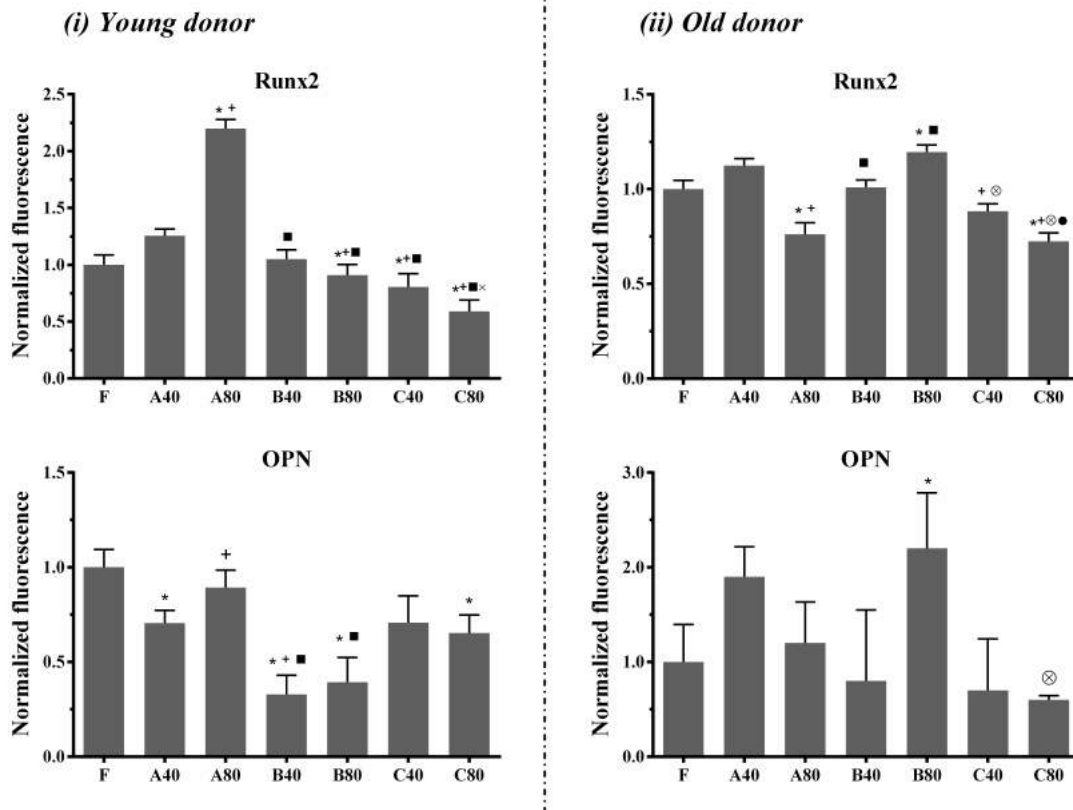
Figure 3.4 – Fluorescence intensity related with the expression of markers for osteoblastic differentiation of hMSCs after 2 weeks of culture on the nanostructured Si samples in basal medium was normalized against flat Si (F) control. (i) Expression in cells from young donor. (ii) Expression in cells from old donor. (* represents significant differences from F, + from A40, ■ from A80, ⊗ from B40, and × from B80).

of the late differentiation marker studied (OPN). In Figure 3.4 i, the fluorescence observed for young cells grown on A80 and C40 samples is similar to the fluorescence observed on control. However, all other nanostructures show a lower signal than the flat control. The population of cells from an old donor have a very heterogeneous expression of OPN (Figure 3.4 ii). Only significant differences are observed between F and B80, and B80 and C80. Expression on B80 pattern is approximately twice the signal observed on the control, which is consistent with the trend observed for Runx2.

To assess if the nanotopographies could potentially be used for the control of differentiation towards chondrocyte or adipocyte lineages, immunofluorescence assays were performed in parallel for cells from a young donor. Sox9 and Col1A2 were selected as markers of chondrogenic differentiation, whereas PPAR-γ and adiponectin were selected as markers of adipogenic differentiation of MSCs [88, 126]. No expression was observed regarding the adipogenic markers on any topography after 2 weeks (data

not shown), indicating that the selected nanoarrays are not suitable to guide hMSCs differentiation towards adipogenic lineage. On the other hand, immunostaining for chondrogenic markers indicated that the pattern B80 was particularly efficient on the enhancement of chondrogenic differentiation of hMSCs, as represented in Figure 3.5.
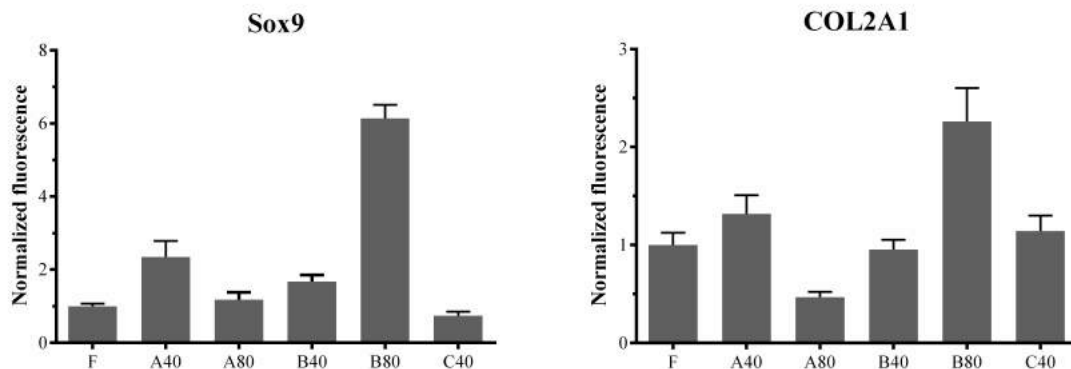
Figure 3.5 – Normalized fluorescence intensity observed hMSCs cultured for 2 weeks on nanotopographies related with the expression with Sox9 and Col1A2, the chondrogenic markers selected. Fluorescence was normalized against the flat control for simplicity of analysis.

3.3. RT-qPCR

Although it is not possible to ensure an accurate correlation between protein and gene expression, the selection of conditions for RT-qPCR assays was based on the previously obtained immunofluorescence results. The difficulties in correlating RNA and protein expression are mainly due to variations in RNA translation efficiency (which depends on ribosome density and their occupancy levels), protein stability, as well as experimental errors and noise associated to the assays [168, 169]. Nevertheless, since RT-qPCR experiments require a large amount of transcriptome, and it was necessary to pool cells from 4 cm² (4 samples for each condition) for such assays, it was decided that gene expression would only be evaluated for the conditions granting the best results for osteogenic differentiation in immunofluorescence. As different tendencies were observed for cells from young and old donors, the best condition after the interpretation of immunofluorescence results for the young donor, i.e., A80, and for the old donor, that is, B80 were selected for the subsequent studies.

After 2 weeks of culture on the selected nanopatterns, the differentiation stage of the cells was investigated. RT-qPCR is a very reliable technique which can detect gene expression even when a small quantity of RNA is available. The expression of genes

73

known to be expressed during early (Runx2, Col1A1) and late (OCN) stages of differentiation of hMSCs into osteoblasts was quantified to further investigate differences on the impact of the nanotopographies on hMSC differentiation (Figure 3.6).
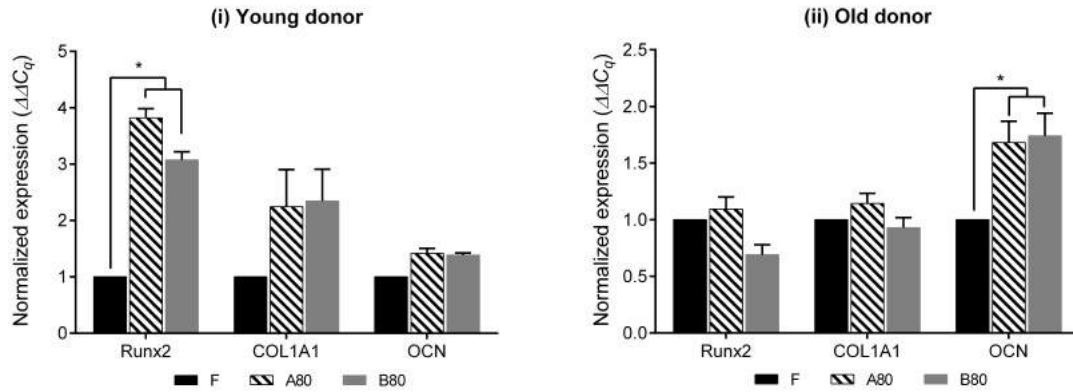
Figure 3.6 – Normalized gene expression ($\Delta\Delta Cq$ method) of Runx2, Col1A1, and OCN in hMSCs after 2 weeks of culture in basal medium on the nanostructured samples, taking the flat Si surface (F) as control. (n=4)

RT-qPCR results were in agreement with the trendlines observed in by immunofluorescence. Concerning hMSCs from a young donor, Runx2 expression was significantly higher on nanostructured samples, especially for the A80 condition. Similarly, the expression of Col1A1, an early differentiation marker as Runx2, appeared to be enhanced on the nanotopographies, though the difference from control was not significant (for the confidence interval selected). OCN expression was comparable on the three substrates. It is therefore reasonable to deduce that, after 2 weeks, these cells were in an early osteoblastic differentiation stage. An extra time point for a longer time in culture would be important to confirm such conclusion. It would be expected that a decrease in the expression of the early markers would decrease for A80 and B80, and that an increase of OCN would be observable.

On the other hand, cells from an older donor are able to differentiate faster on nanostructured surfaces than younger cells. In this case, OCN is over-expressed on nanostructured samples compared with the flat control, whereas Runx2 and Col1A1 expression are similar for all conditions.

4. Discussion

4.1. Nanoscale topographies

The modification of material properties, namely surface chemistry, topography, and mechanical characteristics, has been extensively investigated for the modulation of cell behavior, including their proliferation, adhesion, or differentiation abilities [97, 99, 168–170]. In particular, a controlled modification of the topography of a material at nanoscale has demonstrated to be a powerful tool to control the differentiation of hMSCs into the osteogenic lineage as reviewed by Donelly, or Gui [97, 171]. Still, the creation of nanoscale topographies using traditional lithographic methods used in nanoelectronics, as electron-beam and focused-ion-beam lithography, have inherent drawbacks including high costs and low throughput (due to the time required to process a small die) [15]. Conversely, the use of BCP templates for lithography proves to be a viable alternative, allowing high feature density, with dimensions down to a few nanometers, faster sample processing, and lower costs, since it allows the creation of organized templates *via* a simple spin-coating or dip-coating of BCP solution onto a material [15]. Typically, after coating on a substrate, these templates undergo a step of solvent or thermal annealing above their glass transition temperature, to improve the ordering of the domains on the surface [159, 172, 173]. Such step is very time-consuming, and can actually lead to some non-uniformity across large surface areas, as full wafers (since every extra step of a process introduces a degree of uncertainty). Thus, in this study, reverse micelles of PS-b-P2VP were prepared in a selective solvent, and used for lithography right after spin-coating, as described by Krishnamoorthy [173]. Nanoscale pillar arrays were successfully created on full wafers making use of BCP self-assembly properties and common nanofabrication techniques used in electronic applications. These arrays show low variability of their characteristic dimensions across the wafer surface, and high process reproducibility. It was possible to control each geometrical variable (diameter, spacing, height) independently in steps down to 5 % of their mean value. Such patterns can possibly be applied on different surfaces, namely non-planar, or soft polymeric materials, through the simple application of nanoimprint lithography, which allows a fast imprinting of the negative of the pattern on a resin that can be used as mask to etch the underlying substrate. Although the processing time was reduced following that approach, several parameters were carefully controlled to decrease variability of the coatings. Nevertheless, once the set of variables was fine-

tuned for the expected arrays, sample processing time was considerably shorter than the alternative approaches previously referred, and reproducible pillars arrays on full wafers were produced for subsequent use in cell culture.

The fact that it is known that hMSCs are able to sense differences in topography of a few nanometers, along with the need to replicate the cell studies to investigate statistically relevant cell responses, required the fabrication of highly reproducible and controlled nanoarrays on full wafers to have the sufficient number of nanostructured samples for cell culture. To the extent of our knowledge, there are no published studies on modulation of hMSCs differentiation via nanoscale topographies on Si. Investigation of hMSC response to similar nanoscale topographies is more commonly reported on titanium dioxide or polymeric surfaces[10, 110, 118]. Still, the fabricated Si nanostructures can potentially be interesting model surfaces for bone disease studies.

4.2. Investigation of hMSC response

Nanopillars of cylindrical shape (ensured by the use of a hard mask and highly controlled etching conditions) hexagonally distributed over a large surface (4 inch wafers) were obtained for hMSC studies. The possibility of controlling the characteristics of the fabricated arrays paved the way not only for the investigation of the most interesting range of dimensions of the nanofeatures able to favor hMSC osteogenic differentiation, but also which geometrical variable (diameter, spacing, height) would have more influence on this specific cell response.

The results obtained indicate that the geometries selected can promote osteogenic differentiation in a faster/greater extent than flat silicon surfaces. Still, differences in hMSC response to the patterns were observed between young and old donors. Whereas younger cells show increased expression of osteogenic markers on A80 samples (diameter 100 nm, height 80 nm, spacing 140 nm), old cells seem to differentiate faster on B80 patterns (same diameter and height, but larger spacing of 200 nm). Despite the difference in spacing, it can be concluded that hMSCs are more prone to undergo osteoblastic differentiation when cultured on Si nanopillars of larger dimensions (diameter 100 nm) than on pillars of smaller diameter (50 nm). Such result is in accordance with the work of de Peppo, who observed that larger nanofeature dimensions favor cell adhesion, spreading, and osteogenic differentiation of hMSCs [110]. Still, it is important to note that the substrate material were different (titanium vs. silicon in the

present work), and that, contrary to that study, in the present work cells were always kept in a basal medium, without any further supplementation, as dexamethasone or β-glycerophosphate, to induce osteodifferentiation. The different media composition is not expected to change the differentiation trend among the different patterns, but only the rate of cell differentiation. The utilization of basal media allowed the investigation of the influence of the material topography alone. Cells are not restricted to the differentiation into one lineage, but they can also proliferate maintaining their stemness, or differentiate into other lineages. On the contrary, the use of an osteogenic differentiation medium constrains cell differentiation to this specific lineage. In this case the effect of topography would be observed on the differentiation rate, with cells demonstrating a faster commitment towards the osteoblastic lineages on specific materials. Still it would be necessary to accurately deconvolute the effects of topography and induction medium on cell behavior, including several control samples, which can be simplified using a basal medium for the whole experiment.

Immunofluorescence results indicate that the population of cells from a younger donor is considerably more homogeneous than from older donor, which can be noticed especially by the length or error bars for OPN expression. hMSCs from the old donor show rather longer error bars, evidencing that the expression of OPN diverges within this cell population. Nonetheless, RT-qPCR results confirm that hMSCs from the old donor are undergoing osteoblastic differentiation, notably on the selected nanostructures. Cells cultured on the nanostructures show a significantly increased expression of OCN gene than cells cultured on flat control. Moreover, since the earlier differentiation markers were expressed at similar levels on all surfaces, it can be concluded that cells from the old donor were in a late stage of differentiation of MSC into osteoblasts [24]. On the other hand, RT-qPCR indicated that cells from a younger donor were differentiating preferentially on nanostructured surfaces. Yet, after 2 weeks, these cells were still in an early stage of differentiation and would need a longer time in culture to reach the stage of differentiation of older hMSCs. An extra time point for a longer time in culture would be important to confirm such conclusion. It would then be expected a decrease in the expression of the early markers for A80 and B80, and that an increase of OCN.

Regarding the investigation of chondrogenic commitment, immunofluorescence demonstrated that features with large diameter and height, and with increased separation

(B80) would be the more adequate for the promotion of chondrogenic differentiation of hMSCs from a young donor. To the extent of our knowledge, MSC differentiation into chondrocytes on 2D surfaces without any biochemical modification is hardly feasible [174]. Stimulation of chondrogenesis in vitro is normally achieved using hydrogels (3D) or 2D substrates coated with chondroitin, for instance [26, 174]. Further investigation of the possibility of using the nanopillar arrays prepared for studies of hMSCs differentiation towards chondrogenic lineage would be of great interest. It is also worth noting that the alterations in ability to differentiate of hMSCs with age. Although hMSCs from a young donor were more prone to commit towards chondrogenic lineage when cultured on B80 arrays, the hMSCs from an older donor registered higher expression of osteogenic markers on the same arrays.

We believe that the cell seeding protocol followed in the present study is more adequate for the investigation of the impact of nanoscale topographies on cell behavior than the approaches previously reported. Contrary to most protocols found in literature, where hMSCs are seeded on materials in media with serum, here, the cells are seeded and incubated during the first 4 hours in medium without serum [10, 110, 128]. Therefore, cells have time to adhere directly on the nanostructures, whereas if the medium was supplemented with any sera, proteins would adsorb firstly and very rapidly on the material surface, and cells would adhere to the material coated with proteins. In the latter case, it is important to note that the adsorption of proteins causes not only a change in surface chemistry (that is also known to have an impact on hMSC behavior), but also in surface topography, since the features and proteins have comparable dimensions. These changes demand further characterization of the surface, which can be very troublesome, as protein adsorption cannot be controlled accurately. To avoid such complications, cells can simply be incubated during the first hours after seeding in a medium without proteins, as described here.

5. Conclusions

Periodic nanopillar arrays with precise and independent control over diameter, height and periodicity were fabricated by pattern-transfer of self-assembled BCP colloidal templates into silicon substrates. The approach for nanofabrication provided unique advantage of high-throughput production of nanotopographies needed for cell-

culture, with no compromise on the resolution and quality of samples. The nanopillar arrays are found to enhance osteogenic differentiation of hMSCs, which in turn was found to be dependent on the age of the donor. Cells from young donors showed greatest level of differentiation on large pillar arrays with small pitch, whereas differentiation of cells from an older donor is further augmented on large pillars with larger pitch. Further study of the influence of age on differentiation potential, in parallel with a more exhaustive of the influence of nanoscale structures on the behavior of hMSCs from patients of various ages can contribute for the advance of personalized cell therapies, and in particular for the treatment of bone diseases and defects.

3.2 hMSC response to bioactive nanopillar arrays

Mesenchymal Stem Cell Differentiation Driven by Osteoinductive Bioactive Nanoscale Topographies

Catarina R. Pedrosa [1-4], Christel Chanseau [1-3], Christine Labrugère[5], Sivashankar Krishnamoorthy [4,†,*], Marie-Christine Durrieu [1-3,†,*]

[1]Université de Bordeaux, Chimie et Biologie des Membranes et Nano-Objets (CBMN UMR5248), Pessac, France

[2]CNRS, CBMN UMR5248, Pessac, France

[3]Bordeaux INP, CBMN UMR5248, Pessac, France

[4]Materials Research and Technology (MRT) Department, Luxembourg Institute of Science and Technology (LIST), Belvaux, Luxembourg

[5]PLACAMAT, UMS3626, CNRS - Université de Bordeaux, Pessac, France

*Equally contribution

† corresponding authors:

sivashankar.krishnamoorthy@list.lu, marie-christine.durrieu@inserm.fr

Under preparation

Abstract

Mesenchymal Stem Cells (MSCs) are very responsive to the characteristics of their surrounding microenvironment, which *in vivo* corresponds to their Extracellular Matrix (ECM). The possibility of mimicking such ECM, offers the opportunity to elicit specific cell behaviors, including MSC differentiation. The control of surface properties of a biomaterial, namely its topography and chemistry, at the same scale level of the components of the natural ECM (nanoscale) has the potential to be an effective way of accurately modulating cell response. Ordered nanoscale silicon pillar arrays of distinct periodicities were fabricated using reverse micelles of Block Copolymers (BCPs) on full wafers with standard deviations lower than 15 %. Synthetic peptides were covalently grafted on the nanoarrays to evaluate possible synergies between chemistry and topography on the osteogenic differentiation of MSCs. Silicon functionalization with RGD peptide and BMP-2 mimetic peptide lead to an enhancement of osteogenic differentiation compared with most of the other conditions, with similar levels of marker expression on all topographies. Still, bare nanopillar arrays of reduced pitch were found to be more effective on the promotion of MSC differentiation. Such findings highlight the relevance of investigating possibilities of engineering *in vitro* systems which can be fine-tuned according to the envisaged cell response.

Keywords: nanotopographies, surface functionalization, mimetic peptides, mesenchymal stem cells, osteogenic differentiation

1. Introduction

Biomaterials can be engineered to improve and actively guide cell response in a controlled way [1]. In order to achieve that, material surfaces should be able to mimic the *in vivo* microenvironment to which a cell is normally in contact with, i.e. to mimic its Extracellular Matrix (ECM) [2]. Since most cell-ECM interactions occur at nanoscale (e.g. growth factor-receptor interaction), the control of biomaterial surface properties at this scale level is of utmost importance. Most reported studies rely on the creation of nanoscale topographies or the fine-tuning of the surface chemistry of a material for the specific cell type under investigation to perform such control [12, 16, 26, 175]. Mesenchymal Stem Cell (MSC) have been one of the main cell types used in studies of modulation of cell fate through the control of materials design [16]. MSC culture *in vitro* is not so demanding as for other cell types, and these cells are a very promising option for bone tissue engineering applications, due to their osteogenic differentiation potential (among the potential to differentiate into other lineages, namely adipogenic or chondrogenic) [39].

Nanofabrication methods commonly used in electronic applications grant powerful tools to produce nanoscale features which can be translated into platforms for cell-substrate interaction studies. Though these fabrication methods can potentially be applied to a multitude of materials, state-of-art approaches are normally developed for silicon. Moreover, silicon is a material with adequate mechanical properties for applications in bone replacement, it is a non-toxic material, and any particles that may be released are degraded into silicic acid, which is also non-toxic [7, 8, 176]. Several variations of nanotopographies, namely pillars, rods, pits, grooves, wires, and their organization on the surface (*i.e.* ordered/disordered) have been used in studies investigation MSC differentiation towards osteoblastic lineage [10, 26, 112, 122, 177–179]. Yet, there is no consensus on which geometry is actually the most efficient on the promotion of osteogenic differentiation. Even studies investigating identical nanotopographies can report contradictory results [12, 13]. Material topography is indeed a very powerful parameter for the control of cell behavior, but it is necessary to keep in mind that any slight change of chemistry, both at the level of material surface or of culture media composition, as well as the origin of cells (*e.g.* adipose- or bone marrow-derived MSCs, or donor age) can have an impact on cell response of the same amplitude as topography [16, 148, 154].

Regarding the control of cell response through alterations of surface chemistry of a biomaterial, varied sized molecules, ranging from full-length mating ECM proteins to short linear peptides have been investigated as possible ways of assigning bioactivity to a material surface [16, 17, 28, 66]. Although the use of full length ECM proteins has been proven to be a successful way of controlling cell behavior on bioactive materials, their use has been hindered due to intrinsic limitations, including their poor stability, or safety concerns [17]. In order to overcome these shortcomings, small synthetic peptides encompassing only the amino acids necessary to support a particular biological activity have been investigated [66, 180]. These mimetic peptides can be synthesized with high purity, lower costs, and specific active sites can be engineered in a controlled way. Moreover, contrary to full-length proteins, conformation and density of short molecules can be controlled when bound to a material [17]. The most representative motif used for the improvement of cell adhesion is the sequence of amino acids arginine-glycine-aspartic acid (RGD), which *in vivo* mediates the binding of ECM proteins (e.g. fibronectin, vitronectin) to transmembrane integrin receptors [18, 19, 54]. Additionally, it has been reported that RGD peptide can also contribute for osteogenic differentiation of Human Mesenchymal Stem Cell (hMSC) and osteoblast-like cells when cells are maintained in osteogenic differentiation media [181, 182]. Nevertheless, the growth factors most commonly used for the enhancement of osteogenic differentiation of MSCs are Bone Morphogenetic Protein (BMP), and in particular Bone Morphogenetic Protein 2 (BMP-2) [164, 183]. Due to the factors previously referred, most studies take advantage of only the sequence responsible for the osteogenic activity of this molecule to functionalize biomaterials for bone tissue engineering applications [17, 22, 184]. The combination of a peptide promoting cell adhesion with one promoting cell differentiation for the co-functionalization of a biomaterial surface has been reported to further enhance differentiation when compared with the grafting of only one peptide sequence, such as a BMP-2 mimetic peptide [20, 21, 23, 185]. A few studies can be found in the literature reporting also synergistic effects of combining nanotopographies with chemical cues on osteogenic differentiation of MSCs or osteoblast progenitors [186–188].

Guided by such considerations, this study aimed at investigating osteogenic differentiation of hMSCs cultured on bare nanoscale pillar arrays or functionalized with a RGD peptide and/or a BMP-2 mimetic peptide. The prepared surfaces were carefully characterized by Atomic Force Microscopy (AFM), Scanning Electron Microscopy (SEM)

and X-ray Photoelectron Spectroscopy (XPS). To evaluate to which extent hMSC differentiation was promoted, the expression of early (Runt-related Transcription Factor 2 (Runx2), and Type I Collagen (Col1A1)) and late (Osteopontin (OPN), and Osteocalcin (OCN)) osteogenic differentiation markers was investigated by immunofluorescence and Quantitative Real Time Polymerase Chain Reaction (RT-qPCR).

2. Experimental Section

Materials: Polystyrene-block-poly(2-vinylpyridine) (PS-b-P2VP) (Molecular Weight (M_w) 248000-b-195000 g mol^{-1}, Polydispersity Index (PDI) 1.08) was purchased from Polymer Source Inc (Montreal, Canada) and used without further purification. All solvents, acids and bases were purchased from Sigma Aldrich, unless stated otherwise. Prime grade silicon wafers with 25 nm thick thermally grown SiO_2 film were acquired from Siegert Wafer (Germany). 3-aminopropyltriethoxysilane (APTES) and 3-(Maleimido)propionic acid N-hydroxysuccinimide ester (SMP) were purchased from Sigma Aldrich. Peptides used for surface functionalization (GRGDSPC, afterwards designated as RGD peptide, and KRKIPKASSVPTELSAISMLYLC, afterwards designated as BMP-2 mimetic peptide) were synthesized by Genecust (Luxembourg). Bone marrow-derived Human Mesenchymal Stem Cells (hMSCs) were acquired from Promo-Cell (Germany). Basal culture medium αMEM and Fetal Bovine Serum (FBS) were purchased from Gibco, ThermoFisher Scientific. All the reagents used in DNA digestion and RNA retrotranscription were acquired from ThermoFisher Scientific. Primers used for RT-qPCR were acquired at Sigma-Aldrich. SsoAdvanced™ Universal SYBR® Green Supermix was purchased from Bio-Rad. Bovine Serum Albumin (BSA) and sample mounting media with DAPI (Fluoroshield™ with DAPI) were purchased from Sigma-Aldrich. Primary antibody against Runt-related Transcription Factor 2 (Runx2) (rabbit monoclonal) was purchased from Cell Signaling Technology Europe (Netherlands) and the primary antibody against Osteopontin (OPN) (mouse monoclonal) from Santa Cruz Biotechnology (USA). Secondary antibodies were acquired from Invitrogen, ThermoFisher Scientific.

Nanopillar fabrication: Oxygen plasma Reactive Ion Etching (RIE) (PlasmaTherm 790 RIE, USA) at low DC bias was used for removal of organic contamination from

the substrates, followed by CO_2 snow jet cleaning to remove any remaining small sized particles. Silicon nanopillar arrays were prepared using protocol described by Krishnamoorthy (2011) [14]. PS-b-P2VP was dissolved in anhydrous m-Xylene at a concentration of 0.5 wt% and stirred for 24 h. The reverse micelles obtained were spin-coated on clean wafers at 2000 or 5000 rpm to produce polymer templates distinct periodicities. Samples were afterwards subjected to brief Ar/O_2 plasma descumming (18 sccm Ar / 2 sccm O_2, 4 mTorr, 4 W) for descumming the thin layer of polystyrene between the features, and subsequently transferred into thermal oxide layer by CHF_3/Ar (12 sccm CHF_3 / 38 sccm Ar, at -90 °C, 30 mTorr, 200 W) and then into Si by SF_6/O_2 plasma (50 sccm SF_6 / 10 sccm O_2, 10 mTorr, 25 W). Remaining silica was removed by chemical etching with hydrofluoric acid (2 % v/v). After each step, samples were characterized in detail by AFM (Innova, Bruker, MA, USA) and SEM (FIB- SEM, Helios 650, FEI Company, OR, USA). Nanopatterned wafers were diced in 1 cm^2 chips for easier utilization in systems for cell culture.

Surface functionalization: Sample surfaces were activated in solutions of hydrogen peroxide (30 wt %) and sulfuric acid at a ratio 1:4 for 30 min. Samples were then consecutively sonicated in 5 baths of deionized water for 10 min. Surface functionalization protocol is schematically represented in Figure 3.7, and was based on the work of Porté-Durrieu (2004) [189]. Immediately after surface activation, samples were degassed for 15 h under high vacuum (10^{-5} mbar) at 150 °C. This treatment was followed by a silanization step under an inert atmosphere using a solution of APTES 2 % (v/v) in anhydrous hexane for 3 h. Samples were sonicated twice 15 min in anhydrous hexane to remove silane molecules in excess, and cured for 2 h under high vacuum (10^{-5} mbar) at 100 °C. Amine-terminated surfaces were then conjugated with the SMP crosslinker at a concentration of 4 mM in Dimethylformamide (DMF) for 3 h. Again, samples were sonicated twice 15 min in DMF to remove SMP molecules in excess, and dried for 2 h under high vacuum (10^{-5} mbar) at 70 °C. Finally, RGD peptide, BMP-2 mimetic peptide or a combination of both peptides at a ratio 1:1 were immobilized on the surfaces. Samples were incubated for 24 h with solutions of peptides at 0.1 mM in deionized water. Samples were afterwards sonicated in deionized water to remove unbound peptides and stored in Phosphate Buffered Saline (PBS).
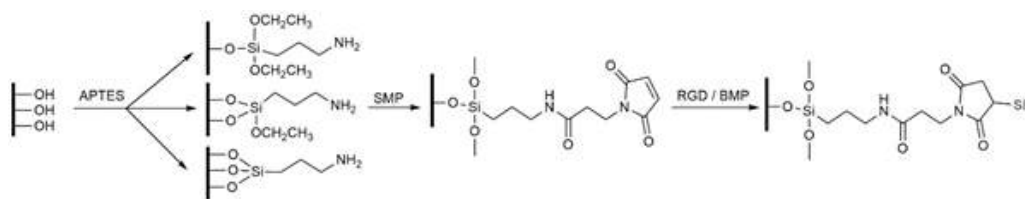
Figure 3.7 – Schematic representation of protocol of surface functionalization. R represents the peptide of interest bound to the crosslinker SMP.

XPS characterization: Samples were characterized by X-ray Photoelectron Spectroscopy (XPS) before surface modification and after each functionalization step to confirm that the reactions were successful. XPS was performed (K-Alpha, ThermoFisher Scientific) with a monochromated AlKα source was utilized at 100 W, spot size of 400 μm. For each condition, five regions were analyzed to confirm the uniformity of the surface treatment.

Cell culture: Nanostructured chips were sterilized in 70 % ethanol overnight prior to their use as in cell culture. Bone marrow hMSCs were seeded at passage five at an initial density of 10^4 cells cm^{-2} on the samples. Cells were seeded in serum-free medium to ensure cell interaction directly to the material, and incubated at 37 °C, 5 % CO_2. After 4 h, medium was changed to αMEM completed with 10 % FBS, which will afterwards be referred as basal medium. Culture medium was replaced twice a week, and hMSCs were cultured for 2 weeks.

Immunofluorescence assays: Immunostaining was performed after the 2 weeks of cell culture to investigate the expression of the selected osteogenic markers. Cells were fixed with paraformaldehyde (4 % v/v), permeabilized with ice-cold methanol and Triton-X 100 (0.5 % v/v). Samples were subsequently incubated with BSA (1 % v/v) to avoid possible non-specific interactions. Samples were then incubated with the primary antibodies against Runx2 and OPN for 1 h at 37 °C. After washing with Tween-20 (0.05 % v/v), samples were incubated for 1 h at 37 °C with the secondary antibodies goat anti-rabbit IgG coupled with AlexaFluor™ 488 and goat anti-mouse IgG coupled with AlexaFluor™ 647. Samples were again washed with a solution of Tween-20 and mounted and counterstained with DAPI. Samples were observed using an epifluorescence microscope Leica DM5500B.

RT-qPCR: Total RNA was isolated using RNeasy Mini Kit, and genomic DNA was removed using TURBO DNA-free kit. Total RNA was quantified using spectrophotometer NanoDrop 1000 (ThermoFisher Scientific) and RNA integrity was evaluated using an Agilent bioanalyzer 2100 with a RNA 6000 Nano kit (Agilent, USA). cDNA was synthesized from 500 ng of total RNA with the help of random primers and Maxima Reverse Transcriptase. RNA retrotranscription reaction was performed in 2 steps: incubation at 50 °C for 1 h, and subsequent incubation at 72 °C for 15 min. Aliquots of cDNA underwent dye-based RT-qPCR for the study of 3 genes expressed during osteoblastic differentiation (primers listed in Table 3.6). RT-qPCR was performed using 4 ng of c DNA, and primers at a concentration of 500 nM, for a final volume of 10 μL. RT-qPCR was performed using a CFX Connect™ Real-Time PCR System (Bio-Rad), using 2 genes of reference: RPC53 and PPIA. 40 PCR amplification cycles were performed for each experiment, and consisted on incubating the solution at 95 °C for 5 s, followed by an incubation at 60 °C for 10 s. *Cq* values for the genes of interest were normalized against 2 reference genes which were selected using BestKeeper: PPIA and RPC53. The relative expression levels were calculated using the comparative method ($\Delta\Delta Cq$) and gene expression was normalized using flat Si sample as control. For each condition, 2 replicates were considered.

Table 3.6 – Primers used in RT-qPCR assays.

Gene	Primer sequence	Amplicon / bp
RPC53	5'-ACCCTGGCTGACCTGACAGA-3' (Forward)	71
	5'-AGGAGTTGCACCCTTCCAGA-3' (Reverse)	
PPIA	5'-CGGGTCCTGGCATCTTGT-3' (Forward)	81
	5'-CAGTCTTGGCAGTGCAGATGA-3' (Reverse)	
Runx2	5'-AAGTGCGGTGCAAACTTTCT-3' (Forward)	90
	5'-TCTCGGTGGCTGGTAGTGA-3' (Reverse)	
COL1A1	5'-ACATGTTCAGCTTTGTGGACC-3' (Forward)	117
	5'-TGATTGGTGGGATGTCTTCGT-3' (Reverse)	
OCN	5'-GACTGTGACGAGTTGGCTGA-3' (Forward)	119
	5'-CTGGAGAGGAGCAGAACTGG-3' (Reverse)	

Statistical analysis: All data are expressed as mean ± standard error of the mean,

except if stated otherwise. Statistical analyses were performed using CFX Maestro Software (Bio-Rad, USA) for RT-qPCR data, and GraphPad Prism (USA) for immunofluorescence data. Significant differences were considered for p-values < 0.05.

3. Results

3.1 Preparation of bioactive nanostructured samples

Silicon nanopillar arrays were fabricated on full wafers with high uniformity and reproducibility. Such characteristics were made possible due to the ability of PS-b-P2VP to self-assemble forming organized, hexagonally distributed templates, with possibility of varying each geometrical variable in steps lower than 5 % of its mean value, as developed by Krishnamoorthy et al. (2011) [14]. Briefly, solutions of reverse micelles were spin-coated on the substrates at 2 distinct speeds for the preparation of polymeric templates of identical diameter, but different periodicity, as summarized in Table 3.7. The SiO$_2$ thin film was used as an intermediate mask to improve the geometric characteristics of the Si nanopillars, due to its superior selectivity for Si etching than the initial BCP film, while preserving the dimensions of the initial reverse micelles. SEM characterization demonstrated (Figure 3.8) that feature heights were close to the 80 nm height originally defined (Table 3.7).
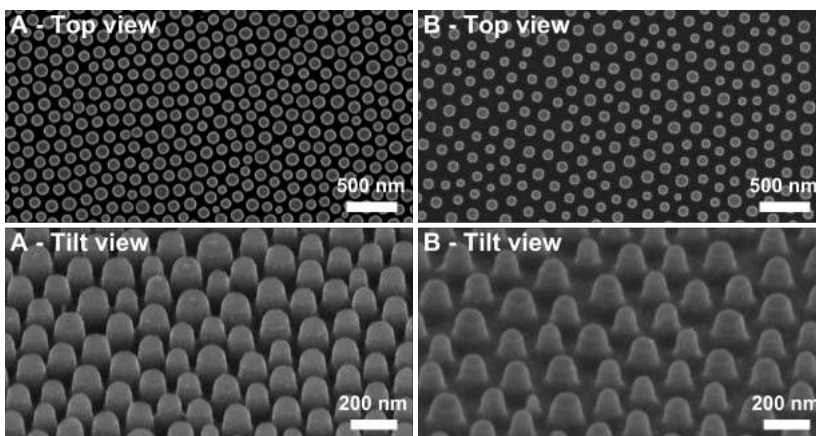
Figure 3.8 – Detail of SEM images of the fabricated nanopillars at top and tilted views.

The success of the process of surface modification was confirmed by XPS after each step on flat Si substrates (Table 3.8) and extrapolated to the nanostructured samples, taking into account the chemical composition observed before and after peptide grafting.

Table 3.7 – Characteristic dimensions of the Si nanopillar arrays determined by AFM and SEM

Label	Spin speed / rpm	Diameter/nm	Periodicity/nm	Height/nm
A	2000	105 ± 14	141 ± 12	75 ± 6
B	5000	104 ± 13	201 ± 23	82 ± 6

Table 3.8 – Chemical surface composition determined by XPS at each step of grafting of BMP-2 mimetic peptide and RGD peptide on flat silicon (represented in Figure 1).

Atomic %	Clean Si	+APTES	+SMP	BMP-2	RGD
Si	56.4 ± 0.2	47.8 ± 0.3	47.8 ± 0.3	43.5 ± 0.4	40.1 ± 0.3
C	12.6 ± 1.3	23.0 ± 0.9	21.2 ± 0.8	27.4 ± 1.1	28.5 ± 0.9
N	0.2 ± 0.1	1.7 ± 0.1	1.7 ± 0.1	3.7 ± 0.2	2.8 ± 0.1
O	30.8 ± 0.6	27.5 ± 0.3	29.3 ± 0.6	25.4 ± 0.2	28.6 ± 0.2
N/C	*0.02*	*0.07*	*0.08*	*0.14*	*0.10*

High resolution spectra for C1s and N1s at each step of surface functionalization are represented in Figure 3.9. Silicon substrates characterized before functionalization exhibited high silicon (56.4 %) and oxygen (30.8 %) percentages, characteristic of the native silicon oxide layer of the substrates. A slight carbon contamination, which was also observed (12.6 %), is impossible to avoid, even if the samples were only exposed to air during mounting on XPS sample holder. Still, this value was within the same set of values reported in previous studies, therefore being in an acceptable range [2, 18, 20]. Nitrogen content was 0.2 %, a value corresponding to measurements at the detection limits of the XPS system.

After silanization, XPS surveys show a decrease in Si content (to 47.8 %), a significant increase in carbon content (to 23.0 %) and the appearance of nitrogen (1.7 %) associated with the formation of an APTES layer on the surface. High resolution C1s spectrum indicated an increase in the number of C-C bounds compared with the clean substrate. Moreover, C-NH$_2$ bonds were observed in the N1s high resolution spectrum, confirming the existence of the silane layer on the treated samples.
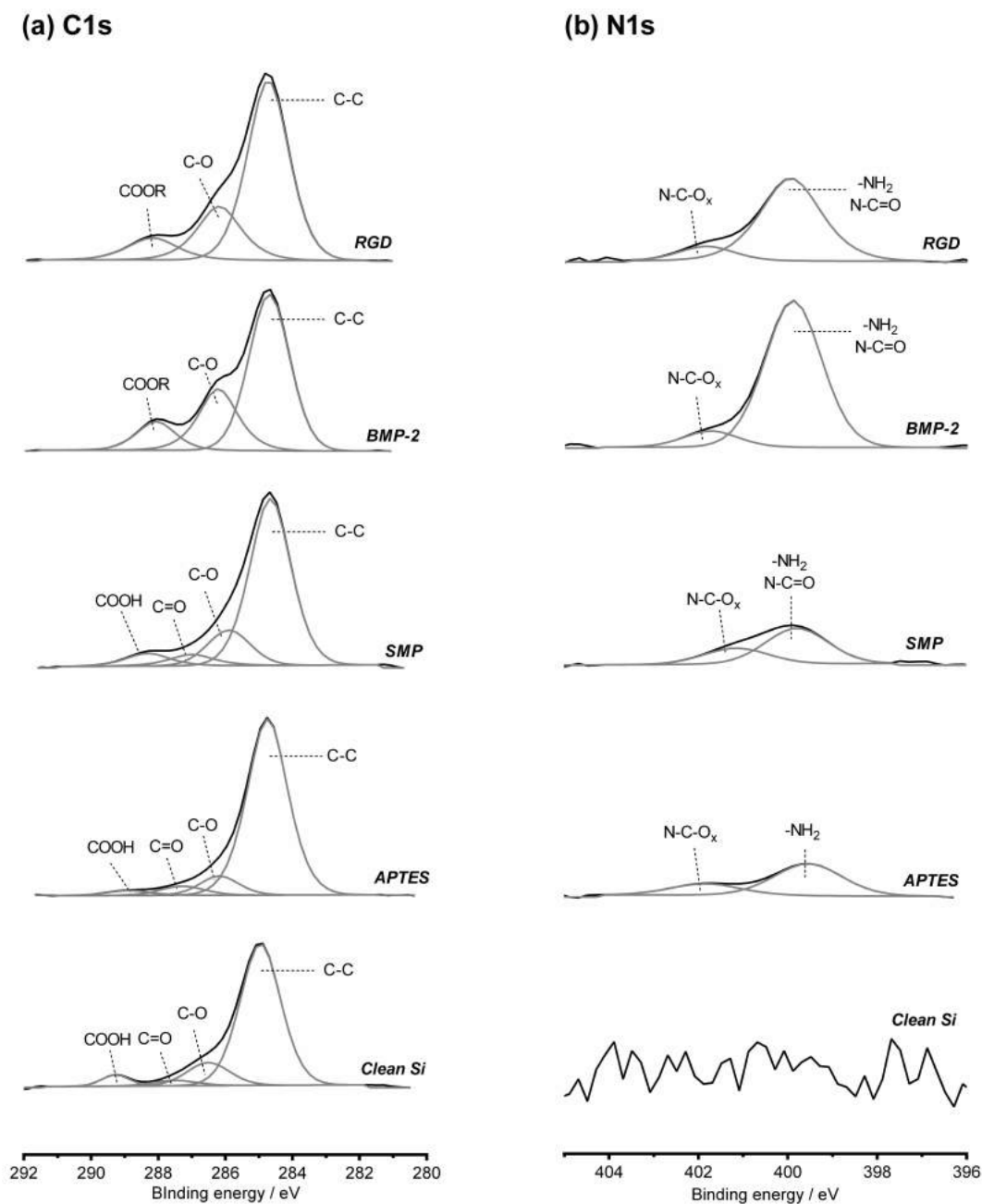
Figure 3.9 – Deconvolution of high resolution XPS spectra of C1s (a) and N1s (b) after each step of surface functionalization for the grafting of RGD or BMP-2 mimetic peptide on flat Silicon samples.

The slight increase of oxygen (to 29.3 %) after reaction of the amine-terminated surfaces with the SMP indicates the presence of the crosslinker on the sample surfaces. Nitrogen remained constant after binding of SMP, which can be a consequence of the existence of only one nitrogen atom in a SMP molecule, which is not sufficient to contribute to a change in the overall percentages of elemental composition. A minor decrease in carbon content was verified, even if each crosslinker molecule has seven

carbon atoms. This fact may be related with a reduced carbon contamination on the new surfaces than on silanized surfaces.

Finally, peptides were bound to the maleimide group of the SMP crosslinker via their cysteine amino acid. The significant decrease on the silicon content observed after BMP-2 mimetic peptide binding can be associated with the large dimensions of this molecule which prevent the possibility of interactions of the x-rays with the silicon substrate. An increase in carbon (to 27.4 %) and nitrogen content (to 3.7 %) are also linked to the immobilization of the mimetic peptide which is constituted by a large number of C and N atoms. Additionally, high resolution C1s spectra shows an increase in C-C bonds. The significant increase of N-C=O bonds alongside with the appearance of N-C=O$_x$ of higher energy in the high resolution N1s spectrum, further confirms the immobilization of the BMP-2 mimetic peptide on the surface. A similar tendency was detected after the grafting of RGD peptide. It is worth noting the reduced standard deviations observed in all measurements, confirming the uniformity of immobilization of the molecules on the surfaces.

In order to confirm that the surface chemistry of the different samples was identical, samples were characterized by XPS right after cleaning, and after functionalization with RGD peptide or BMP-2 mimetic peptide. The results obtained after the deconvolution of the high resolution spectra for the case of BMP-2 mimetic peptide grafting are summarized in Table 3.9. Similar results were obtained for RGD peptide grafting.

3.2. Immunofluorescence assays

After two weeks of cell culture on the selected nanostructures either plain or functionalized with RGD or/and BMP-2 mimetic peptide, hMSCs were fixed and stained to investigate the expression of Runx2, an early osteogenic differentiation marker, and OPN, a marker of late osteogenic differentiation, by immunofluorescence. These results are summarized in Figure 3.10. Figure 3.11 represents an example of the intracellular distribution of the markers selected.

It was observed that, independently of the surface chemistry (RGD or/and BMP-2 functionalization), Runx2 expression was higher on nanotopography A (pillars with reduced spacing). Regarding flat silicon surfaces, it was observed that expression of Runx2 could be enhanced if the substrate was functionalized with RGD peptide or, to a lesser extent, co-functionalized with both peptides. Still, for all cases the fluo-

Table 3.9 – Deconvolution of high resolution XPS spectra for the three surfaces analyzed flat, A, and B, before functionalization (Clean) and after BMP-2 mimetic peptide grafting (BMP-2).

At%	Bond	F		A		B	
		Clean	BMP-2	Clean	BMP-2	Clean	BMP-2
Si	Si^0	50.3	39.1	41.6	33.5	45.5	32.9
	$SiOC_3$	2.1	2.3	3.4	4.1	1.8	4.0
	SiO_2C_2, SiO_3C	5.6	5.2	7.7	5.2	8.3	4.6
C	C-C	10.3	16.8	14.4	19.1	12	19.6
	C-O	3.2	5.3	3.3	5.1	3.0	6.1
	COOR	0	3.7	0	3.2	0	3.6
	COOH	0.6	0	0.7	0	0.5	0
N	NH_2-C,N-C=O	0	3.2	0	3.0	0	2.9
	$N-C-O_x$	0.3	0.2	0.2	0.4	0.3	0.5
O	O=C	0.4	6.5	0.3	4.7	0	6.0
	O-C	27.3	17.7	28.4	21.7	28.5	19.9

rescence signal detected on flat samples was approximately half of the signal observed on nanoarrays of type A. Runx2 expression on bare B nanotopographies was similar to the level observed on plain flat surfaces. The same was noticeable for surface B grafted with RGD peptide and flat modified with the same peptide. Yet, the grafting of BMP-2 mimetic peptide or the combination of the 2 peptides leads to an increase in expression of Runx2 on nanostructures B (approximately 2-fold).

On the other hand, OPN expression appeared to be dependent not only on the topography but also strongly on surface chemistry, with higher fluorescence signal being detected on non-modified flat and on nanopillars with reduced pitch (condition A). The change of surface chemistry of these 2 topologies (flat and nanoarray A), achieved via the grafting of the peptides induced a decrease in OPN expression to roughly two thirds of the signal on plain surfaces. Such decrease was notably evident for the nanoarray A modified with RGD peptide.

3.3. RT-qPCR assays

After 2 weeks of cell culture, total RNA was extracted, and RT-qPCR was performed to investigate the expression of the selected markers. Considering the large number of conditions to be compared, for each gene, results were normalized to a flat, bare silicon control. Hence, differences between nanotopographies and/or surface

Figure 3.10 – Expression of Runx2 and OPN from hMSCs cultured for 2 weeks on plain silicon (Clean Si) or functionalized samples with RGD peptide (RGD), BMP-2 mimetic peptide (BMP), or a combination of the 2 molecules (RGDBMP). Tables summarize significant differences between conditions (* represents $p < 0.05$, ** $p < 0.01$, *** $p < 0.001$).

modifications can be easily distinguished. These results are summarized in Figure 3.12.

It is interesting to note that similar levels of gene expression could be obtained on all topographies when RGD peptide and BMP-2 mimetic peptide were co-immobilized on the different surfaces, and that such level of expression was indeed the maximum observed.

Taking a closer look at the results, for the case of non-functionalized surfaces, nanostructures A appeared to be the most relevant for promotion of osteogenic differentiation of hMSCs. The expression of the 3 markers on nanopillars of type A was significantly higher than their expression on flat substrates (as high as 4-fold in the case of Runx2). Nevertheless, the differences in expression between cells cultured on nanoarrays A and B were not significant for the interval of confidence considered, yet gene expression on B samples was slightly lower.

Functionalization with RGD peptide caused an increase in expression, especially of early differentiation markers (Runx2 and Col1A1). OCN level suffered a significant increase on flat surfaces after functionalization. Yet, for the other topographies, OCN
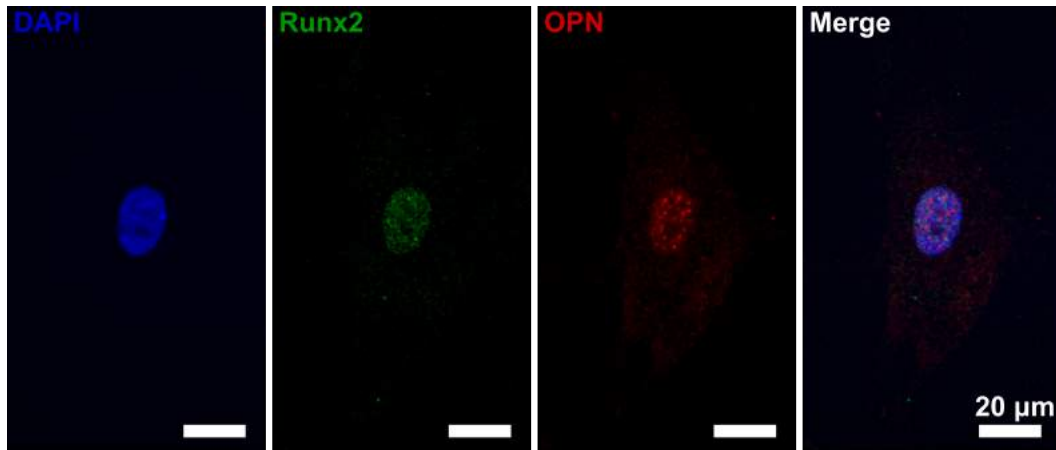
Figure 3.11 – Immunofluorescence micrograph of a cell cultured for 2 weeks on non-functionalized nanoarray A. Identical intra-cellular distribution of the markers was observed on all topographies.

expression did not considerably change.

BMP-2 mimetic peptide grafting had distinct effects on gene expression on each topology. Regarding Runx2 expression, this surface modification caused a significant increase in expression of cells cultured on flat samples (comparing both with no modification or grafting of RGD peptide). However, Runx2 expression on nanostructures A and B was similar to the one observed after functionalization with RGD peptide. The impact of BMP-2 on the remaining 2 markers was rather different. Expression of Col1A1 on flat surfaces did not significantly change compared with the previous conditions, as well as on surfaces B. On the contrary, its expression on nanostructures A was significantly lower than on bare nanostructures. The same was observed for OCN expression on these surfaces. Similarly to Runx2, no significant changes were observed on the level of expression of OCN on flat and nanostructures B grafted with BMP-2 mimetic peptide.

Finally, co-immobilization of the 2 molecules had a positive impact on all topographies as previously referred. Concerning flat surfaces, a significant increase on expression of all markers was noticeable when comparing with bare surfaces (roughly 14-fold for Runx2, 1.5-fold for Col1A1, 2-fold for OCN). However, gene expression of flat surfaces grafted with RGD and/or BMP-2 mimetic peptide did not show significant differences between themselves. The same tendency was observed for nanotopography B. On the contrary, gene expression of cells cultured on topography A benefited from the co-immobilization of peptides for the enhancement of osteogenic differentiation markers. Runx2 level for this last functionalization was approximately 3.5 times
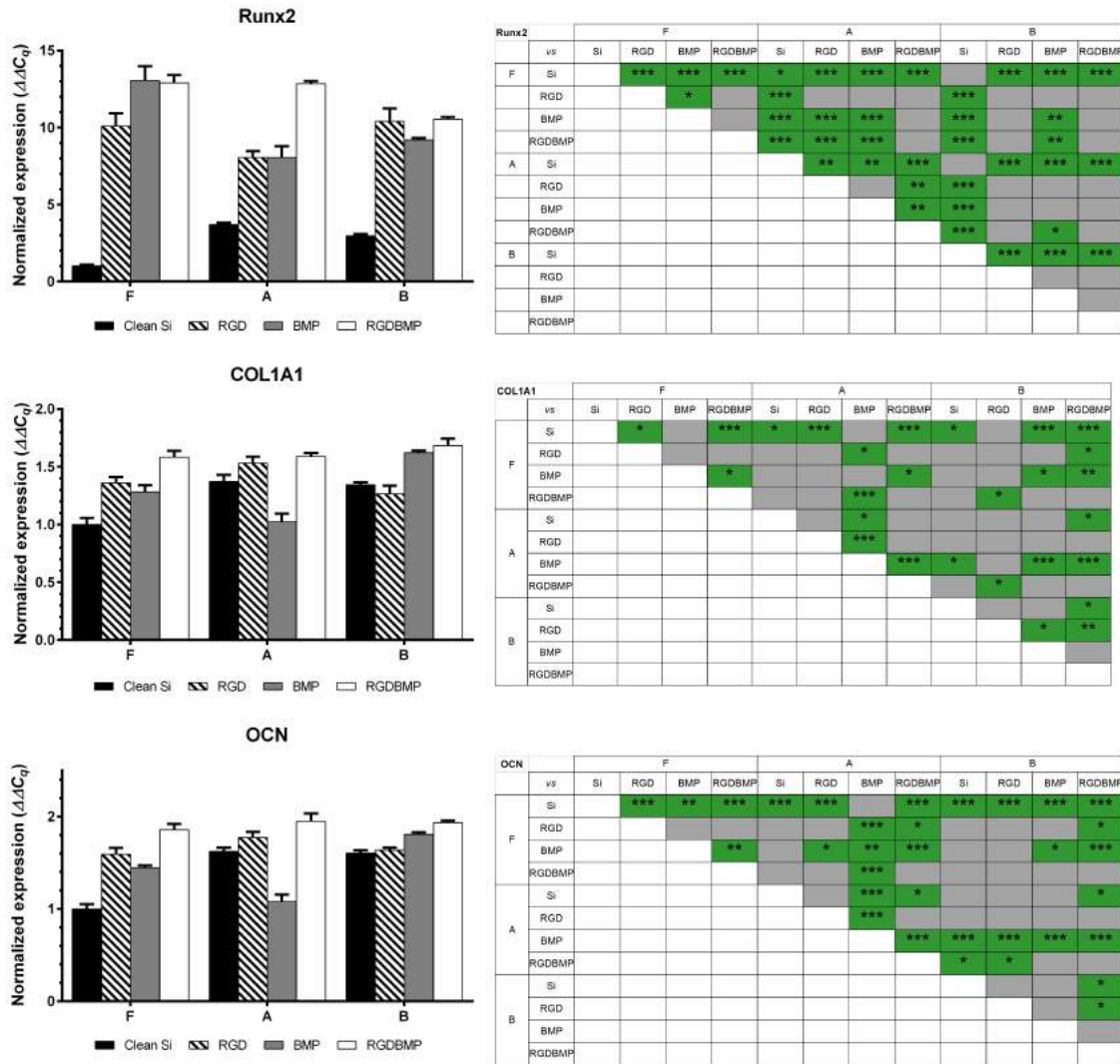
Figure 3.12 – Expression of Runx2 and OPN from hMSCs cultured for 2 weeks on plain silicon (Clean Si) or functionalized samples with RGD peptide (RGD), BMP-2 mimetic peptide (BMP), or a combination of the 2 molecules (RGDBMP). Tables summarize significant differences between conditions (* represents $p < 0.05$, ** $p < 0.01$, *** $p < 0.001$).

higher than for non-modified surface, and 1.5 times higher than for the nanostructures functionalized with only one of the peptides (RGD or BMP-2). Col1A1 expression level was similar to the levels observed on plain and RGD-grafted nanostructures A. On the other hand, OCN expression was slightly higher than non-modified nanoarrays.

4. Discussion

4.1. Sample fabrication

Reverse micelles of block copolymers granted the possibility of creating ordered polymeric arrays with uniformity over large areas (full wafers) which could be afterwards used as masks for the patterning of the underlying substrate with high processing reproducibility. Such characteristics are essential for the subsequent use of silicon nanopillars obtained on hMSC studies of differentiation. Biological tests at least the 3 replicates of the experiment to confirm their reproducibility. Additionally, techniques as RT-qPCR demand the use of a large number of cells, which cannot be ensured using only one chip of 1 cm^2, being therefore necessary to use cells from 4 chips.

XPS characterization showed that surface modification process was successful on the topographies tested. Moreover, no significant differences in surface chemistry between the 2 nanopatterns studied were observed, which can possibly be due to the large spot size of the XPS system compared with the nanofeature dimensions. When averaging the results obtained per region analyzed, the differences in topography become negligible given the difference in scale.

4.2. Investigation of hMSC differentiation

hMSCs were cultured for 2 weeks in basal medium independently of the assay (immunofluorescence or RT-qPCR). Flat or nanopatterned samples were tested either right after fabrication or functionalized with RGD or/and BMP-2 mimetic peptide to investigate which could be the best surface for the promotion of osteogenic differentiation of hMSCs.

Non-modified nanoarray A seemed to be the best surface for the control of hMSC commitment and differentiation towards the osteoblastic lineage, as shown by immunofluorescence andRT-qPCR results. When comparing the expression of the different markers from cells cultured on this pattern with the remaining samples (flat or B), significantly higher levels were observed on nanotopography A.

Such agreement between immunofluorescence and RT-qPCR results was not verified for biofunctionalized samples. Nonetheless, precise correlations between proteomic and genomic analysis are normally impossible to establish[168, 169]. It is necessary to consider protein stability issues, variations in the efficiency of RNA translation,

along with possible experimental errors and background noise related with each assay [168, 169]. Immunofluorescence results indicate that non-functionalized surface A lead to the highest expression of osteogenic markers, being therefore the best choice for hMSC osteogenic differentiation. Grafting of peptides on surfaces F and A did not cause a great alteration of Runx2 levels, but was responsible for a decrease in OPN expression of approximately 30 - 50 % of the signal observed on non-modified samples. That can indicate that hMSC differentiation occurred slower on the new functionalized samples. On the contrary, Runx2 expression was enhanced on B nanoarrays after surface functionalization. Than increase in signal was particularly high (2-fold) for grafting of BMP-2 mimetic peptide and co-grafting of RGD and BMP-2 peptide. Still, no significant differences were observed regarding OPN expression.

RT-qPCR did not show the same trend between the expression of non-modified surfaces and surfaces with grafted peptides. In these assays, Runx2 expression is significantly enhanced with peptide grafting, particularly in the case of co-functionalization of RGD and BMP-2 mimetic peptide independently of surface topology. Similar observations can be taken from the levels of expression of Col1A1 and OCN, though the differences between conditions are not as noteworthy as for Runx2.

Taken together, it is possible to conclude that the impact of surface topography appears to be more effective on the modulation of hMSC differentiation than the surface modification tested. Taking into account that proteins are produced after mRNA translation, and that Runx2 and Col1A1 are markers of early osteogenic differentiation, whereas OPN and OCN are late markers of differentiation, it can be assumed that A is indeed the best topography for the promotion of osteogenesis [24, 190]. The low level of expression of Runx2 observed in RT-qPCR indicates that the gene encoding for Runx2 is no longer being expressed (or being expressed at a decreased level), whereas the corresponding mRNA is being translated at high rate into proteins (immunofluorescence results). The quantity of OPN detected in the cells is significantly higher on non-modified nanoarray A, which indicates that cells cultured on such surfaces were able to commit and differentiate faster into the osteoblastic lineage, than cells cultured on the other conditions tested.

5. Conclusions

The approach followed for the fabrication of nanopillars permitted a reproducible patterning of full wafers with high uniformity. Peptides improving adhesion and promoting osteogenic differentiation of hMSCs were successfully grafted onto the patterned silicon. Immunofluorescence and RT-qPCR assays of hMSCs culture on such samples demonstrated that nanostructuring *per se* can enhance osteoblastic differentiation. Co-immobilization of the two peptides appeared to be an alternative approach to achieve similar stage of cell differentiation without patterning the substrate. Taken together, these findings suggest that fine-tuning of the surface chemistry and/or topography at nanoscale can modulate cell differentiation without the need of an induction medium. Different mimetic peptides could potentially be evaluated in combination of the engineered nanotopographies for a further enhancement of hMSC differentiation.

3.3 Intermediate studies

The main results obtained during the development of the protocol to fabricate nanoscale pillar arrays, as well as the main considerations behind them, the optimization of their surface modification process, and preliminary results regarding hMSC response to the bioactive surfaces are summarized and discussed in the present section.

3.3.1 Block copolymer templates

Amphiphilic BCPs, as PS-b-P2VP, are very interesting candidates for the formation of nanoscale polymer templates on large areas, as their colloidal properties allow their micellization under specific conditions. When coated on flat surfaces, reverse micelles form arrays of *quasi*-hexagonal distribution.

With that objective, solutions of PS-b-P2VP with concentrations between 0.4 and 1.0 wt % in anhydrous m-xylene were prepared for the characterization of the possible attainable micellar systems. Solutions were stirred for 24 hours, and coated on clean silicon wafers at spin-speeds between 2000 and 8000 rpm. The resultant arrays were characterized by SEM and AFM. As expected, no significant differences were observed for micelle diameter. A Delaunay triangulation of the results was performed on ImageJ to determine average periodicity. These results are summarized in Table 3.10 for the BCP of M_w 248-b-195 kg mol $^{-1}$, and in Table 3.11 for the BCP of M_w 55-b-50 kg mol $^{-1}$. For easier understanding of the results obtained, these values were plotted in Figure 3.13.

Table 3.10 − Periodicity of polymeric templates prepared with PS-b-P2VP of M_w 248-b-195 kg mol $^{-1}$ at different concentrations and coated on Si chips at different spin-coating speeds. (※sample not characterized)

Concentration	Spin speed / rpm			
wt %	2000	4000	6000	8000
0.4	174 ± 14 nm	206 ± 18 nm	214 ± 30 nm	230 ± 28 nm
0.6	※	212 ± 28 nm	221 ± 28 nm	235 ± 43 nm
0.8	116 ± 10 nm	145 ± 23 nm	154 ± 18 nm	165 ± 29 nm
1.0	※	143 ± 13 nm	157 ± 17 nm	160 ± 19 nm

Table 3.11 – Periodicity of polymeric templates prepared with PS-b-P2VP of M_w 55-b-50 kg mol $^{-1}$ at different concentrations and coated on Si chips at different spin-coating speeds. (a: patchy coverage; b: impossible to define spacing between micelle cores)

Concentration	Spin speed / rpm			
wt %	2000	4000	6000	8000
0.4	68 ± 10 nm	a	a	a
0.6	65 ± 9 nm	68 ± 6 nm	72 ± 7 nm	73 ± 6 nm
0.8	b	61 ± 7 nm	66 ± 6 nm	67 ± 6 nm
1.0	b	b	61 ± 9 nm	70 ± 13 nm
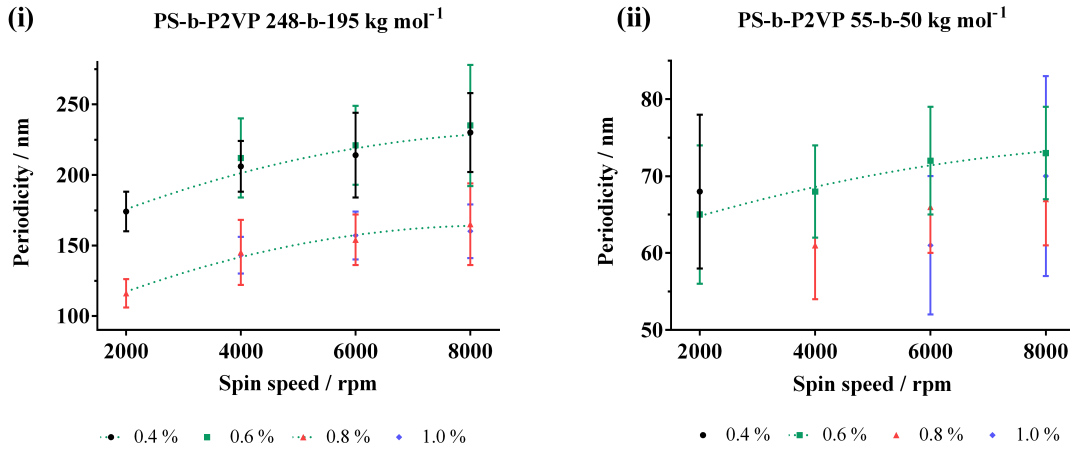
Figure 3.13 – Center-to center distances obtained for the range of concentrations and coating conditions tested. (i) BCP of M_w 248-b-195 kg mol $^{-1}$; (ii) BCP of M_w 55-b-50 kg mol $^{-1}$.

The BCP of largest M_w allowed the formation of homogeneous micellar films on silicon substrates for the range of concentrations and spin-coating speeds. On the other hand, films of PS-b-P2VP of reduced M_w showed patchy coverage of the surface for low solution concentration (0.4 wt %) and coating at higher spin speed ($\geq$ 4000 rpm). Moreover, when the concentration is increased, coating at lower speeds does not ensure the formation of a monolayer. Instead, multilayers of micelles are observed on the chips when coated at spin speeds lower than 6000 rpm for a concentration of 1 wt%, or 4000 rpm for a concentration of 0.8 wt%.

Once it was understood which concentrations and spin-coating speeds could be used for the creation of uniform monolayer films, a single condition was selected for the following studies, for ease of processing. Hence, subsequent tests were performed

for PS-b-P2VP solutions with concentration of 0.5 wt%, and coating at 5000 rpm, for both BCPs (M_w 55-b-50 kg mol^{-1} and 248-b-195 kg mol^{-1}). First of all, 4 inch wafers were coated with micellar films of both BCP and the characteristic dimensions and variation of distribution were characterized in detail. These results are summarized in Table 3.12 and Table 3.13, respectively.

Table 3.12 – Average characteristic dimensions of the polymer templates after spin-coating of solutions of concentration 0.5 wt% at 5000 rpm on Si wafers. (Values presented as mean ± standard deviation)

M_w / kg mol^{-1}	Diameter / nm	Periodicity / nm
248-b-195	60 ± 8	197 ± 23
55-b-50	52 ± 4	68 ± 4

Table 3.13 – Variations of polymer arrays from a true hexagonal distribution on Si wafers. CVs for feature diameter and periodicity across wafers, percentage of features in a correct hexagonal packing, and density of features for the two BCPs (at 0.5 wt %) coated at 5000 rpm on 4 inch wafers.

M_w kg mol^{-1}	Region	CV diam.	CV pitch	Coordination number 6	Density
	Center	11 %	12 %	51 %	115 µm^{-2}
55-b-50	Mid	9 %	10 %	65 %	136 µm^{-2}
	Edge	8 %	11 %	58 %	106 µm^{-2}
	Center	12 %	12 %	62 %	26 µm^{-2}
148-b-195	Mid	12 %	10 %	54 %	22 µm^{-2}
	Edge	10 %	12 %	57 %	21 µm^{-2}

Representative AFM images of these arrays are shown in Figure 3.14.

In addition, Delaunay triangulation along with Voronoi diagrams performed on SEM images offered the possibility of investigating defects from the expected hexagonal distribution. These algorithms allow the determination of the nearest neighbors of each micelle, therefore allowing the assessment of packing of these features on the substrate. Examples of the Voronoi diagrams obtained after the triangulation are represented in Figures 3.15 and 3.16 for the large and the small systems, respectively. For each particle, the number of edges of the corresponding Voronoi polygon was calculated. In this analysis, only polygons with 6 (the ideal polygons), 5 and 7 edges (defects) were
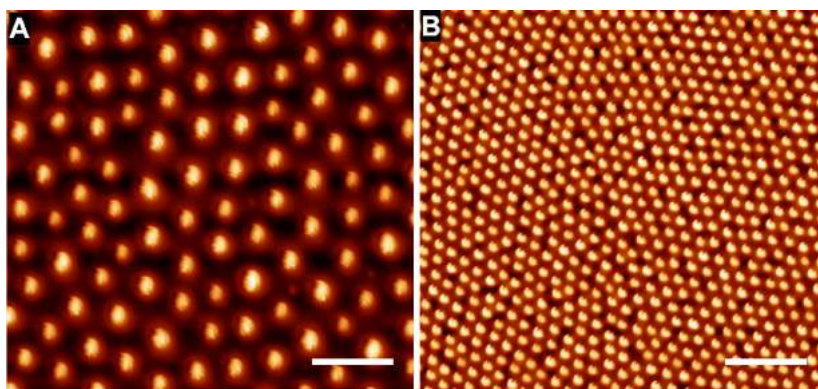
Figure 3.14 – Representative AFM images of the BCP arrays coated from a 0.5 % solution at 5000 rpm. (A) M_w 248-b-195 kg mol $^{-1}$. (B) M_w 55-b-50 kg mol $^{-1}$. (Scale bar 400 nm)

considered, in order to discard all the possible interference due to the particles close to the boundary of the images. This study showed that approximately 70% of the micelles of PS-b-P2VP 248-b-195 kg mol $^{-1}$ are correctly distributed on the surface, whereas for the micelles of PS-b-P2VP 55-b-50 kg mol $^{-1}$ this value was about 87%.
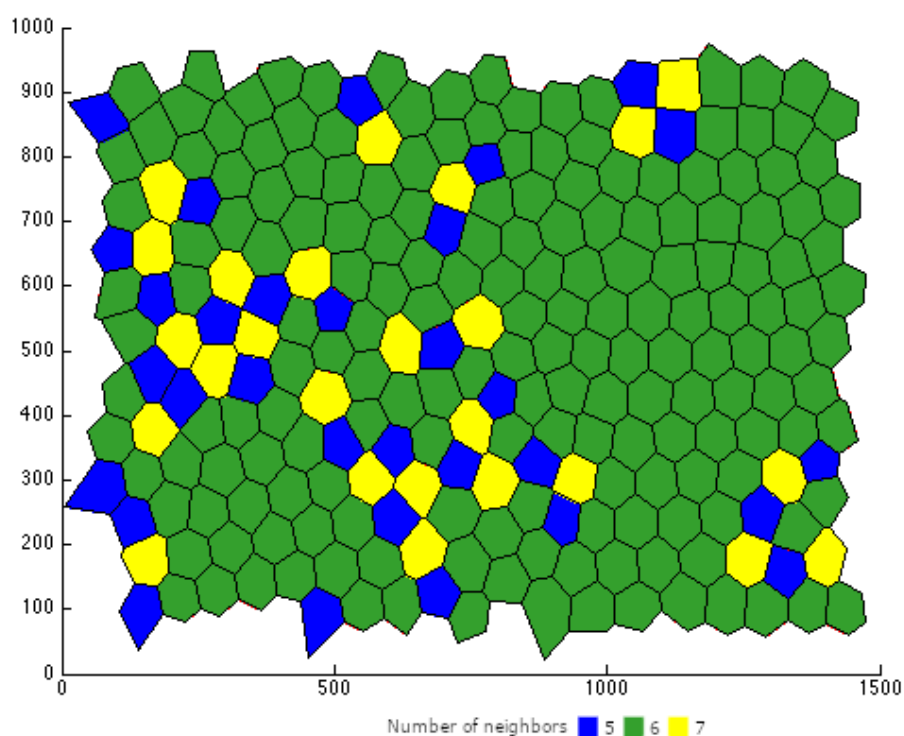
Figure 3.15 – Example of Voronoi diagram obtained from an acsem image of PS-b-P2VP 248-b-195 kg mol $^{-1}$. Axis in pixel, only for better orientation in the image.
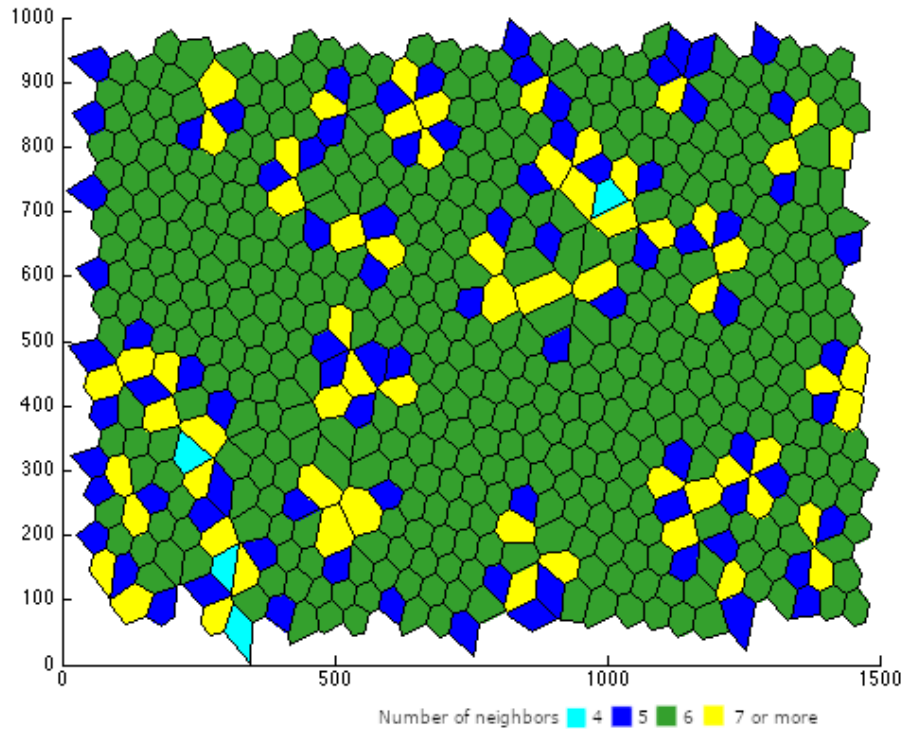
Figure 3.16 – Example of Voronoi diagram obtained from an SEM image of PS-b-P2VP 55-b-50 kg mol $^{-1}$. Axis in pixel, only for better orientation in the image.

3.3.2   Hard masks

Due to the low selectivity of the thin polymer layer to silicon etching, it was necessary to include an intermediate mask with better selectivity for pattern transfer. Two approaches developed by Krishnamoorthy *et al.* (2011) were tested: the use of a thermally grown thin silica film as mask, and the incorporation of titania particles into the reverse micelles to be used as hard mask [14].

SiO₂ masks

Wafers with thermally grown thin silica films were directly purchased from the supplier. BCP reverse micelles were spin-coated on these wafers, and RIE conditions were optimized in order to get silica nanoparticles with dimensions similar to those of the initial polymer templates.

TiO₂ masks

TiO$_2$ was selected as a possible material for such hard mask, as it can be easily incorporated into the cores of BCP by sequential vapor infiltration in an ALD reactor,

at highly controlled conditions, which allows a fine-tuning of the mask dimensions.

As introduced before, selective incorporation of a metal oxide in the micelle cores is possible due to the chemical differences between the polymer blocks forming the core and corona of the micelles. Polar precursors of TiO_2 ($TiCl_4$ and H_2O, in this study) are able to diffuse through the PS layer, and react with the pyridyl groups of the P2VP block, which allows the maintenance of the structural uniformity of the initial micelles. Furthermore, the control of the characteristics of the titania mask was possible *via* the tuning of precursor concentrations and speed of deposition.

When performed within an ALD reactor, these characteristics can be accurately controlled, as this equipment grants the possibility of a precise regulation of the deposition parameters, including temperature, pressure, chemical environment, and dosing of precursors. Moreover, each exposure to the precursors is followed by a step of purging, which leads to the removal of unbound precursors and by-products of the reaction, further contributing to the control of the deposition.

Although the organization of the TiO_2 nanoparticles obtained after the incorporation of the precursors depends exclusively on the spatial arrangement of the initial block copolymer micelles, the dimensions of the oxide particles are related with the number of cycles of exposure to the precursors. After exhausting all pyridyl groups from the P2VP micelle cores, the precursors are still able to react with the already formed TiO_2 nanoparticles, which can give rise to nanoparticles with larger dimensions than the initial P2VP cores. However, it is expected that after a large number of precursor exposure cycles, as all P2VP pyridyl groups reacted with the precursors, the precursors will tend to react between themselves, and to get deposited on the polymer layer, following a classic atomic layer deposition process. Therefore, it was necessary to investigate the characteristics of the TiO_2 features fabricated by sequential vapor infiltration on polymeric templates as a function of the number of ALD cycles, in order to define the maximum number of exposure cycles that still grants a correct hard mask for substrate etching. Incorporation process was performed for 25, 50, 75 and 100 precursor cycles. Samples were characterized by SEM and AFM right after TiO_2 incorporation and after removal of the residual polymer layer by oxygen plasma. SEM characterization aimed at investigating changes in nanoparticle diameter, whereas the AFM analysis offered the possibility of characterizing height of the titania nanoparticles. The results concerning particle diameter are summarized in Table 3.14, and

particle height in Table 3.15.

Table 3.14 – Average micelle diameter before and after polymer removal as a function of number of precursor cycles, obtained by SEM.

Number of cycles	Before removal / nm	After removal / nm
0	70 ± 6	0
25	77 ± 7	61 ± 10
50	79 ± 8	62 ± 10
75	82 ± 13	83 ± 11
100	85 ± 14	87 ± 13

Table 3.15 – Average micelle height before and after polymer removal as a function of number of precursor cycles, obtained by AFM.

Number of cycles	Before removal / nm	After removal / nm
0	40 ± 6	0
25	42 ± 5	25 ± 5
50	44 ± 5	29 ± 5
75	48 ± 6	33 ± 7
100	36 ± 5	36 ± 7

Concerning the large BCP system, particle height was found to increase from 42 nm to 48 nm with the number of cycles, up to 75 cycles. However, for 100 exposure cycles, the average micelle height measured was lower, which can be a consequence of the deposition of a TiO_2 layer on the PS layer, or of the increase of particle diameter that can prevent a correct characterization by AFM. Nevertheless, such conclusion can only be considered after the comparison with the average height measured after RIE. As expected, particle diameter tended to increase with the number of precursor exposure cycles for all conditions. Particularly, it was seen that the particles enlarged even after 25 cycles for all conditions, when compared with the initial dimensions of the polymeric template.

In order to obtain a TiO_2 particle hard mask from the previous samples, it was necessary to remove the polymer layer used as template for the sequential vapor incorporation of TiO_2. The removal of the polymer could be achieved subjecting the samples to an oxygen plasma, which is able to cause photo-oxidation of the polymer layer, leading to its degradation. As represented in Figure 3.17, AFM characterization

showed that the average feature height decreases when the polymer layer was removed, independently of the number of exposure cycles. On the other hand, particle diameter
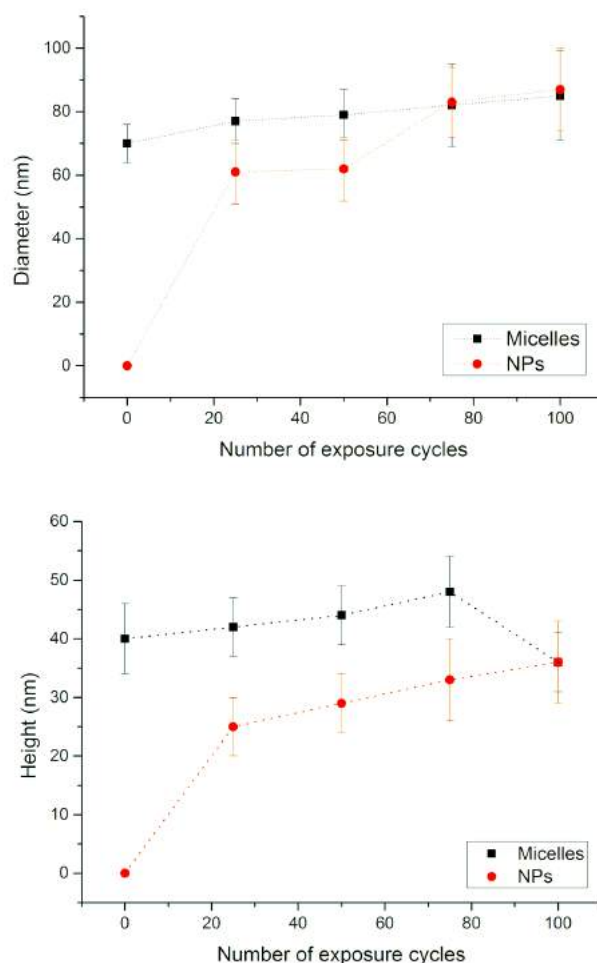
Figure 3.17 – Feature height and diameter after incorporation of TiO_2 before (micelles) and after (NPs) polymer removal.

saturates after a definite number of cycles: it was observed that the removal of the polymer is possible only up to 50 exposure cycles. Afterwards, the TiO_2 starts to be deposited following an ALD process covering the polymer layer, which prevents its exposure to the oxygen plasma. Thus, the optimal number of exposure cycles for the utilization of the titania NPs is 50.

As it was possible to create hard silica masks of feature dimensions resembling the ones of the PS-b-P2VP templates, this approach was not further optimized. The fabrication of a silica mask is less troublesome and time demanding. It is important to note that for smaller features, the sequential vapor incorporation strategy could be indispensable to pattern the substrate with high uniformity and reproducibility. Nevertheless, for the present range of dimensions, the SiO_2 was adequate.

Chromium masks for nanopore arrays

Fabrication of nanopore arrays based on BCP micelle templates was also investigated as possible topographies for cell studies. With that objective, 10 nm thick chromium films were evaporated on silicon wafers coated with the polymer templates and processed following BCP-assisted lithography approach developed by Popa *et al.* [146]. Briefly, chromium coated samples were polished in order to create a porous mask, whose features respect the distribution and have similar diameter of the initial polymer template.

Although four approaches were evaluated for sample polishing (chromium lift-off by ultrasonication, lift-off assisted by a thermosensitive polymer, CMP using a suspension of micron-sized diamond particles, or CMP using a suspension of silica NPs), it was only possible to create uniform and reproducible nanopore arrays on full wafers by mechanically-assisted lift-off using a suspension of colloidal silica NPs (Figure 3.18).
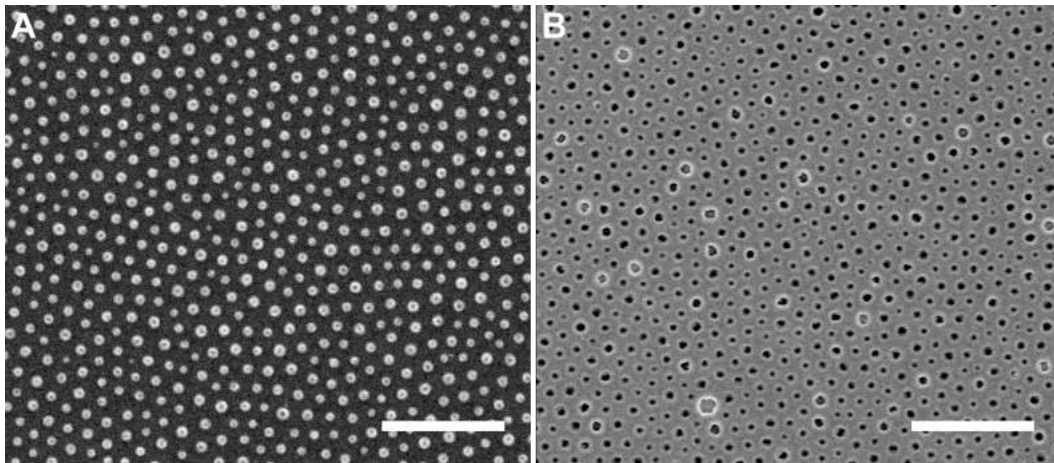
Figure 3.18 – Detail of a sample before (A) and after (B) CMP. (Scale bar 1 µm)

3.3.3 Nanostructures: Titanium vs. Silicon

Although it had been initially planned to prepare nanopillar arrays of Ti-6Al-4V for investigation of hMSC differentiation, due to time constraints it was necessary to change the approach and fabricate the nanostructures in silicon. Titanium alloys are usually the first choice for orthopedic implants due to their very good mechanical properties and corrosion resistance, and due to their bioinertness [28]. However, the crystalline structure characteristic of titanium in its elemental form is lost once the alloying elements are introduced, which hinders the possibility of having a controlled

way of patterning Ti-6Al-4V at nanoscale level [28]. On the contrary, silicon is a crystalline material thoroughly studied for applications in electronics. Moreover, it is also a biocompatible material, as well as any particles that may be released if implanted [7, 8].

Given the difficulties in patterning this titanium allow at nanoscale with high uniformity, the approach consisted on the engineering of controlled nanopillar arrays in silicon, followed by the deposition of the Ti-6Al-4V by Physical Vapor Deposition (PVD) on the patterned surfaces. Initial investigations of the deposition of thin alloy films (10 nm thick) on planar silicon substrates were performed and characterized by AFM. Such characterization confirmed the expected film thickness as well as a low surface roughness, important for the subsequent deposition on nanostructured samples. Additionally, it was necessary to assess the degree of adhesion of the titanium alloy films to silicon. Samples were characterized before and after testing to detect any possible alterations or damages of the films. Coated samples were sonicated for one hour in different solvents, namely PBS and acetone, and immersed in those solvents overnight. No changes were observed on the tested films, which confirmed a suitable adhesion of the Ti-6Al-4V to the silicon substrate, and indicated that the samples would withstand subsequent cell culture. PVD of thin Ti-6Al-4V films was also performed on nanostructured silicon. According to a preliminary SEM characterization, the deposited films appear to conform adequately to the structures, as represented in Figure 3.19. Nonetheless, further SEM characterization along with characterization of surface chemistry would be required prior to the utilization of Ti-6Al-4V nanopillars for any application.
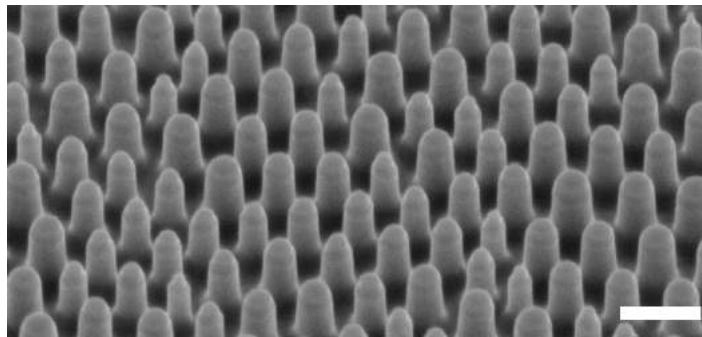
Figure 3.19 – Detail of nanopillar array after coating with a thin Ti-6Al-4V film characterized by SEM. Scale bar 250 nm.

In parallel, the deposition of a 10 nm thick titanium oxide layer on the nanostructured samples was tested by ALD. Once titanium or its alloys are exposed to air, a

thin oxide layer forms on their surface, stabilizing the material. Hence, the deposition of a titania thin film on the nanostructured samples would allow the contact of MSCs with a surface resembling the surface of Ti-6Al-4V. Moreover, ALD can ensure a better adhesion of the deposited film on the substrate, as it relies on the adsorption until saturation of each material precursor, intercalated with the cycles of purging to remove any unbound molecules [191].

Nonetheless, it was not possible to complete the fine-tuning of all the parameters and subsequent sample characterization of Ti-6Al-4V or titania films on silicon nanostructures due to time limitations. Therefore, silicon nanostructures were used as substrates for cell studies.

3.3.4   Nanoimprint lithography

As previously described, NIL is a lithography technique based on the mechanical deformation of polymers which can be hardened by temperature and pressure changes or by crosslinking by UV light [141]. In the current study, this technique was utilized with two main objectives: to simplify the creation of masks for the patterning of silicon wafers, and to investigate the impact of softer nanopillars on hMSC differentiation. However, due to time constraints, it was not possible to complete the optimization of these processes. Therefore, only a brief summary of the results obtained will be presented here.

The starting molds used for NIL tests were indeed silicon nanopillar arrays fabricated as previously described. A solution of reverse micelles of PS-b-P2VP was spin-coated onto a SiO_2 thin film on a silicon wafer, and the formed polymeric templates were used as masks for the patterning of the intermediary silica mask. This hard mask was afterwards used to protect the regions of interest during RIE of the silicon substrate. The nanoscale pillar arrays obtained were then used for NIL.

A set of polymers sensitive to temperature (thermosetting or thermoplastic) or to UV light (crosslinkable) were tested to investigate which approach would be the more suited for the imprinting of uniform features on full wafers, with dimensions identical to the initial dimensions of the silicon master mold. A series of difficulties requiring optimization were faced, namely poor adhesion of the polymer film to the substrate (Figure 3.20A), air bubbles between mold and polymer (notably challenging to prevent for imprintings on large surface areas, as full wafers) (Figure 3.20B), and defects on the

imprinted features due to their reduced dimensions (Figure 3.20C). After optimization
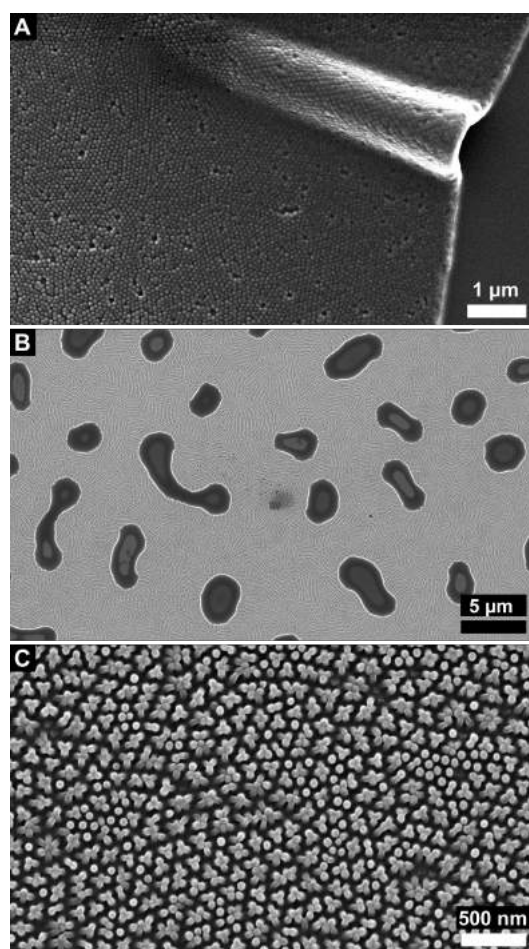
Figure 3.20 – Difficulties faced during optimization of NIL. (A) Poor adhesion of the polymer to the substrate. (B) Air bubbles between mold and polymer. (C) Nanoscale polymer features adhere to each other after imprinting.

of imprinting conditions, it was possible to fabricate uniform nanopillar arrays on full wafers and on soft substrates of similar area. The imprinted features showed dimensions identical to the silicon nanopillar molds used for NIL. A detail of one of the imprinted samples is presented in Figure 3.21.

3.3.5   Peptide grafting: characterization

The success of a surface biofunctionalization process is usually assessed by fluorescence microscopy, as it is a simple approach requiring only that the peptide (or other molecule of interest) is previously labelled with a fluorochrome (*e.g.* fluorescein) [20, 21, 23, 170]. Besides giving information about the success of grafting, it can also be used to determine the concentration of grafted fluorescently-labeled molecules on the surface given a calibration curve, as described by Bilem *et al.* [20]. Such approach
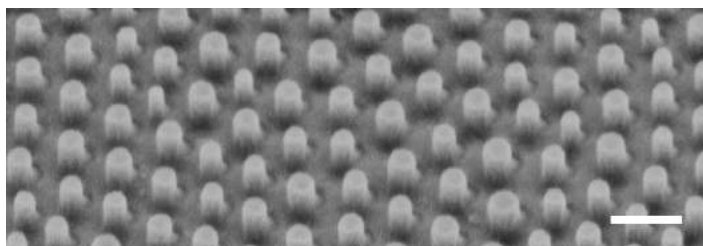
Figure 3.21 – SEM image of polymeric nanopillars with average height of 85 nm obtained by NIL. (Scale bar 250 nm)

was also tested on the samples prepared during this project to evaluate the efficiency of peptide grafting. Nonetheless, no fluorescence was ever observed, which raised the question of whether the biofunctionalization protocol was not effective or the characterization method was not adequate (even on flat silicon samples). It was reported by Bras *et al.* that the detection of fluorescent molecules grafted on silicon oxide on silicon substrates required the fine-tuning of the thickness of the oxide layer allowing the build-up of a constructive interference between excitation and emission beams [192]. In particular, the authors reported, that for very thin oxide layers (as the native oxide of our silicon samples, which had a thickness of approximately 2 nm) destructive interference for excitation and emission wavelengths is observed, hindered the detection of the fluorescence signal by epifluorescence.

Biofunctionalized samples were also characterized by confocal laser microscopy, which successfully showed fluorescence related with the grafting of fluorescently-labeled peptides on flat and on a set of the nanostructured silicon samples. Hence, it could be concluded that peptide grafting was indeed successful, but fluorescent methods could not be used for quantification of peptide density on the surface. It is important to note that similar ordered nanostructures are also used for applications including plasmonic resonance and surface enhanced plasmonic spectroscopy or solid-state lightning, given the possibility of controlling the optical properties of the structured material *via* the fine-tuning of the characteristic dimensions of the arrays [193]. Therefore, every test where light was utilized during this project had to be carefully analyzed to try to deconvolute the effect of the molecule under study with the effects due to the periodic arrays.

Finally, surface functionalization was successfully characterized on all types of samples by XPS, a more complex characterization method which grants the possibility of an accurate analysis of surface chemistry of a material [194]. To have an estimation of

the thickness of the layer bound to silicon (APTES+SMP+BMP-2 mimetic peptide, due to a larger size than RGD peptide), the Beer-Lamber law (Equation 3.1) as used taking into consideration the attenuation of the XPS signal for Si 2p on a flat sample [70?].

$$I = I_0 e^{-\frac{d}{\lambda \sin \theta}} \tag{3.1}$$

where I is the final intensity, I_0 the intensity on bare silicon, d the layer thickness, λ the inelastic mean free path, and θ the take-off angle (90°). λ can be correlated with the kinetic energy, KE, of the emitted photoelectrons using the Equation 3.2.

$$\lambda = B\sqrt{KE} \tag{3.2}$$

with $B = 0.087$ nm eV$^{-1/2}$ for organix materials [70, 195].

Hence, the estimated thickness of the organic layer was 0.36 nm, which is in accordance with previous reported works [70].

4 | Conclusions and Prospects

In this study, bioactive nanoscale structures were fabricated for the investigation of hMSC behavior, and in particular their osteogenic differentiation, in order to better understand the impact of bioactive nanoscale structures on stem cell differentiation, and to potentially ameliorate the currently available technologies and materials having such aim.

Nanotopography geometries and dimensions were selected based on the literature analyzed. Still, difficulties in finding systematic ways of analyzing the results reported in the literature, hindered the choice of nanoscale topographies. Although numerous studies have been published on this specific field of research, non-coherent or even contradictory results were often reported, as previously discussed here. hMSCs are extremely sensitive to culture conditions, which contributes to such variability in results found in the literature. Even small divergences in culture media composition can have a strong impact on how MSCs proliferate, migrate, differentiate, *etc.* Nevertheless, it is understood that stiff materials and culture conditions leading to increased cytoskeleton tension are able to enhance osteogenic differentiation of MSCs.

Therefore, nanoscale pillars were selected as base topographies for the present studies. These nanostructures were fabricated taking advantage of the self-assembly properties of amphiphilic BCPs in selective solvents. This technique allowed the fabrication of nanopillar arrays of different dimensions with high uniformity and reproducibility over full wafers, with control over each geometric variable (diameter, spacing, and height) in steps of less than 5% of their mean value. Such results are not easily accessible using other common nanofabrication techniques, namely EBL. Since it is currently understood that such topographies have different refractive indexes depending on their geometry, which may have an influence on results obtained by fluorescence (either characterization of the grafting of peptides labeled with a fluorochrome or immunofluorescence assays), it would be important to characterize the reflectance spectra

especially in the range of wavelengths used during subsequent experiments.

A high-throughput nanofabrication approach was mandatory for the preparation of the nanostructured samples due to the high requirements of biological experiments, and of the optimization of all the fundamental steps for the creation of bioactive nanostructured samples. Also, it was observed that the chips cut closer to the edge of the wafers did not exhibited the level of uniformity in terms of feature geometry required for this project. Regarding biological experiments, it was necessary to keep in mind that each test needs to be reproduced for at least n=3. In the case of immunofluorescence assays, the number of samples needed for each experiment is dependent on the number of fluorescence filters available on the fluorescence microscope. Therefore, it was only possible to use two markers (plus a marker for cell nuclei) per sample. On the other hand, RT-qPCR requires a minimum quantity of RNA which is correlated with the number of cells from which RNA is extracted. It was verified that five chips with cells per condition would be required to extract sufficient RNA for the performance of RT-qPCR tests. Moreover, all the characterization and optimization steps of nanofabrication and surface modification required the utilization of several chips that were then unsuitable for reuse in cell culture. NIL was also tested as a potential approach for a easier replication of the templates to be used for the patterning of the underlying silicon substrate. Yet, lack of time hindered the optimization of this method, and a more common protocol for the engineering of the nanoarrays was followed.

Six nanopillar arrays were finally tested for their ability to modulated hMSC response compared to a flat silicon control, aiming at determining the best condition for the enhancement of osteogenic differentiation. The age of the cell donor was perceived as a central parameter influencing the selection of the most suited nanotopography for osteogenic differentiation. Spacing between features was the main geometric parameter modulating differentiation of hMSCs from donors of different age. Whereas osteoblastic differentiation is enhanced on nanopillars of reduced separation for cells from a young donor, cells of an older donor are more prone to differentiate into the osteoblastic lineage on pillars of larger separation. Nevertheless, in both cases, it was observed that hMSCs were more prone to undergo osteoblastic differentiation on features of larger diameter and height (100 nm diameter, 80 nm height). It can be expected that such topographies are the ones leading to higher cytoskeleton tension, though further testing must be performed, including the characterization of organization of actin fil-

aments within cells. In order to investigate if these topographies could potentially be used in other applications, namely for studies of hMSC commitment and differentiation towards other lineages, preliminary immunofluorescence assays were performed for a small number of hMSCs from a young donor. These tests aimed at evaluating the expression of markers of MSC adipogenic and chondrogenic differentiation by cells cultured on the nanostructured substrates. No expression of adipogenic markers was observed on samples (flat or patterned), which can be due to the intrinsic high stiffness of silicon not offering adequate environment for adipogenic differentiation. On the other hand, cells cultured on nanostructured silicon expressed chondrogenesis markers, and in particular those grown on nanopillar arrays of large diameter, separation and height (100 nm diameter, 200 nm center-center spacing, 80 nm height). It is interesting to note the alterations with age of the donor on the ability of cells to respond to a specific stimulus. Whereas this array was able to direct the differentiation of hMSCs from a young towards the chondrogenic lineage, it enhanced osteogenic differentiation of cells of an older donor. These results highlight the importance of having treatments adjusted to an individual patient or at least age group. Still, it would be relevant to have a larger batch of cell donors to have a better understanding of how age (and possibly gender) may constrain cell response to a particular surface.

The subsequent study of the possible enhancement of cell differentiation due to synergies between surface chemistry and topography was not performed for all the nanoarrays considered initially. That was due to the fact that it has been previously observed that not all topographies selected were able to direct hMSC differentiation towards the osteoblastic lineage, and due to constraints related with the number of substrates necessary for cell culture. Still, the selected conditions were sufficient for a multiplex evaluation of the control of hMSC differentiation by nanoscale topography and/or chemistry, of possible interactions between chemistry and topology of the material, and of potential synergistic effects between surface chemistry and topography on the modulation of cell differentiation.

No synergistic effects between physical and chemical cues were observed regarding cell differentiation after 2 weeks of culture. Instead, it was observed that, independently, nanopillars or surface biofunctionalization (with a combination of an adhesive peptide and a mimetic peptide promoting differentiation) were able to induce osteogenic differentiation of hMSCs to the same extent. Such fact indicates that both approaches

can be effective on the modulation of cell behavior. These findings may be interesting for the development of novel biomaterials or model surfaces where both types of stimuli cannot be applied simultaneously, since it may be possible to engineer material surfaces enhancing cell differentiation *via* physical or chemical cues.

In the future, nanostructure functionalization could be tested using different peptides or combination of peptides (*e.g.* RGD and PHSRN to improve adhesion along with a BMP-2 mimetic peptide) to survey the possibility of having faster hMSC differentiation without the need for any induction media. Also, the use of microvesicles from hMSCs or osteoblasts has been reported as a possible tool for the improvement of osteogenic differentiation of hMSCs [196]. Taking into consideration the results obtained for cells cultured on bare nanotopographies, the combination of nanostructures with microvesicles (possibly in solution) could potentially be an alternative approach for such differentiation studies. Alternatively, co-culture of **mcs!**s (**mcs!**s) with endothelial cells, for instance, could possibly be a way of enhancing MSC differentiation, as endothelial cells secrete various regulatory molecules for differentiation and activity of bone forming cells [197]. Complementary studies of potential cell differentiation towards other lineages (*e.g.* chondrogenic, adipogenic) or preservation of stemness characteristics should be performed to complete the preliminary tests performed during this project. The fabricated samples can potentially be applied in cartilage treatment or disease models, taking into consideration the results here obtained.

Although there was not the possibility to test the effectiveness of NIL-based polymeric nanotopographies, the investigation of the feasibility of application of such nanostructures on hMSC differentiation appear to be of extreme interest. In addition, the comparison of the impact of a particular nanotopography prepared on materials with very distinct stiffness (as silicon and a polymer) can give relevant insights on how cells would respond to such combination of mechanical and physical cues. Furthermore, from a materials perspective, it would be of extreme interest to evaluate the local stiffness of the material to which cells are in contact with, which could performed by AFM infrared spectroscopy, for instance. When describing a nanotopography of a material, one takes into consideration the bulk stiffness of a material. Yet, the mechanical properties of a biomaterial need to be adjusted to the dimensions of the nanofeatures, since it is known that cells are only able to interact with the top part of the pillars, which surely possess a lower young modulus than the bulk material. Other nanoscale

topographies, namely holes or grooves, could be used for further investigation of the impact of geometry variables on stem cell differentiation, in order to further improve the understanding of the impact of material topography on MSC behavior.

Moreover, cell culture should be performed for additional time points. The selection of a specific time point granted an initial understanding of the processes and response of cells to the prepared surfaces. Nonetheless, it would be important to investigate the how cell differentiation progresses with time on the different bioactive nanostructured surfaces. Although it was not possible to perform during this work, the fraction of cells which is actually able to adhere to the samples after seeding should also be investigated, as it is understood that cell density has an impact on cell differentiation. Furthermore, it would be interesting to compare the number of adherent cells for younger and older cell donors, to infer if age also influences cell adhesion abilities. Additionally, SEM could be performed to observe cell shape and the way of adhering to the different nanotopographies. Other techniques of characterization of osteoblastic differentiation (*e.g.* alizarin red staining, ALP activity testing, or western blot) could also be used to further investigate the impact of material properties on MSC differentiation, even if they may require the use of a larger number of cells.

Bibliography

[1] D. F. Williams, "On the nature of biomaterials," *Biomaterials*, vol. 30, no. 30, pp. 5897–5909, Oct. 2009.

[2] R. Fraioli, F. Rechenmacher, S. Neubauer, J. M. Manero, J. Gil, H. Kessler, and C. Mas-Moruno, "Mimicking bone extracellular matrix: Integrin-binding peptidomimetics enhance osteoblast-like cells adhesion, proliferation, and differentiation on titanium," *Colloids and Surfaces B: Biointerfaces*, vol. 128, pp. 191–200, Apr. 2015.

[3] M. M. Stevens, "Biomaterials for bone tissue engineering," *Materials Today*, vol. 11, no. 5, pp. 18–25, May 2008.

[4] J. Kobolak, A. Dinnyes, A. Memic, A. Khademhosseini, and A. Mobasheri, "Mesenchymal stem cells: Identification, phenotypic characterization, biological properties and potential for regenerative medicine through biomaterial microengineering of their niche," *Methods*, vol. 99, pp. 62–68, Apr. 2016.

[5] S. Kern, H. Eichler, J. Stoeve, H. Klüter, and K. Bieback, "Comparative Analysis of Mesenchymal Stem Cells from Bone Marrow, Umbilical Cord Blood, or Adipose Tissue," *STEM CELLS*, vol. 24, no. 5, pp. 1294–1301, 2006.

[6] J. Liu, F. Yu, Y. Sun, B. Jiang, W. Zhang, J. Yang, G.-T. Xu, A. Liang, and S. Liu, "Concise Reviews: Characteristics and Potential Applications of Human Dental Tissue-Derived Mesenchymal Stem Cells," *STEM CELLS*, vol. 33, no. 3, pp. 627–638, 2014.

[7] S. P. Low, N. H. Voelcker, L. T. Canham, and K. A. Williams, "The biocompatibility of porous silicon in tissues of the eye," *Biomaterials*, vol. 30, no. 15, pp. 2873–2880, May 2009.

[8] K. Dashnyam, A. El-Fiqi, J. O. Buitrago, R. A. Perez, J. C. Knowles, and H.-W. Kim, "A mini review focused on the proangiogenic role of silicate ions released from silicon-containing biomaterials," *Journal of Tissue Engineering*, vol. 8, p. 2041731417707339, Jan. 2017.

[9] M. J. P. Biggs, R. G. Richards, and M. J. Dalby, "Nanotopographical modification: A regulator of cellular function through focal adhesions," *Nanomedicine: Nanotechnology, Biology and Medicine*, vol. 6, no. 5, pp. 619–633, Oct. 2010.

[10] T. Sjöström, L. E. McNamara, R. M. D. Meek, M. J. Dalby, and B. Su, "2D and 3D Nanopatterning of Titanium for Enhancing Osteoinduction of Stem Cells at Implant Surfaces," *Advanced Healthcare Materials*, vol. 2, no. 9, pp. 1285–1293, Sep. 2013.

[11] S. Oh, K. S. Brammer, Y. S. J. Li, D. Teng, A. J. Engler, S. Chien, and S. Jin, "Stem cell fate dictated solely by altered nanotube dimension," *Proceedings of the National Academy of Sciences*, vol. 106, no. 7, pp. 2130–2135, Feb. 2009.

[12] K. Metavarayuth, P. Sitasuwan, X. Zhao, Y. Lin, and Q. Wang, "Influence of Surface Topographical Cues on the Differentiation of Mesenchymal Stem Cells in Vitro," *ACS Biomaterials Science & Engineering*, vol. 2, no. 2, pp. 142–151, Feb. 2016.

[13] M. J. Dalby, N. Gadegaard, and R. O. C. Oreffo, "Harnessing nanotopography and integrin-matrix interactions to influence stem cell fate," *Nature Materials*, vol. 13, no. 6, pp. 558–569, Jun. 2014.

[14] S. Krishnamoorthy, K. K. Manipaddy, and F. L. Yap, "Wafer-Level Self-Organized Copolymer Templates for Nanolithography with Sub-50 nm Feature and Spatial Resolutions," *Advanced Functional Materials*, vol. 21, no. 6, pp. 1102–1112, Mar. 2011.

[15] O. M. Ishchenko, S. Krishnamoorthy, N. Valle, J. Guillot, P. Turek, I. Fechete, and D. Lenoble, "Investigating Sequential Vapor Infiltration Synthesis on Block-Copolymer-Templated Titania Nanoarrays," *The Journal of Physical Chemistry C*, vol. 120, no. 13, pp. 7067–7076, Apr. 2016.

[16] M. J. Dalby, A. J. García, and M. Salmeron-Sanchez, "Receptor control in mesenchymal stem cell engineering," *Nature Reviews Materials*, vol. 3, p. 17091, Jan. 2018.

[17] C. Mas-Moruno, "Surface functionalization of biomaterials for bone tissue regeneration and repair," in *Peptides and Proteins as Biomaterials for Tissue Regeneration and Repair.* Elsevier, 2018, pp. 73–100.

[18] M. Porté-Durrieu, F. Guillemot, S. Pallu, C. Labrugère, B. Brouillaud, R. Bareille, J. Amédée, N. Barthe, M. Dard, and C. Baquey, "Cyclo-(DfKRG) peptide grafting onto Ti–6Al–4V: Physical characterization and interest towards human osteoprogenitor cells adhesion," *Biomaterials*, vol. 25, no. 19, pp. 4837–4846, Aug. 2004.

[19] Z. A. Cheng, O. F. Zouani, K. Glinel, A. M. Jonas, and M.-C. Durrieu, "Bioactive Chemical Nanopatterns Impact Human Mesenchymal Stem Cell Fate," *Nano Letters*, vol. 13, no. 8, pp. 3923–3929, Aug. 2013.

[20] I. Bilem, P. Chevallier, L. Plawinski, E. D. Sone, M. C. Durrieu, and G. Laroche, "RGD and BMP-2 mimetic peptide crosstalk enhances osteogenic commitment of human bone marrow stem cells," *Acta Biomaterialia*, vol. 36, pp. 132–142, May 2016.

[21] O. F. Zouani, C. Chollet, B. Guillotin, and M.-C. Durrieu, "Differentiation of pre-osteoblast cells on poly(ethylene terephthalate) grafted with RGD and/or BMPs mimetic peptides," *Biomaterials*, vol. 31, no. 32, pp. 8245–8253, Nov. 2010.

[22] O. F. Zouani, L. Rami, Y. Lei, and M.-C. Durrieu, "Insights into the osteoblast precursor differentiation towards mature osteoblasts induced by continuous BMP-2 signaling," *Biology Open*, p. BIO20134986, Jul. 2013.

[23] I. Bilem, P. Chevallier, L. Plawinski, E. D. Sone, M.-C. Durrieu, and G. Laroche, "Interplay of Geometric Cues and RGD/BMP-2 Crosstalk in Directing Stem Cell Fate," *ACS Biomaterials Science & Engineering*, vol. 3, no. 10, pp. 2514–2523, Oct. 2017.

[24] R. Miron and Y. Zhang, "Osteoinduction: A Review of Old Concepts with New Standards," *Journal of Dental Research*, vol. 91, no. 8, pp. 736–744, Aug. 2012.

[25] P.-Y. Wang, H. Thissen, and P. Kingshott, "Modulation of human multipotent and pluripotent stem cells using surface nanotopographies and surface-immobilised bioactive signals: A review," *Acta Biomaterialia*, vol. 45, pp. 31–59, Nov. 2016.

[26] H. Donnelly, M. J. Dalby, M. Salmeron-Sanchez, and P. E. Sweeten, "Current approaches for modulation of the nanoscale interface in the regulation of cell behavior," *Nanomedicine: Nanotechnology, Biology and Medicine*, vol. 14, no. 7, pp. 2455–2464, Oct. 2018.

[27] D. F. Williams and European Society for Biomaterials, "Definitions in biomaterials: Proceedings of a consensus conference of the european society for biomaterials, Chester, England, March 3-5, 1986." Amsterdam: Elsevier, 1987, oCLC: 489912247.

[28] B. D. Ratner, A. S. Hoffmann, F. J. Schoen, and J. E. Lemons, Eds., *Biomaterials Science: An Introduction to Materials in Science*, 3rd ed. Canada: Elsevier, 2013.

[29] E. Rabkin and F. J. Schoen, "Cardiovascular tissue engineering," *Cardiovascular Pathology*, vol. 11, no. 6, pp. 305–317, Nov. 2002.

[30] F. Zivic, S. Affatato, M. Trajanovic, M. Schnabelrauch, and N. Grujovic, Eds., *Biomaterials in Clinical Practice: Advances in Clinical Research and Medical Devices*. Switzerland: Springer, 2018, oCLC: 1007925805.

[31] D. F. Williams, "On the mechanisms of biocompatibility," *Biomaterials*, vol. 29, no. 20, pp. 2941–2953, Jul. 2008.

[32] B. Weyand, M. Dominici, R. Hass, R. Jacobs, and Kasper, Eds., *Mesenchymal Stem Cells: Basics and Clinical Applications I*, ser. Advances in Biochemical Engineering/Biotechnology. Springer, 2013, no. 129.

[33] I. n. de Miguel-Beriain, "The ethics of stem cells revisited," *Advanced Drug Delivery Reviews*, vol. 82-83, pp. 176–180, Mar. 2015.

[34] F. D. Price, K. Kuroda, and M. A. Rudnicki, "Stem cell based therapies to treat muscular dystrophy," *Biochimica et Biophysica Acta (BBA) - Molecular Basis of Disease*, vol. 1772, no. 2, pp. 272–283, Feb. 2007.

[35] S. Yamanaka, "A Fresh Look at iPS Cells," *Cell*, vol. 137, no. 1, pp. 13–17, Apr. 2009.

[36] K. Takahashi, K. Tanabe, M. Ohnuki, M. Narita, T. Ichisaka, K. Tomoda, and S. Yamanaka, "Induction of Pluripotent Stem Cells from Adult Human Fibroblasts by Defined Factors," *Cell*, vol. 131, no. 5, pp. 861–872, Nov. 2007.

[37] A. I. Caplan, "Mesenchymal stem cells," *Journal of Orthopaedic Research*, vol. 9, no. 5, pp. 641–650, 1991.

[38] A. Uccelli, L. Moretta, and V. Pistoia, "Mesenchymal stem cells in health and disease," *Nature Reviews Immunology*, vol. 8, no. 9, pp. 726–736, Sep. 2008.

[39] A. I. Caplan, "Adult mesenchymal stem cells for tissue engineering versus regenerative medicine," *Journal of Cellular Physiology*, vol. 213, no. 2, pp. 341–347, Nov. 2007.

[40] M. E. Bernardo, F. Locatelli, and W. E. Fibbe, "Mesenchymal stromal cells," *Annals of the New York Academy of Sciences*, vol. 1176, pp. 101–117, Sep. 2009.

[41] D. Spruyt, C. Gillet, and J. Rasschaert, "Bone and Bone Marrow, Interactions," in *Reference Module in Biomedical Sciences*. Elsevier, Jan. 2018.

[42] D. B. Burr and M. R. Allen, *Basic and Applied Bone Biology*. Elsevier Science, 2013.

[43] F. F. Safadi, M. F. Barbe, S. M. Abdelmagid, M. C. Rico, R. A. Aswad, J. Litvin, and S. N. Popoff, "Bone Structure, Development and Bone Biology," in *Bone Pathology*. Humana Press, 2009, pp. 1–50.

[44] "OSTEOCORD: Bone from Blood," www.york.ac.uk/res/bonefromblood/, Jul. 2018.

[45] National Institutes of Health, "National Institute of Arthritis and Musculoskeletal and Skin Diseases," www.niams.nih.gov, Jul. 2018.

[46] N. Rucci and A. Teti, "Bone Cells: Osteoblast/Osteoclast/Osteocyte," in *Reference Module in Biomedical Sciences*. Elsevier, Jan. 2018.

[47] J. Baldwin, J. Henkel, and D. W. Hutmacher, "6.3 Engineering the Organ Bone," in *Comprehensive Biomaterials II*, P. Ducheyne, Ed. Oxford: Elsevier, Jan. 2017, pp. 54–74.

[48] I. Schoen, B. L. Pruitt, and V. Vogel, "The Yin-Yang of Rigidity Sensing: How Forces and Mechanical Properties Regulate the Cellular Response to Materials," *Annual Review of Materials Research*, vol. 43, no. 1, pp. 589–618, 2013.

[49] R. J. McMurray, M. J. Dalby, and P. M. Tsimbouri, "Using biomaterials to study stem cell mechanotransduction, growth and differentiation," *Journal of Tissue Engineering and Regenerative Medicine*, vol. 9, no. 5, pp. 528–539, May 2015.

[50] H. J. Anderson, J. K. Sahoo, R. V. Ulijn, and M. J. Dalby, "Mesenchymal Stem Cell Fate: Applying Biomaterials for Control of Stem Cell Behavior," *Frontiers in Bioengineering and Biotechnology*, vol. 4, May 2016.

[51] S. C. Neves, R. F. Pereira, M. Araújo, and C. C. Barrias, "Bioengineered peptide-functionalized hydrogels for tissue regeneration and repair," in *Peptides and Proteins as Biomaterials for Tissue Regeneration and Repair*, M. A. Barbosa and M. C. L. Martins, Eds. Woodhead Publishing, Jan. 2018, pp. 101–125.

[52] J. E. Phillips, T. A. Petrie, F. P. Creighton, and A. J. García, "Human mesenchymal stem cell differentiation on self-assembled monolayers presenting different surface chemistries," *Acta Biomaterialia*, vol. 6, no. 1, pp. 12–20, Jan. 2010.

[53] J. M. Curran, R. Chen, and J. A. Hunt, "The guidance of human mesenchymal stem cell differentiation in vitro by controlled modifications to the cell substrate," *Biomaterials*, vol. 27, no. 27, pp. 4783–4793, Sep. 2006.

[54] S. L. Bellis, "Advantages of RGD peptides for directing cell association with biomaterials," *Biomaterials*, vol. 32, no. 18, pp. 4205–4210, Jun. 2011.

[55] T. G. Kapp, F. Rechenmacher, S. Neubauer, O. V. Maltsev, E. A. Cavalcanti-Adam, R. Zarka, U. Reuning, J. Notni, H.-J. Wester, C. Mas-Moruno, J. Spatz, B. Geiger, and H. Kessler, "A Comprehensive Evaluation of the Activity and Selectivity Profile of Ligands for RGD-binding Integrins," *Scientific Reports*, vol. 7, Jan. 2017.

[56] X. Chen, P. Sevilla, and C. Aparicio, "Surface biofunctionalization by covalent co-immobilization of oligopeptides," *Colloids and Surfaces B: Biointerfaces*, vol. 107, pp. 189–197, Jul. 2013.

[57] R. Fraioli, K. Dashnyam, J.-H. Kim, R. A. Perez, H.-W. Kim, J. Gil, M.-P. Ginebra, J. M. Manero, and C. Mas-Moruno, "Surface guidance of stem cell behavior: Chemically tailored co-presentation of integrin-binding peptides stimulates osteogenic differentiation in vitro and bone formation in vivo," *Acta Biomaterialia*, vol. 43, pp. 269–281, Oct. 2016.

[58] K. M. Hennessy, B. E. Pollot, W. C. Clem, M. C. Phipps, A. A. Sawyer, B. K. Culpepper, and S. L. Bellis, "The effect of collagen I mimetic peptides on mesenchymal stem cell adhesion and differentiation, and on bone formation at hydroxyapatite surfaces," *Biomaterials*, vol. 30, no. 10, pp. 1898–1909, Apr. 2009.

[59] A. M. Wojtowicz, A. Shekaran, M. E. Oest, K. M. Dupont, K. L. Templeman, D. W. Hutmacher, R. E. Guldberg, and A. J. García, "Coating of biomaterial scaffolds with the collagen-mimetic peptide GFOGER for bone defect repair," *Biomaterials*, vol. 31, no. 9, pp. 2574–2582, Mar. 2010.

[60] P. Gentile, A. M. Ferreira, J. T. Callaghan, C. A. Miller, J. Atkinson, C. Freeman, and P. V. Hatton, "Multilayer Nanoscale Encapsulation of Biofunctional Peptides to Enhance Bone Tissue Regeneration In Vivo," *Advanced Healthcare Materials*, vol. 6, no. 8, p. 1601182, Feb. 2017.

[61] A. E. Rodda, L. Meagher, D. R. Nisbet, and J. S. Forsythe, "Specific control of cell–material interactions: Targeting cell receptors using ligand-functionalized polymer substrates," *Progress in Polymer Science*, vol. 39, no. 7, pp. 1312–1347, Jul. 2014.

[62] N. O. Enemchukwu and A. J. García, "Peptide- and Protein-Modified Surfaces," in *Comprehensive Biomaterials II*, P. Ducheyne, Ed. Oxford: Elsevier, Jan. 2017, pp. 200–220.

[63] U. Hersel, C. Dahmen, and H. Kessler, "RGD modified polymers: Biomaterials for stimulated cell adhesion and beyond," *Biomaterials*, vol. 24, no. 24, pp. 4385–4415, Nov. 2003.

[64] R. Tejero, E. Anitua, and G. Orive, "Toward the biomimetic implant surface: Biopolymers on titanium-based implants for bone regeneration," *Progress in Polymer Science*, vol. 39, no. 7, pp. 1406–1447, Jul. 2014.

[65] R. Beutner, J. Michael, B. Schwenzer, and D. Scharnweber, "Biological nano-functionalization of titanium-based biomaterial surfaces: A flexible toolbox," *Journal of The Royal Society Interface*, vol. 7, no. Suppl 1, pp. S93–S105, Feb. 2010.

[66] C. Mas-Moruno, R. Fraioli, F. Rechenmacher, S. Neubauer, T. G. Kapp, and H. Kessler, "avβ3- or a5β1-Integrin-Selective Peptidomimetics for Surface Coating," *Angewandte Chemie International Edition*, vol. 55, no. 25, pp. 7048–7067, 2016.

[67] Y.-S. Huang, V. Bertrand, D. Bozukova, C. Pagnoulle, C. Labrugère, E. De Pauw, M.-C. De Pauw-Gillet, and M.-C. Durrieu, "RGD Surface Functionalization of the Hydrophilic Acrylic Intraocular Lens Material to Control Posterior Capsular Opacification," *PLoS ONE*, vol. 9, no. 12, pp. 1–32, Dec. 2014.

[68] M. Kantlehner, P. Schaffner, D. Finsinger, J. Meyer, A. Jonczyk, B. Diefenbach, B. Nies, G. Hölzemann, S. L. Goodman, and H. Kessler, "Surface Coating with Cyclic RGD Peptides Stimulates Osteoblast Adhesion and Proliferation as well as Bone Formation," *ChemBioChem*, vol. 1, no. 2, pp. 107–114, Aug. 2000.

[69] A. Mardilovich and E. Kokkoli, "Biomimetic Peptide-Amphiphiles for Functional Biomaterials: The Role of GRGDSP and PHSRN," *Biomacromolecules*, vol. 5, no. 3, pp. 950–957, May 2004.

[70] C. Mas-Moruno, R. Fraioli, F. Albericio, J. M. Manero, and F. J. Gil, "Novel Peptide-Based Platform for the Dual Presentation of Biologically Active Peptide Motifs on Biomaterials," *ACS Applied Materials & Interfaces*, vol. 6, no. 9, pp. 6525–6536, May 2014.

[71] J. Marchand-Brynaert, E. Detrait, O. Noiset, T. Boxus, Y.-J. Schneider, and C. Remacle, "Biological evaluation of RGD peptidomimetics, designed for the covalent derivatization of cell culture substrata, as potential promotors of cellular adhesion," *Biomaterials*, vol. 20, no. 19, pp. 1773–1782, Oct. 1999.

[72] A. Grauer and B. König, "Peptidomimetics – A Versatile Route to Biologically Active Compounds," *European Journal of Organic Chemistry*, vol. 2009, no. 30, pp. 5099–5111, Oct. 2009.

[73] K. Anselme, "Osteoblast adhesion on biomaterials," *Biomaterials*, vol. 21, no. 7, pp. 667–681, Apr. 2000.

[74] H. Mao and Y. Ito, "Growth Factors and Protein-Modified Surfaces and Interfaces," in *Comprehensive Biomaterials II*, P. Ducheyne, Ed. Oxford: Elsevier, Jan. 2017, vol. 4, pp. 321–359.

[75] B. M. Gumbiner, "Cell Adhesion: The Molecular Basis of Tissue Architecture and Morphogenesis," *Cell*, vol. 84, no. 3, pp. 345–357, Feb. 1996.

[76] S. J. Shattil, C. Kim, and M. H. Ginsberg, "The final steps of integrin activation: The end game," *Nature Reviews Molecular Cell Biology*, vol. 11, no. 4, pp. 288–300, Apr. 2010.

[77] M. Vicente-Manzanares, C. K. Choi, and A. R. Horwitz, "Integrins in cell migration – the actin connection," *Journal of Cell Science*, vol. 122, no. 2, pp. 199–206, Jan. 2009.

[78] M. C. Siebers, P. J. ter Brugge, X. F. Walboomers, and J. A. Jansen, "Integrins as linker proteins between osteoblasts and bone replacing materials. A critical review," *Biomaterials*, vol. 26, no. 2, pp. 137–146, Jan. 2005.

[79] P. Kanchanawong, G. Shtengel, A. M. Pasapera, E. B. Ramko, M. W. Davidson, H. F. Hess, and C. M. Waterman, "Nanoscale architecture of integrin-based cell adhesions," *Nature*, vol. 468, no. 7323, pp. 580–584, Nov. 2010.

[80] R. G. Lebaron, "Extracellular Matrix Cell Adhesion Peptides: Functional Applications in Orthopedic Materials," *ResearchGate*, 2000.

[81] B. B. Shotorbani, E. Alizadeh, R. Salehi, and A. Barzegar, "Adhesion of mesenchymal stem cells to biomimetic polymers: A review," *Materials Science and Engineering: C*, vol. 71, pp. 1192–1200, Feb. 2017.

[82] P. Gentile, C. Ghione, C. Tonda-Turo, and D. M. Kalaskar, "Peptide functionalisation of nanocomposite polymer for bone tissue engineering using plasma surface polymerisation," *RSC Advances*, vol. 5, no. 97, pp. 80 039–80 047, Sep. 2015.

[83] G. M. Harbers and K. E. Healy, "The effect of ligand type and density on osteoblast adhesion, proliferation, and matrix mineralization," *Journal of Biomedical Materials Research Part A*, vol. 75A, no. 4, pp. 855–869, 2005.

[84] B. F. Bell, M. Schuler, S. Tosatti, M. Textor, Z. Schwartz, and B. D. Boyan, "Osteoblast response to titanium surfaces functionalized with extracellular matrix peptide biomimetics," *Clinical Oral Implants Research*, vol. 22, no. 8, pp. 865–872, Aug. 2011.

[85] A. A. Sawyer, K. M. Hennessy, and S. L. Bellis, "The effect of adsorbed serum proteins, RGD and proteoglycan-binding peptides on the adhesion of mesenchymal stem cells to hydroxyapatite," *Biomaterials*, vol. 28, no. 3, pp. 383–392, Jan. 2007.

[86] N. Broggini, S. Tosatti, S. J. Ferguson, M. Schuler, M. Textor, M. M. Bornstein, D. D. Bosshardt, and D. Buser, "Evaluation of chemically modified SLA implants (modSLA) biofunctionalized with integrin (RGD)- and heparin (KRSR)-binding peptides," *Journal of Biomedical Materials Research. Part A*, vol. 100, no. 3, pp. 703–711, Mar. 2012.

[87] J. O. Hollinger, P. Alvarez-Urena, P. Ducheyne, A. Srinivasan, J. Baskin, H. Waters, and R. Gruber, "Bone Tissue Engineering: Growth Factors and Cytokines," in *Comprehensive Biomaterials II*, P. Ducheyne, Ed. Oxford: Elsevier, Jan. 2017, pp. 20–53.

[88] J. D. Lamplot, S. Denduluri, X. Liu, J. Wang, L. Yin, R. Li, W. Shui, H. Zhang, N. Wang, G. Nan, J. Angeles, L. L. Shi, R. C. Haydon, H. H. Luu, S. Ho, and T.-C. He, "Major Signaling Pathways Regulating the Proliferation and Differentiation of Mesenchymal Stem Cells," in *Essentials of Mesenchymal Stem Cell Biology and Its Clinical Translation*, R. C. Zhao, Ed. Springer Netherlands, 2013, pp. 75–100.

[89] B. Bragdon, O. Moseychuk, S. Saldanha, D. King, J. Julian, and A. Nohe, "Bone Morphogenetic Proteins: A critical review," *Cellular Signalling*, vol. 23, no. 4, pp. 609–620, Apr. 2011.

[90] W. F. McKay, S. M. Peckham, and J. M. Badura, "A comprehensive clinical review of recombinant human bone morphogenetic protein-2 (INFUSE® Bone Graft)," *International Orthopaedics*, vol. 31, no. 6, pp. 729–734, Dec. 2007.

[91] O. F. ZOUANI, "Compounds for Inducing Tissue Formation and Uses Thereof," Patent US2 018 208 635 (A1), Jul., 2018, cIB: C07K14/51.

[92] A. S. G. Curtis and M. Varde, "Control of Cell Behavior: Topological Factors," *JNCI: Journal of the National Cancer Institute*, vol. 33, no. 1, pp. 15–26, Jul. 1964.

[93] R. A. Gittens, T. McLachlan, R. Olivares-Navarrete, Y. Cai, S. Berner, R. Tannenbaum, Z. Schwartz, K. H. Sandhage, and B. D. Boyan, "The effects of combined micron-/submicron-scale surface roughness and nanoscale features on cell proliferation and differentiation," *Biomaterials*, vol. 32, no. 13, pp. 3395–3403, May 2011.

[94] A. Curtis and C. Wilkinson, "Topographical control of cells," *Biomaterials*, vol. 18, no. 24, pp. 1573–1583, Dec. 1997.

[95] M. J. Dalby, S. J. Yarwood, H. J. H. Johnstone, S. Affrossman, and M. O. Riehle, "Fibroblast signaling events in response to nanotopography: A gene array study," *IEEE Transactions on NanoBioscience*, vol. 1, no. 1, pp. 12–17, Mar. 2002.

[96] M. M. Stevens and J. H. George, "Exploring and Engineering the Cell Surface Interface," *Science*, vol. 310, no. 5751, pp. 1135–1138, Nov. 2005.

[97] N. Gui, W. Xu, D. E. Myers, R. Shukla, H. P. Tang, and M. Qian, "The effect of ordered and partially ordered surface topography on bone cell responses: A review," *Biomaterials Science*, vol. 6, no. 2, pp. 250–264, 2018.

[98] I. Lauria, M. Höner, S. Kant, R. Davtalab, T. Weik, K. Sternberg, and H. Fischer, "Response of umbilical cord mesenchymal stromal cells to varying titanium topographical signals," *Journal of Biomedical Materials Research Part A*, vol. 106, no. 1, pp. 180–191, Jan. 2018.

[99] A. Cunha, O. F. Zouani, L. Plawinski, A. M. Botelho do Rego, A. Almeida, R. Vilar, and M.-C. Durrieu, "Human mesenchymal stem cell behavior on femtosecond laser-textured Ti-6Al-4V surfaces," *Nanomedicine*, vol. 10, no. 5, pp. 725–739, Mar. 2015.

[100] P. Bertoncini, S. L. Chevalier, S. Lavenus, P. Layrolle, and G. Louarn, "Early adhesion of human mesenchymal stem cells on TiO2 surfaces studied by single-cell force spectroscopy measurements," *Journal of Molecular Recognition*, vol. 25, no. 5, pp. 262–269, May 2012.

[101] D. V. Nazarov, V. M. Smirnov, E. Zemtsova, N. M. Yudintceva, M. A. Shevtsov, and R. Z. Valiev, "Enhanced osseointegrative properties of the ultrafine-grained titanium implants modified by the chemical etching and atomic layer deposition." *ACS Biomaterials Science & Engineering*, Jul. 2018.

[102] T. Sjöström, M. J. Dalby, A. Hart, R. Tare, R. O. C. Oreffo, and B. Su, "Fabrication of pillar-like titania nanostructures on titanium and their interactions with human skeletal stem cells," *Acta Biomaterialia*, vol. 5, no. 5, pp. 1433–1441, Jun. 2009.

[103] Q.-R. Xiao, N. Zhang, X. Wang, X.-Y. Man, K. Yang, L.-X. Lü, and N.-P. Huang, "Oriented Surface Nanotopography Promotes the Osteogenesis of Mesenchymal Stem Cells," *Advanced Materials Interfaces*, vol. 4, no. 3, p. 1600652, Feb. 2017.

[104] J. Park, S. Bauer, K. A. Schlegel, F. W. Neukam, K. von der Mark, and P. Schmuki, "TiO2 Nanotube Surfaces: 15 nm—An Optimal Length Scale of Surface Topography for Cell Adhesion and Differentiation," *Small*, vol. 5, no. 6, pp. 666–671, Mar. 2009.

[105] K. S. Brammer, C. J. Frandsen, and S. Jin, "TiO2 nanotubes for bone regeneration," *Trends in Biotechnology*, vol. 30, no. 6, pp. 315–322, Jun. 2012.

[106] J. Fiedler, B. Özdemir, J. Bartholomä, A. Plettl, R. E. Brenner, and P. Ziemann, "The effect of substrate surface nanotopography on the behavior of multipotnent mesenchymal stromal cells and osteoblasts," *Biomaterials*, vol. 34, no. 35, pp. 8851–8859, Nov. 2013.

[107] P. Tsimbouri, N. Gadegaard, K. Burgess, K. White, P. Reynolds, P. Herzyk, R. Oreffo, and M. J. Dalby, "Nanotopographical Effects on Mesenchymal Stem Cell Morphology and Phenotype," *Journal of Cellular Biochemistry*, vol. 115, no. 2, pp. 380–390, Feb. 2014.

[108] S. Watari, K. Hayashi, J. A. Wood, P. Russell, P. F. Nealey, C. J. Murphy, and D. C. Genetos, "Modulation of osteogenic differentiation in hMSCs cells by submicron topographically-patterned ridges and grooves," *Biomaterials*, vol. 33, no. 1, pp. 128–136, Jan. 2012.

[109] M. T. Raimondi, S. M. Eaton, M. Laganà, V. Aprile, M. M. Nava, G. Cerullo, and R. Osellame, "Three-dimensional structural niches engineered via two-photon laser polymerization promote stem cell homing," *Acta Biomaterialia*, vol. 9, no. 1, pp. 4579–4584, Jan. 2013.

[110] G. M. de Peppo, H. Agheli, C. Karlsson, K. Ekström, H. Brisby, M. Lennerås, S. Gustafsson, P. Sjövall, A. Johansson, E. Olsson, J. Lausmaa, P. Thomsen, and S. Petronis, "Osteogenic response of human mesenchymal stem cells to well-defined nanoscale topography in vitro," *International Journal of Nanomedicine*, vol. 9, pp. 2499–2515, May 2014.

[111] L. E. McNamara, T. Sjöström, K. Seunarine, R. D. Meek, B. Su, and M. J. Dalby, "Investigation of the limits of nanoscale filopodial interactions," *Journal of Tissue Engineering*, vol. 5, p. 2041731414536177, Jan. 2014.

[112] L. E. McNamara, T. Sjöström, K. E. V. Burgess, J. J. W. Kim, E. Liu, S. Gordonov, P. V. Moghe, R. M. D. Meek, R. O. C. Oreffo, B. Su, and M. J. Dalby, "Skeletal stem cell physiology on functionally distinct titania nanotopographies," *Biomaterials*, vol. 32, no. 30, pp. 7403–7410, Oct. 2011.

[113] G. Abagnale, M. Steger, V. H. Nguyen, N. Hersch, A. Sechi, S. Joussen, B. Denecke, R. Merkel, B. Hoffmann, A. Dreser, U. Schnakenberg, A. Gillner, and W. Wagner, "Surface topography enhances differentiation of mesenchymal stem cells towards osteogenic and adipogenic lineages," *Biomaterials*, vol. 61, pp. 316–326, Aug. 2015.

[114] I. A. Janson, Y. P. Kong, and A. J. Putnam, "Nanotopographic Substrates of Poly (Methyl Methacrylate) Do Not Strongly Influence the Osteogenic Phenotype of Mesenchymal Stem Cells In Vitro," *PLOS ONE*, vol. 9, no. 3, p. e90719, Mar. 2014.

[115] B. K. K. Teo, S. T. Wong, C. K. Lim, T. Y. S. Kung, C. H. Yap, Y. Ramagopal, L. H. Romer, and E. K. F. Yim, "Nanotopography Modulates Mechanotransduction of Stem Cells and Induces Differentiation through Focal Adhesion Kinase," *ACS Nano*, vol. 7, no. 6, pp. 4785–4798, Jun. 2013.

[116] K. Kulangara, Y. Yang, J. Yang, and K. W. Leong, "Nanotopography as modulator of human mesenchymal stem cell function," *Biomaterials*, vol. 33, no. 20, pp. 4998–5003, Jul. 2012.

[117] J. Park, S. Bauer, A. Pittrof, M. S. Killian, P. Schmuki, and K. von der Mark, "Synergistic Control of Mesenchymal Stem Cell Differentiation by Nanoscale Surface Geometry and Immobilized Growth Factors on TiO2 Nanotubes," *Small*, vol. 8, no. 1, pp. 98–107, Jan. 2012.

[118] R. J. McMurray, N. Gadegaard, P. M. Tsimbouri, K. V. Burgess, L. E. McNamara, R. Tare, K. Murawski, E. Kingham, R. O. C. Oreffo, and M. J. Dalby, "Nanoscale surfaces for the long-term maintenance of mesenchymal stem cell phenotype and multipotency," *Nature Materials*, vol. 10, no. 8, pp. 637–644, Aug. 2011.

[119] M. J. Dalby, N. Gadegaard, R. Tare, A. Andar, M. O. Riehle, P. Herzyk, C. D. W. Wilkinson, and R. O. C. Oreffo, "The control of human mesenchymal cell differentiation using nanoscale symmetry and disorder," *Nature Materials*, vol. 6, no. 12, pp. 997–1003, Dec. 2007.

[120] M. J. P. Biggs, R. G. Richards, N. Gadegaard, C. D. W. Wilkinson, and M. J. Dalby, "The effects of nanoscale pits on primary human osteoblast adhesion formation and cellular spreading," *Journal of Materials Science: Materials in Medicine*, vol. 18, no. 2, pp. 399–404, Feb. 2007.

[121] J. Tang, R. Peng, and J. Ding, "The regulation of stem cell differentiation by cell-

cell contact on micropatterned material surfaces," *Biomaterials*, vol. 31, no. 9, pp. 2470–2476, Mar. 2010.

[122] K. S. Brammer, S. Oh, C. J. Cobb, L. M. Bjursten, H. van der Heyde, and S. Jin, "Improved bone-forming functionality on diameter-controlled TiO2 nanotube surface," *Acta Biomaterialia*, vol. 5, no. 8, pp. 3215–3223, Oct. 2009.

[123] J. S. Park, H. N. Yang, S. Y. Jeon, D. G. Woo, K. Na, and K.-H. Park, "Osteogenic differentiation of human mesenchymal stem cells using RGD-modified BMP-2 coated microspheres," *Biomaterials*, vol. 31, no. 24, pp. 6239–6248, Aug. 2010.

[124] J. Park, S. Bauer, K. von der Mark, and P. Schmuki, "Nanosize and Vitality: TiO2 Nanotube Diameter Directs Cell Fate," *Nano Letters*, vol. 7, no. 6, pp. 1686–1691, Jun. 2007.

[125] A. S. G. Curtis, N. Gadegaard, M. J. Dalby, M. O. Riehle, C. D. W. Wilkinson, and G. Aitchison, "Cells react to nanoscale order and symmetry in their surroundings," *IEEE Transactions on NanoBioscience*, vol. 3, no. 1, pp. 61–65, Mar. 2004.

[126] M. J. P. Biggs, M. Fernandez, D. Thomas, R. Cooper, M. Palma, J. Liao, T. Fazio, C. Dahlberg, H. Wheadon, A. Pallipurath, A. Pandit, J. Kysar, and S. J. Wind, "The Functional Response of Mesenchymal Stem Cells to Electron-Beam Patterned Elastomeric Surfaces Presenting Micrometer to Nanoscale Heterogeneous Rigidity," *Advanced Materials*, vol. 29, no. 39, pp. n/a–n/a, Oct. 2017.

[127] C. Allan, A. Ker, C.-A. Smith, P. M. Tsimbouri, J. Borsoi, S. O'Neill, N. Gadegaard, M. J. Dalby, and R. Dominic Meek, "Osteoblast response to disordered nanotopography," *Journal of Tissue Engineering*, vol. 9, p. 2041731418784098, Jan. 2018.

[128] L. C. Y. Lee, N. Gadegaard, M. C. de Andrés, L.-A. Turner, K. V. Burgess, S. J. Yarwood, J. Wells, M. Salmeron-Sanchez, D. Meek, R. O. C. Oreffo, and M. J. Dalby, "Nanotopography controls cell cycle changes involved with skeletal stem cell self-renewal and multipotency," *Biomaterials*, vol. 116, pp. 10–20, Feb. 2017.

[129] F. Mussano, T. Genova, F. Serra, M. Carossa, L. Munaron, S. Carossa, F. Mussano, T. Genova, F. G. Serra, M. Carossa, L. Munaron, and S. Carossa, "Nano-Pore Size of Alumina Affects Osteoblastic Response," *International Journal of Molecular Sciences*, vol. 19, no. 2, p. 528, Feb. 2018.

[130] A. M. Loye, E. R. Kinser, S. Bensouda, M. Shayan, R. Davis, R. Wang, Z. Chen, U. D. Schwarz, J. Schroers, and T. R. Kyriakides, "Regulation of Mesenchymal Stem Cell Differentiation by Nanopatterning of Bulk Metallic Glass," *Scientific Reports*, vol. 8, no. 1, p. 8758, Jun. 2018.

[131] G. Riess, "Micellization of block copolymers," *Progress in Polymer Science*, vol. 28, no. 7, pp. 1107–1170, Jul. 2003.

[132] S. Förster and M. Konrad, "From self-organizing polymers to nano- and biomaterials," *Journal of Materials Chemistry*, vol. 13, no. 11, pp. 2671–2688, Oct. 2003.

[133] J. Rodríguez-Hernández, F. Chécot, Y. Gnanou, and S. Lecommandoux, "Toward 'smart' nano-objects by self-assembly of block copolymers in solution," *Progress in Polymer Science*, vol. 30, no. 7, pp. 691–724, Jul. 2005.

[134] R. J. Thibault and V. M. Rotello, "Molecular Self-Assembly," in *Encyclopedia of Polymer Science and Technology*. American Cancer Society, 2004.

[135] T. Liu, L. Z. Liu, and B. Chu, "Formation of Amphiphilic Block Copolymer Micelles in Nonaqueous Solution**Acknowledgements: BC gratefully acknowledge the support of their work by the Department of Energy (DE-FGO286ER45237.012), and the National Center for Human Genome Research (1R01HG0138601). He also wishes to thank many of his colleagues and scientists who have graciously sent him their reprints and preprints, in particular to A. Eisenberg, I.A. Katime, A.P. Gast, T. Nose, C. Frank, S.P. Nunes and J.L. Fulton." in *Amphiphilic Block Copolymers*, P. Alexandridis and B. Lindman, Eds. Amsterdam: Elsevier Science B.V., Jan. 2000, pp. 115–149.

[136] S. Förster, M. Zisenis, E. Wenz, and M. Antonietti, "Micellization of strongly segregated block copolymers," *The Journal of Chemical Physics*, vol. 104, no. 24, pp. 9956–9970, Jun. 1996.

[137] S. Krishnamoorthy, C. Hinderling, and H. Heinzelmann, "Nanoscale patterning with block copolymers," *Materials Today*, vol. 9, no. 9, pp. 40–47, Sep. 2006.

[138] M. Park, C. Harrison, P. M. Chaikin, R. A. Register, and D. H. Adamson, "Block Copolymer Lithography: Periodic Arrays of ˜1011 Holes in 1 Square Centimeter," *Science*, vol. 276, no. 5317, pp. 1401–1404, May 1997.

[139] J. P. Spatz, S. Mößmer, and M. Möller, "Mineralization of Gold Nanoparticles in a Block Copolymer Microemulsion," *Chemistry – A European Journal*, vol. 2, no. 12, pp. 1552–1555, Dec. 1996.

[140] L. TOPPAN PRINTING CO., "Nanoimprint solution," https://www.toppan.co.jp/electronics/english/semicon/nano_in_print/, Sep. 2018.

[141] L. J. Guo, "Nanoimprint Lithography: Methods and Material Requirements," *Advanced Materials*, vol. 19, no. 4, pp. 495–513, Feb. 2007.

[142] F. Hua, Y. Sun, A. Gaur, M. A. Meitl, L. Bilhaut, L. Rotkina, J. Wang, P. Geil, M. Shim, J. A. Rogers, and A. Shim, "Polymer Imprint Lithography with Molecular-Scale Resolution," *Nano Letters*, vol. 4, no. 12, pp. 2467–2471, Dec. 2004.

[143] H. Lan and Y. Ding, "Nanoimprint Lithography," in *Lithography*, M. Wang, Ed. Croatia: Intech Open, 2010, p. 656.

[144] S. Y. Chou, P. R. Krauss, W. Zhang, L. Guo, and L. Zhuang, "Sub-10 nm imprint lithography and applications," *Journal of Vacuum Science & Technology B: Microelectronics and Nanometer Structures Processing, Measurement, and Phenomena*, vol. 15, no. 6, pp. 2897–2904, Nov. 1997.

[145] W. Zhou, *Nanoimprint Lithography: An Enabling Process for Nanofabrication*. Berlin, Heidelberg: Springer Berlin Heidelberg, 2013.

[146] A.-M. Popa, P. Niedermann, H. Heinzelmann, J. A. Hubbell, and R. Pugin, "Fabrication of nanopore arrays and ultrathin silicon nitride membranes by block-copolymer-assisted lithography," *Nanotechnology*, vol. 20, no. 48, p. 485303, Dec. 2009.

[147] M. W. Pfaffl, A. Tichopad, C. Prgomet, and T. P. Neuvians, "Determination of stable housekeeping genes, differentially regulated target genes and sample integrity: BestKeeper – Excel-based tool using pair-wise correlations," *Biotechnology Letters*, vol. 26, no. 6, pp. 509–515, Mar. 2004.

[148] K. H. Vining and D. J. Mooney, "Mechanical forces direct stem cell behaviour in development and regeneration," *Nature Reviews Molecular Cell Biology*, p. nrm.2017.108, Nov. 2017.

[149] S. M. Nalluri, M. J. Hill, and D. Sarkar, "Control of Mesenchymal Stem Cells with Biomaterials," in *Essentials of Mesenchymal Stem Cell Biology and Its Clinical Translation*, R. C. Zhao, Ed. Springer Netherlands, 2013, pp. 139–159.

[150] R. G. Harrison, "On the Stereotropism of Embryonic Cells," *Science*, vol. 34, no. 870, pp. 279–281, Sep. 1911.

[151] M. J. Dalby, "Cellular response to low adhesion nanotopographies," *International Journal of Nanomedicine*, vol. 2, no. 3, pp. 373–381, Sep. 2007.

[152] C. Vater, P. Kasten, and M. Stiehler, "Culture media for the differentiation of mesenchymal stromal cells," *Acta Biomaterialia*, vol. 7, no. 2, pp. 463–477, Feb. 2011.

[153] S. Hagmann, B. Moradi, S. Frank, T. Dreher, P. W. Kämmerer, W. Richter, and T. Gotterbarm, "Different culture media affect growth characteristics, surface marker distribution and chondrogenic differentiation of human bone marrow-derived mesenchymal stromal cells," *BMC Musculoskeletal Disorders*, vol. 14, no. 1, p. 223, Jul. 2013.

[154] M. Kim, C. Kim, Y. S. Choi, M. Kim, C. Park, and Y. Suh, "Age-related alterations in mesenchymal stem cells related to shift in differentiation from osteogenic to adipogenic potential: Implication to age-associated bone diseases and defects," *Mechanisms of Ageing and Development*, vol. 133, no. 5, pp. 215–225, May 2012.

[155] M. Maredziak, K. Marycz, K. A. Tomaszewski, K. Kornicka, and B. M. Henry, "The Influence of Aging on the Regenerative Potential of Human Adipose Derived Mesenchymal Stem Cells," *Stem Cells International*, vol. 2016, no. Article ID 2152435, p. 15, 2016.

[156] S. Zhou, J. S. Greenberger, M. W. Epperly, J. P. Goff, C. Adler, M. S. LeBoff, and J. Glowacki, "Age-related intrinsic changes in human bone-marrow-derived mesenchymal stem cells and their differentiation to osteoblasts," *Aging Cell*, vol. 7, no. 3, pp. 335–343, Jun. 2008.

[157] E. U. Alt, C. Senst, S. N. Murthy, D. P. Slakey, C. L. Dupin, A. E. Chaffin, P. J. Kadowitz, and R. Izadpanah, "Aging alters tissue resident mesenchymal stem cell properties," *Stem Cell Research*, vol. 8, no. 2, pp. 215–225, Mar. 2012.

[158] P. Ganguly, J. J. El-Jawhari, P. V. Giannoudis, A. N. Burska, F. Ponchel, and E. A. Jones, "Age-related Changes in Bone Marrow Mesenchymal Stromal Cells: A Potential Impact on Osteoporosis and Osteoarthritis Development," *Cell Transplantation*, vol. 26, no. 9, pp. 1520–1529, Sep. 2017.

[159] K. Brassat, D. Kool, J. Bürger, and J. K. N. Lindner, "Hierarchical nanopores formed by block copolymer lithography on the surfaces of different materials pre-patterned by nanosphere lithography," *Nanoscale*, vol. 10, no. 21, pp. 10 005–10 017, May 2018.

[160] R. Katsumata, M. N. Yogeesh, H. Wong, S. X. Zhou, S. M. Sirard, T. Huang, R. D. Piner, Z. Wu, W. Li, A. L. Lee, M. C. Carlson, M. J. Maher, D. Akinwande, and C. J. Ellison, "Large area fabrication of graphene nanoribbons by wetting transparency-assisted block copolymer lithography," *Polymer*, vol. 110, pp. 131–138, Feb. 2017.

[161] S. Coppola, V. Vespini, F. Olivieri, G. Nasti, M. Todino, B. Mandracchia, V. Pagliarulo, and P. Ferraro, "Direct self-assembling and patterning of semiconductor quantum dots on transferable elastomer layer," *Applied Surface Science*, vol. 399, pp. 160–166, Mar. 2017.

[162] C. Cummins, A. P. Bell, and M. A. Morris, "Creating Active Device Materials for Nanoelectronics Using Block Copolymer Lithography," *Nanomaterials*, vol. 7, no. 10, p. 304, Sep. 2017.

[163] P. A. George, M. R. Doran, T. I. Croll, T. P. Munro, and J. J. Cooper-White, "Nanoscale presentation of cell adhesive molecules via block copolymer self-assembly," *Biomaterials*, vol. 30, no. 27, pp. 4732–4737, Sep. 2009.

[164] E. H. Schwab, T. L. M. Pohl, T. Haraszti, G. K. Schwaerzer, C. Hiepen, J. P. Spatz, P. Knaus, and E. A. Cavalcanti-Adam, "Nanoscale Control of Surface Immobilized BMP-2: Toward a Quantitative Assessment of BMP-Mediated Signaling Events," *Nano Letters*, vol. 15, no. 3, pp. 1526–1534, Mar. 2015.

[165] H. L. Khor, Y. Kuan, H. Kukula, K. Tamada, W. Knoll, M. Moeller, and D. W. Hutmacher, "Response of Cells on Surface-Induced Nanopatterns: Fibroblasts and Mesenchymal Progenitor Cells," *Biomacromolecules*, vol. 8, no. 5, pp. 1530–1540, May 2007.

[166] F. L. Yap and S. Krishnamoorthy, "Fabricating 2D arrays of chemical templates for in situ synthesis of inorganic nanostructures using self-assembly based nanolithography," vol. 20, no. 45, pp. 10 211–10 216, Nov. 2010.

[167] W. L. Murphy, T. C. McDevitt, and A. J. Engler, "Materials as stem cell regulators," *Nature Materials*, vol. 13, no. 6, pp. 547–557, May 2014.

[168] T. Maier, M. Güell, and L. Serrano, "Correlation of mRNA and protein in complex biological samples," *FEBS Letters*, vol. 583, no. 24, pp. 3966–3973, Dec. 2009.

[169] C. Vogel and E. M. Marcotte, "Insights into the regulation of protein abundance from proteomic and transcriptomic analyses," *Nature Reviews Genetics*, vol. 13, no. 4, pp. 227–232, Apr. 2012.

[170] R. K. Das, O. F. Zouani, C. Labrugère, R. Oda, and M.-C. Durrieu, "Influence of Nanohelical Shape and Periodicity on Stem Cell Fate," *ACS Nano*, vol. 7, no. 4, pp. 3351–3361, Apr. 2013.

[171] H. Donnelly, M. Salmeron-Sanchez, and M. J. Dalby, "Designing stem cell niches for differentiation and self-renewal," *Journal of The Royal Society Interface*, vol. 15, no. 145, p. 20180388, Aug. 2018.

[172] M. A. Chavis, D.-M. Smilgies, U. B. Wiesner, and C. K. Ober, "Widely Tunable Morphologies in Block Copolymer Thin Films Through Solvent Vapor Annealing Using Mixtures of Selective Solvents," *Advanced Functional Materials*, vol. 25, no. 20, pp. 3057–3065, Apr. 2015.

[173] C. Park, J. Yoon, and E. L. Thomas, "Enabling nanotechnology with self assembled block copolymer patterns," *Polymer*, vol. 44, no. 22, pp. 6725–6760, Oct. 2003.

[174] Q. Zhang, S. Lin, Q. Li, D. Zhao, and X. Cai, "Cellular Response to Surface Topography and Substrate Stiffness," in *Cartilage Regeneration*, ser. Stem Cell Biology and Regenerative Medicine, Y. Lin, Ed.   Cham: Springer International Publishing, 2017, pp. 41–57.

[175] Z. Chen, A. Bachhuka, F. Wei, X. Wang, G. Liu, K. Vasilev, and Y. Xiao, "Nanotopography-based strategy for the precise manipulation of osteoimmunomodulation in bone regeneration," *Nanoscale*, vol. 9, no. 46, pp. 18 129–18 152, Nov. 2017.

[176] S. P. Low, K. A. Williams, L. T. Canham, and N. H. Voelcker, "Evaluation of mammalian cell adhesion on surface-modified porous silicon," *Biomaterials*, vol. 27, no. 26, pp. 4538–4546, Sep. 2006.

[177] Q. Zhou, Z. Zhao, Z. Zhou, G. Zhang, R. C. Chiechi, and P. van Rijn, "Directing Mesenchymal Stem Cells with Gold Nanowire Arrays," *Advanced Materials Interfaces*, vol. 5, no. 14, p. 1800334, Jul. 2018.

[178] S. Zhang, B. Ma, F. Liu, J. Duan, S. Wang, J. Qiu, D. Li, Y. Sang, C. Liu, D. Liu, and H. Liu, "Polylactic Acid Nanopillar Array-Driven Osteogenic Differentiation of Human Adipose-Derived Stem Cells Determined by Pillar Diameter," *Nano Letters*, vol. 18, no. 4, pp. 2243–2253, Apr. 2018.

[179] E. P. Su, D. F. Justin, C. R. Pratt, V. K. Sarin, V. S. Nguyen, S. Oh, and S. Jin, "Effects of titanium nanotubes on the osseointegration, cell differentiation, mineralisation and antibacterial properties of orthopaedic implant surfaces," *The Bone & Joint Journal*, vol. 100-B, no. 1_Supple_A, pp. 9–16, Jan. 2018.

[180] J. H. Collier and T. Segura, "Evolving the use of peptides as components of biomaterials," *Biomaterials*, vol. 32, no. 18, pp. 4198–4204, Jun. 2011.

[181] X. Wang, S. Li, C. Yan, P. Liu, and J. Ding, "Fabrication of RGD Micro/Nanopattern and Corresponding Study of Stem Cell Differentiation," *Nano Letters*, vol. 15, no. 3, pp. 1457–1467, Mar. 2015.

[182] S. Wu, X. Yang, W. Li, L. Du, R. Zeng, and M. Tu, "Enhancing osteogenic differentiation of MC3T3-E1 cells by immobilizing RGD onto liquid crystal substrate," *Materials Science and Engineering: C*, vol. 71, pp. 973–981, Feb. 2017.

[183] E. Migliorini, A. Valat, C. Picart, and E. A. Cavalcanti-Adam, "Tuning cellular responses to BMP-2 with material surfaces," *Cytokine & Growth Factor Reviews*, vol. 27, pp. 43–54, Feb. 2016.

[184] M.-J. Kim, B. Lee, K. Yang, J. Park, S. Jeon, S. H. Um, D.-I. Kim, S. G. Im, and S.-W. Cho, "BMP-2 peptide-functionalized nanopatterned substrates for enhanced osteogenic differentiation of human mesenchymal stem cells," *Biomaterials*, vol. 34, no. 30, pp. 7236–7246, Oct. 2013.

[185] Y. Ma, G. M. Policastro, Q. Li, J. Zheng, R. Jacquet, W. J. Landis, and M. L. Becker, "Concentration-Dependent hMSC Differentiation on Orthogonal Concentration Gradients of GRGDS and BMP-2 Peptides," *Biomacromolecules*, vol. 17, no. 4, pp. 1486–1495, Apr. 2016.

[186] G. Kaur, C. Wang, J. Sun, and Q. Wang, "The synergistic effects of multivalent ligand display and nanotopography on osteogenic differentiation of rat bone marrow stem cells," *Biomaterials*, vol. 31, no. 22, pp. 5813–5824, Aug. 2010.

[187] M. Lai, Z. Jin, and Z. Su, "Surface modification of TiO2 nanotubes with osteogenic growth peptide to enhance osteoblast differentiation," *Materials Science and Engineering: C*, vol. 73, pp. 490–497, Apr. 2017.

[188] X. Gao, X. Zhang, J. Song, X. Xu, A. Xu, M. Wang, B. Xie, E. Huang, F. Deng, and S. Wei, "Osteoinductive peptide-functionalized nanofibers with highly ordered structure as biomimetic scaffolds for bone tissue engineering," *International Journal of Nanomedicine*, Nov. 2015.

[189] M. C. Durrieu, S. Pallu, F. Guillemot, R. Bareille, J. Amédée, C. Baquey, C. Labrugère, and M. Dard, "Grafting RGD containing peptides onto hydroxyapatite to promote osteoblastic cells adhesion," *Journal of Materials Science: Materials in Medicine*, vol. 15, no. 7, pp. 779–786, Jul. 2004.

[190] B. Alberts, D. Bray, K. Hopkin, A. D. Johnson, J. Lewis, M. Raff, K. Roberts, and P. Walter, *Essential Cell Biology.* Garland Science, Jan. 2015.

[191] A. Foroughi-Abari and K. Cadien, "Atomic Layer Deposition for Nanotechnology," in *Nanofabrication: Techniques and Principles*, M. Stepanova and S. Dew, Eds. Vienna: Springer Vienna, 2012, pp. 143–161.

[192] M. Bras, V. Dugas, F. Bessueille, J. P. Cloarec, J. R. Martin, M. Cabrera, J. P. Chauvet, E. Souteyrand, and M. Garrigues, "Optimisation of a silicon/silicon dioxide substrate for a fluorescence DNA microarray," *Biosensors and Bioelectronics*, vol. 20, no. 4, pp. 797–806, Nov. 2004.

[193] S. Krishnamoorthy, S. Krishnan, P. Thoniyot, and H. Y. Low, "Inherently Reproducible Fabrication of Plasmonic Nanoparticle Arrays for SERS by Combining Nanoimprint and Copolymer Lithography," *ACS Applied Materials & Interfaces*, vol. 3, no. 4, pp. 1033–1040, Apr. 2011.

[194] J. F. Moulder, W. F. Stickle, P. E. Sobol, and K. D. Bomben, *Handbook of X-Ray Photoelectron Spectroscopy*, J. Chastain and R. C. King, Eds. Minnesota, USA: Physical Electronics, Inc, 1992, vol. 3.

[195] M. P. Seah and W. A. Dench, "Quantitative electron spectroscopy of surfaces: A standard data base for electron inelastic mean free paths in solids," *Surface and Interface Analysis*, vol. 1, no. 1, pp. 2–11, Feb. 1979.

[196] S. Otsuru, L. Desbourdes, A. J. Guess, T. J. Hofmann, T. Relation, T. Kaito, M. Dominici, M. Iwamoto, and E. M. Horwitz, "Extracellular vesicles released from mesenchymal stromal cells stimulate bone growth in osteogenesis imperfecta," *Cytotherapy*, vol. 20, no. 1, pp. 62–73, Jan. 2018.

[197] C. R. Correia, T. C. Santos, R. P. Pirraco, M. T. Cerqueira, A. P. Marques, R. L. Reis, and J. a. F. Mano, "In vivo osteogenic differentiation of stem cells inside compartmentalized capsules loaded with co-cultured endothelial cells," *Acta Biomaterialia*, vol. 53, pp. 483–494, Apr. 2017.

A | Scientific communications

A.1 Publications

C.R. Pedrosa, D. Arl, P. Grysan, I. Khan, S. Durrieu, S. Krishnamoorthy, M.-C. Durrieu; Controlled Nanoscale Topographies for Osteogenic Differentiation of Mesenchymal Stem Cells; Submitted to *Biomaterials*.

C.R. Pedrosa, C. Chanseau, C. Labrugère, S. Krishnamoorthy, M.-C. Durrieu; Mesenchymal Stem Cell Differentiation Driven by Osteoinductive Bioactive Nanoscale Topographies; under preparation.

A.2 Oral communications

Obs.: Presenting author underlined.

Mesenchymal stem cell stemness or differentiation for bone tissue engineering
EJD-FunMat training school 2016 (Bordeaux – France, March 13th-18th 2016)
<u>C. R. Pedrosa</u>, L. Plawinski, S. Krishnamoorthy, M.-C. Durrieu

Mesenchymal stem cell stemness or differentiation for bone tissue engineering
EJD-FunMat training school 2017 (Aveiro – Portugal, March 26th-31st 2017)
<u>C. R. Pedrosa</u>, L. Plawinski, S. Krishnamoorthy, M.-C. Durrieu

2D model surfaces of controlled chemistry and nanotopography for bone tissue engineering

2eme Journées Plénières GDR B2I (Bordeaux – France, June 28th - 29th 2017)

C. R. Pedrosa, D. Arl, P. Grysan, J.-B. Chemin, L. Plawinski, S. Krishnamoorthy, M.-C. Durrieu

Mesenchymal stem cell stemness or differentiation for bone tissue engineering

EJD-FunMat training school 2018 (Luxembourg – Luxembourg, March 18th - 23rd 2018)

C. R. Pedrosa, S. Krishnamoorthy, M.-C. Durrieu

Bioactive nanostructured materials to control mesenchymal stem cell differentiation

Journée Scientifique du CBMN, (Pessac – France, May ^{31st} 2018)

C. R. Pedrosa, D. Arl, P. Grysan, L. Plawinski, C. Chanseau, I. Khan, S. Krishnamoorthy, M.-C. Durrieu

Nanoscale pillars as modulators of mesenchymal stem cell behaviour

29th Annual Conference of the European Society for Biomaterials (Maastricht – Netherlands, September 9th - 14th 2018)

C. R. Pedrosa, D. Arl, P. Grysan, L. Plawinski, C. Chanseau, I. Khan, S. Krishnamoorthy, M.-C. Durrieu

Controlling mesenchymal stem cell differentiation via engineered bioactive nanoscale topographies

Matériaux 2018 (Strasbourg – France, November 19th - 23rd 2018)

C. R. Pedrosa, D. Arl, P. Grysan, L. Plawinski, C. Chanseau, I. Khan, S. Krishnamoorthy, M.-C. Durrieu

A.3   Poster presentations

Obs.: Presenting author underlined.

Controlled nano-engineered interfaces to model cell-substrate interactions
EMRS Fall Meeting 2016 (Warsaw – Poland, September 18th - 22th 2016)
<u>C. R. Pedrosa</u>, D. Arl, P. Grysan, J.-B. Chemin, L. Plawinski, M.-C. Durrieu, S. Krishnamoorthy

Controlled nanoscale topographies as model substrates for bone tissue engineering
2nd Workshop of Regenerative Medicine in Bordeaux (Bordeaux – France, October 24th - 26th 2016)
<u>C. R. Pedrosa</u>, D. Arl, P. Grysan, J.-B. Chemin, L. Plawinski, S. Krishnamoorthy, M.-C. Durrieu

Controlled nanoscale topographies as model substrates for bone tissue engineering
EJD-FunMat training school 2017 (Aveiro - Portugal, March 26th - 31st 2017)
<u>C. R. Pedrosa</u>, D. Arl, P. Grysan, J.-B. Chemin, L. Plawinski, S. Krishnamoorthy, M.-C. Durrieu

Engineered nanoscale topographies to model cell-substrate interactions for bone tissue engineering
10 Years of Research at CBMN (Talence – France, April 6th - 7th 2017)
<u>C. R. Pedrosa</u>, D. Arl, P. Grysan, J.-B. Chemin, L. Plawinski, S. Krishnamoorthy, M.-C. Durrieu

Engineered nanoscale topographies to model cell-substrate interactions for bone tissue engineering
19e Journée de l'École Doctorale des Sciences Chimiques de l'Université de Bordeaux (Bordeaux – France, May 5th 2017)
<u>C. R. Pedrosa</u>, D. Arl, P. Grysan, J.-B. Chemin, L. Plawinski, S. Krishnamoorthy, M.-C. Durrieu

Engineered nanoscale topographies to model cell-substrate interactions for Bone Tissue Engineering

Young scientist day FR TransBioMed TecSan (Bordeaux – France, May 17th 2017)

<u>C. R. Pedrosa</u>, D. Arl, P. Grysan, J.-B. Chemin, L. Plawinski, S. Krishnamoorthy, M.-C. Durrieu

Tuneable nanoscale topographies for modulation of mesenchymal stem cell response for bone tissue engineering

Journée Scientifique de la FR TecSan (Bordeaux – France, June 22nd 2017) – FLASH POSTER

<u>C. R. Pedrosa</u>, D. Arl, P. Grysan, J.-B. Chemin, L. Plawinski, S. Krishnamoorthy, M.-C. Durrieu

Controlled nanoscale topographies for investigation of cell-substrate interactions applied to bone tissue engineering

28th Annual Conference of the European Society for Biomaterials (Athens – Greece, September 4th - 8th 2017)

<u>C. R. Pedrosa</u>, D. Arl, P. Grysan, J.-B. Chemin, L. Plawinski, S. Krishnamoorthy, M.-C. Durrieu

Bioactive nanostructured materials for stem cell differentiation

EJD-FunMat training school 2018 (Luxembourg, March 18th - 23rd 2018)

<u>C. R. Pedrosa</u>, D. Arl, P. Grysan, Stephanie Durrieu, L. Plawinski, C. Chanseau, S. Krishnamoorthy, M.-C. Durrieu

Nanoscale, bioactive topographies as 2D model surfaces for investigation of mesenchymal stem cell differentiation

Journée de la FR TecSan (Pessac – France, May 15th 2018) – FLASH POSTER

<u>C. R. Pedrosa</u>, D. Arl, P. Grysan, L. Plawinski, C. Chanseau, I. Khan, S. Krishnamoorthy, M.-C. Durrieu